

Molecular films and their role in controlling interface properties

Dmitri D. Iarikov

Dissertation submitted to the faculty of the Virginia Polytechnic Institute and State University in partial fulfillment of the requirements for the degree of

Doctor of Philosophy
In
Chemical Engineering

William A. Ducker, Committee Chair
Bahareh Behkam
Richey M. Davis
Steve M. Martin

September 13, 2013
Blacksburg, VA

Keywords: antimicrobial surfaces, poly(allylamine), lateral force microscopy, atomic force microscopy, peptide synthesis, self-assembled monolayers

Molecular films and their role in controlling interface properties

Dmitri D. Iarikov

ABSTRACT

In the first part of this study, frictional and normal forces in aqueous solutions were measured between a glass particle and oligopeptide films grafted from a glass plate. Homopeptide molecules consisting of 11 monomers of different amino acids were each “grafted from” an oxidized silicon wafer using microwave-assisted solid phase peptide synthesis. Oligopeptides increased the magnitude of friction compared to a bare hydrophilic silicon wafer. Friction was a strong function of the nature of the monomer unit and was lower for hydrophilic films. There was a strong adhesion and therefore friction between surfaces of opposite charges. Changes in adhesion and friction depended on the hydrophobicity and electrostatic forces: hydrophobic films and oppositely charged films produced high friction, whereas hydrophilic and like-charges produced low friction. Friction was lower in phosphate buffered saline than in pure water due to the screening of the double layer attraction for oppositely charged surfaces and additional lubrication by hydrated salt ions. We also investigated antimicrobial action of poly (allyl amine) (PA) when covalently bonded to glass. Glass surfaces were prepared by a two-step procedure where the glass was first functionalized with epoxide groups using 3-glycidoxypropyltrimethoxy silane (GOPTS) and then exposed to PA to bind via reaction of a fraction of its amine groups. Antibacterial properties of these coatings were evaluated by spraying aqueous suspensions of bacteria on the functionalized glass slides, incubating them under agar, and counting the number of surviving cell colonies. The PA film displayed strong anti-microbial activity against both Gram-positive and Gram-negative bacteria. Films that were prepared by allowing the PA to self assemble onto the solid via electrostatic interactions were ineffective antimicrobials. Such films had an insufficient positive charge and did not extend far from the solid. Thus we found that antimicrobial activity was correlated with a combination of the ability of the polymer chain to extend into solution and a positive surface potential.

Acknowledgements

I would like to extend my appreciation and sincere gratitude to the people that made it possible for me to earn my graduate degree. Here is the incomplete list: my PhD advisor, Dr. William A. Ducker, my co-advisor Dr. Bahareh Behkam, members of my PhD advisory committee: Dr. Davis and Dr. Martin, the Chemical Engineering department chairs Dr. John Walz and Dr. David Cox, my labmates, past and present, Dr. Chris Honig, Dr. Adam Bowles, Dean Mastropietro, Milad Radiom, Lauren Russel, Katelyn Gause, Akhil Jindal, my coworkers at the Virginia Bioinformatics Institute Mehdi Kargar and Ali Sahari, my parents Drs. Dmitri and Elena Iarikov and my sister Polina Iarikova, and the Chemical Engineering department staff Tina Kirk, Diane Cannaday, Nora Bentley, Riley Chain, and Mike Vaught.

Table of Contents

Chapter 1: Introduction	1
1.1 Motivation	1
1.2 Alkoxysilane self-assembled monolayers	3
1.3 Surface characterization	6
1.4 Atomic force microscopy	8
1.5 Surface imaging	11
1.6 Force measurements	12
References	17
Chapter 2: Measurements of friction using lateral force microscopy	18
2.1 Introduction	18
2.2 Calibration methods for lateral force microscopy	22
2.3 Photodiode calibration methods	30
2.4 Contact compliance and in-plane deflection	38
2.5 Hydration lubrication	40
2.6 Friction control using polymer films	41

References	43
Chapter 3: Effects of grafted oligopeptides on friction measured with lateral force microscopy	45
Abstract	45
3.1 Introduction	46
3.2 Materials and methods	50
3.3 Results and discussion	56
3.4 Conclusions	70
References	73
Chapter 4: Introduction to antimicrobial films and atomic force microscopy	76
4.1 Introduction	76
4.2 Bacterial organisms used in this study	78
4.3 Proposed mechanism of action of antimicrobial compounds	82
4.4 Review of the recent work in antimicrobial films	85
References	90

Chapter 5: Antimicrobial surfaces using covalently-bound polyallylamine	92
Abstract	92
5.1 Introduction	93
5.2 Materials and methods	97
5.3 Results and discussion	102
5.4 Conclusions	116
References	120
Chapter 6. Antimicrobial peptide films	122
Abstract	122
6.1 Introduction	123
6.2 Materials and methods	124
6.3 Results and discussion	125
6.4 Conclusions	130
References	131
Chapter 7. Conclusions	132

List of figures

Figure 1.1 GOPTS (a) and APTES (b) attached to a silicon surface.....	4
Figure 1.2 Schematic of hydroxyl and condensation reactions of silanes with a silica substrate.....	6
Figure 1.3 Schematic illustration of the AFM tip, piezoelectric translation stage, and the force detection assembly.....	10
Figure 1.4 Photo-diode response as a function of the z -piezo position (left), and the corresponding surface force-separation plot (right).....	13
Figure 1.5 Examples of surface force versus separation plots.....	15
Figure 2.1. Friction loop measured with lateral force microscopy.....	21
Figure 2.2 Schematic of the torsional rotation of a rectangular AFM cantilever.....	22
Figure 2.3 Voltage to displacement conversion for a lateral cantilever (error bars represent the standard deviation).....	37
Figure 2.4 Schematic of the torsional (left) and in-plane (right) displacement of the AFM cantilever.....	39
Figure 3.1 Schematic of grafted peptide (top) and sequence of the P ₁₁ -9 peptide (bottom).....	49
Figure 3.2 X-ray photoelectron spectroscopy analysis of the APTES and APTES-peptide surfaces.	57

Figure 3.3 A. Normal forces and B. frictional forces between a glass probe and the polylysine-grafted silica wafer.	59
Figure 3.4 A. Normal forces and B. typical frictional forces between a glass probe and the poly(glutamic acid)-grafted silica wafer.....	61
Figure 3.5 A. Normal forces and B. frictional forces between a glass probe and the poly-leucine grafted silica wafer.....	62
Figure 3.6 A. Normal forces and B. frictional forces between a glass probe and the polyphenylalanine-grafted silica wafer.....	63
Figure 3.7 A. Normal forces and B. frictional forces between a glass probe and the polyglutamine-grafted silica wafer.	64
Figure 3.8 A. Normal forces and B. frictional forces between a glass probe and the P ₁₁ -9-grafted silica wafer.	65
Figure 3.9 Frictional force versus normal load for two poly-glutamic acid films, 11 amino acid long (a) and 22 amino acid long (b) in water.....	66
Figure 3.10 Relationship between measured adhesion and friction.	68
Figure 5.1 Schematic of covalent attachment of PA to glass. The primary amine groups become protonated at neutral pH.....	99
Figure 5.2 N1s peak of the XPS spectrum of a 15,000 MW PAA film.	103
Figure 5.3 ATR-IR spectrum of a 15,000MW PAA/GOPTS film on a silicon wafer.....	104

Figure 5.4 The atomic force microscope image of a silicon wafer that was GOPTS treated for 6 min (a) and 60 min (b).....105

Figure 5.5 Atomic force microscopy images of the bare silicon wafer (a), the GOPTS coated silicon wafer (b), 15,000 MW PAA (c) and 58,000 MW PAA (d).....106

Figure 5.6 Zeta potential of (a) covalently-bound PAA/GOPTS films after an hour-long GOPTS application, and (b) two dipped 15,000MW PAA films.....107

Figure 5.7 Cartoon of the proposed difference in the binding conformation of the electrostatically adsorbed (a) and covalently bound (b) PA.....108

Figure 5.8 Typical force curve between a PA/GOPTS film and a (negatively charged) silicon nitride cantilever (60 min. GOPTS reaction, measurement performed in PBS).109

Figure 5.9 Extension of the PA chains into solution as measured using AFM.....111

Figure 5.10 *S. aureus* colonies on a control glass slide (left) and the GOPTS/PA treated surface (right) after a 24 hour incubation period.....113

Figure 6.1 S2s peak in the XPS spectrum showing the presence of sulfur, which could only occur if amine groups had been present to bind cysteine.....125

Figure 6.2 Secondary ion mass spectrometry for a Pexiganan which would have a mass of $m/z=2363.5$ if only the intended product were formed.....126

Figure 6.3 The XPS spectrum of the glass film following a 24 hour APTES deposition (a), a 4 minute APTES deposition (b), and of a clean glass control (c).....127

Figure 6.4 Bacterial colonies on a clean glass slide (left), APTES-Pexiganan coating (middle), and GOPTS-PEGDA-Pexiganan (right).....128

List of Tables

Table 3.1 Amino acid R-groups used in the synthesis of peptide films with charges at pH 7....	71
Table 3.2 Friction coefficients and adhesive forces at zero load.	72
Table 4.1 An overview of AFM studies of bacterial cell interactions with antimicrobial compounds.....	89
Table 5.1 Killing efficiency of different surfaces compared with a clean glass control.....	117
Table 5.2 The polymer ECL and the standard error of the PA films.....	118
Table 5.3 Values for the XPS analysis of the clean, GOPTS-coated, and GOPTS/PA coated wafers, and also the GOPTS/PA coated wafers after a reaction with Fmoc-protected Cysteine amino acids.....	119

List of abbreviations

AFM	atomic force microscopy
APTES	(3-aminopropyl) triethoxysilane
ATR-IR	attenuated total reflectance Fourier transform infrared spectroscopy
ECL	extended chain length
GOPTS	3-glycidyloxypropyltriethoxysilane
HA	hyaluronic acid
HBTU	o-Benzotriazole-N,N,N',N'-tetramethyl-uronium-hexafluoro-phosphate
LB	lysogeny broth
LFM	lateral force microscopy
LPS	lipopolysaccharide
MALDI TOF	Matrix assisted laser desorption ionization time of flight
MRSA	methicillin resistant <i>S. aureus</i>
MW	molecular weight
NMP	n-Methyl-2-pyrrolidone
PA	polyallylamine
PAA	poly(acrylic acid)
PBS	phosphate buffered saline

PEI	N,N-dodecyl,methyl-polyethylenimine
PLL	poly-L-lysine
PSD	photo-sensitive diode
QA	quaternary ammonium
QCM	quartz crystal microbalance
rms	root mean square
SAM	self-assembled monolayer
SEM	scanning electron microscopy
SFA	surface forces apparatus
SIMS	secondary ion mass spectrometry
SPPS	solid phase peptide synthesis
TEM	transmission electron microscopy
TFA	trifluoroacetic acid
TSB	tryptic soy broth
UHP	ultra-high purity
UV	ultra-violet
XPS	X-ray photoelectron spectroscopy

Preface/Attribution

Manuscript 1 – Effects of grafted oligopeptides on friction measured with lateral force microscopy (Chapter 3)

Published in *Langmuir*, 2013, 29 (19), pp 5760–5769

Authors:

Dmitri D. Iarikov – performed all of the work reported in the manuscript including synthesis and characterization of surfaces and friction force measurements and was the primary author on the manuscript.

William A. Ducker – principal investigator.

Manuscript 2 – Antimicrobial surfaces using covalently-bound polyallylamine (Chapter 5)

Authors:

Dmitri D. Iarikov – performed most of the experimental work and was the primary author of the manuscript, performed all of the synthesis and characterization work and the majority of the bacterial assays, developed protocols for the synthesis procedures and for the bacterial assay.

Mehdi Kargar – assisted with developing the protocol for the bacterial assay and conducted a portion of the bacterial assay experiments.

Ali Sahari – assisted with bacterial assay experiments.

Lauren Russel – assisted with film synthesis and bacterial assay experiments.

Katelyn Gause – assisted with bacterial assay experiments.

Bahareh Behkam – co-principal investigator.

William A. Ducker – principal investigator.

Manuscript 3 – Antimicrobial peptide films (Chapter 6)

Authors:

Dmitri D. Iarikov – performed the experimental work and was the primary author of the manuscript.

William A. Ducker – principal investigator.

Chapter 1

Introduction

1.1 Motivation

Synovial lubrication in mammalian joints is an incredibly efficient way to reduce friction in an aqueous environment. Friction coefficients can be as low as 0.001 – 0.01 between two cartilage surfaces. This ability to maintain extremely low friction under highly dynamic conditions is explained by the complex cartilage structure and self-assembled phospholipids and surface biomacromolecules at the interface.¹ One of the goals of this project was to determine the effect of various chemical groups, e.g. carboxylic acids, amines and hydrophobic groups, on the magnitude of friction between model surfaces in water. This investigation is relevant because previous work has shown that surface-bound molecules strongly affect friction at the aqueous interfaces.² For example, in one study, self-assembled peptides were evaluated as a potential alternative to hyaluronic acid injections for the treatment of osteoarthritis.³ Different peptides were synthesized and allowed to self-assemble into fibrils which formed nematic fluids to be used as cartilage lubricant replacing hyaluronic acid injections. A nematic fluid refers to a liquid crystalline phase where the long axis of the particle is aligned. In our study we took a different approach and grafted short-chain peptides (oligopeptides) to the interface. The frictional response of these films was evaluated using lateral force microscopy (LFM).

The second goal of this study was to modify the silane-coated surfaces to impart antimicrobial functionality. The interest in antimicrobial surfaces stems from the ever-growing demand for healthier and cleaner living conditions among the world population. Pathogenic microbial strains cause millions of deaths every year and new materials that can kill or repel microbes and harmful bacteria are constantly being sought.⁴ Treatment of microbial infections has become more and more difficult due to the increasing presence of antibiotic-resistant pathogens.⁵ For example, the number of deaths from the methicillin resistant strain of *S.aureus* alone in the USA recently surpassed the number of deaths attributed to the HIV.⁶ Many infections are caused or introduced by medical implants. For these infections a possible treatment is to modify the surface of the implant to kill bacteria. This is particularly important in hospital environments where infections spread by the way of transplants or subdermal medical devices.⁷ One advantage of this treatment is that only a small portion of the body is exposed to the antimicrobial, rather than the entire body, as in oral antibiotic treatments. Effective antimicrobial coatings could prevent urinary tract infections and sepsis associated with prolonged exposure to subdermal catheterization. Therefore, we developed polyallylamine (PA) surfaces with significant anti-microbial activity. Test surfaces were first functionalized with epoxy groups using 3-glycidoxypropyl-trimethoxy silane (GOPTS) to allow PA attachment to glass to form a microbicidal layer. The PA films displayed strong anti-microbial capabilities compared with untreated glass. The antibacterial capability of these coatings was evaluated by spraying aqueous suspensions of bacterial cells on PA-functionalized glass slides, incubating them on the surface, and counting the number of surviving cell colonies.

1.2 Alkoxysilane self-assembled monolayers

Self-assembled monolayers (SAMs) have come to scientific attention in 1980⁸ and include systems such as thiol/gold surfaces and alkylsilane/silicon (glass) surfaces. These SAMs form spontaneously on a solid substrate from solution, a property that allows for fine control over the surface chemistry.⁹ The addition of SAMs to silicon or glass surfaces can impart different types of molecular functionality to the substrate (i.e. wettability, electrical or thermal conductivity, friction, adhesion, or antimicrobial properties). Alkylsilane SAMs are chemically and physically robust and find direct applications in various technological systems in the fields of electronics, nanotechnology, protein binding, antibacterial coatings, cell adhesion, and others.¹⁰⁻¹² The typical alkylsilane molecule consists of three portions: the head group, the alkyl chain, and the terminal end group (Figure 1.1).¹⁰ The head group (triethoxy- or trimethoxysilane) anchors the molecule to the substrate. The alkyl chain has a significant influence on the SAM ordering, and the terminal end group is responsible for the chemical functionality of the resultant surface-bound silane layer. In the work in this thesis, the functionality is the ability to bind a polymer. Following the SAM self-assembly, the silane monolayers were further functionalized with oligopeptide molecules (Chapter 3) to modify surface friction or with PA to give the film antimicrobial capabilities (Chapter 5).

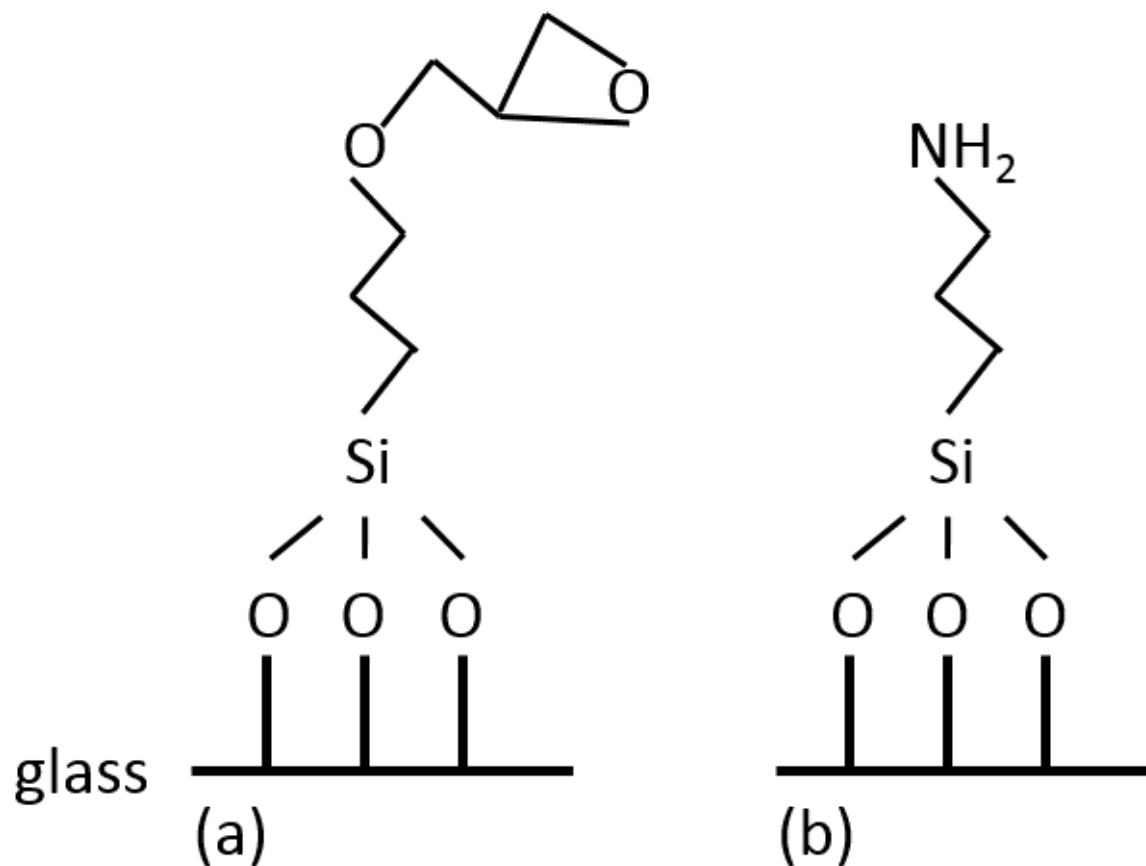
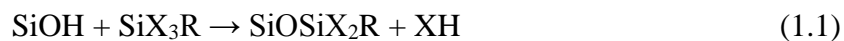


Figure 1.1 GOPTS (a) and APTES (b) attached to a silicon surface.

Silanes react with the silanol groups (SiOH) present on the silica surface according to the following reaction schematic:¹³



where X is the head group and R is the alkyl chain and the terminal end group. The idealized depiction of the two alkylsilanes attached covalently to a substrate is shown in Figure 1.1. It was originally proposed by Sagiv⁸ that the formation of the SAM is initialized with the hydrolysis reaction of silane molecules followed by reaction with the exposed –OH groups on the surface. Others also suggested that the reaction occurs between the self-assembling molecules and

surface-bound residual water molecules and this reaction results in a two-dimensional, cross-linked network of Si-O-Si bonds. The reaction between alkylsilanes and a glass surface is carried out in either organic solvents (such as toluene) or in a vapor phase under vacuum. An alkylsilane molecule can form more than one bond with the silicon substrate. The silanol (“hydroxyl”) groups have to first be “exposed” by a reaction with a strong acid, i.e. concentrated sulfuric acid and hydrogen peroxide mixture. Alternatively, hydroxyl groups on the silicon surface can be formed by exposing the surface to UV/ozone or to oxygen plasma.^{14,15} The initial reaction (“condensation”) is initiated when the head group of the silane reacts with the trace molecules of water on the substrate surface to form silanol groups (hydrolysis).¹³ This is followed by hydrogen bond formation between the silane compounds and the surface and eventually condensation on the surface. The schematic of the hydrolysis and the condensation reactions can be seen in Figure 1.2.⁹ An alternative route to the reaction is the initial adsorption of the silane molecule to the surface followed by a reaction with the exposed hydroxyl groups. It is important to exclude water from the reaction as it promotes uncontrolled further polymerization of the alkylsilanes on the substrate. Exclusion of water can be achieved by exposing the solvent to dry molecular sieves. The self-assembly process generally depends on different factors such as reaction time, reaction temperature, silane concentration, and presence of moisture.

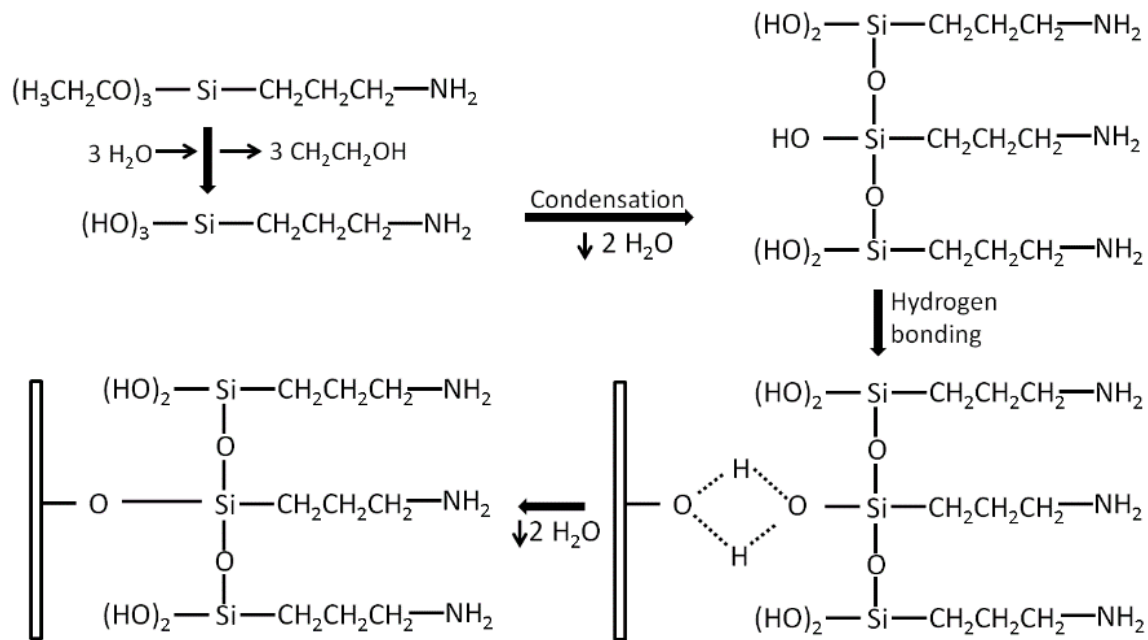


Figure 1.2 The schematic of hydroxyl and condensation reactions of silanes with a silica substrate. Modified from a paper by Arslan et al.⁹

1.3 Surface characterization

In the fields of interface and surface science, it is critical to be able to control and predict the chemical composition and physical structure of thin films and coatings. The analysis of the film structure and composition can be achieved using several techniques such as x-ray photoelectron spectroscopy (XPS), ellipsometry, secondary-ion mass spectrometry (SIMS), atomic force microscopy (AFM), quartz crystal microbalance (QCM), (surface-sensitive) attenuated total internal reflection infra-red spectroscopy (ATR-IR), and fluorescent microscopy.⁹ This section serves as a brief overview for these techniques and instruments.

The XPS is a spectroscopic technique that can be used to estimate the elemental composition and bonding of material present on the surface.¹⁶ This is achieved by using monochromatic X-ray to irradiate the sample followed by analysis of the energy of electrons that escape from the sample surface. The XPS can “probe” the surface on the order of 1 to 10 nm depending on the intensity of the X-ray and the angle of irradiation.

Ellipsometry is a specular optical technique that investigates dielectric properties of thin films that makes it possible to estimate the thickness and refractive index of very thin films.¹⁷ The measured signal is the change in polarization of light as the incident radiation interacts with the film substrate. The difficulties associated with this technique are in the modeling of the experimental data and a requirement for a reflective substrate.

SIMS is used to analyze the composition of thin films by sputtering the surface with an ion beam and collecting and analyzing secondary ions.¹⁸ The mass spectrometer then is used to determine the mass to charge ratios of the sputtered material, which is then used to infer the mass of the compounds that were on the solid surface. The probing depth where SIMS is effective is in the range of 1 to 2 nm.

The QCM is a relatively new technique that is used to measure the total mass adsorbed to a surface and thus the mass per unit area if the area is known.¹⁹ The surface is usually a quartz crystal sputter-coated with a gold layer, which is further functionalized with thiol molecules. However, coatings other than gold or silicon can be used. Minute changes in mass (down to

below 1 ug/cm^2) arising from adsorption lead to measurable changes in the resonant vibrational frequency of the quartz crystal. The adsorbed mass includes solvent molecules. Using QCM it is possible to detect a mass addition of a single molecular monolayer. Energy dissipation at the surface can also be measured. The energy dissipation is a qualitative characterization technique, which gives insight into the organization of the surface film.

The ATR-IR is a surface-sensitive technique that can be used to measure the chemical bonding in a thin film.¹⁶ In this thesis, a particular version of ATR-IR was used where the sample was pressed against a germanium crystal. An evanescent wave, created at the surface of the germanium prism, penetrates into the sample. Adsorption by the sample leads to diminished intensity (attenuation) of the light that passes through the germanium prism. The attenuated intensity, normalized by the attenuation without the sample, as a function of frequency is known as the “spectrum”. Comparison between the measured spectrum and the spectra of known compounds allows identification of the adsorbed material.

AFM can be used to measure surface forces, frictional forces, and the surface topography. These methods are discussed in great detail later in this chapter.

1.4 Atomic force microscopy

AFM was the principal experimental technique used in experiments described in this thesis, and will be described in some detail. The next several paragraphs will allow the reader to gain

understanding and appreciation for this technique. Unlike traditional microscopes where imaging is performed with an incident beam, the AFM imaging is achieved by sensing the force between a sharp probe and a sample surface.²⁰ In an AFM the object is scanned with a microscopic “tip” that has a radius of curvature on the order of a few nanometers. The tip is located at the end of a soft cantilever spring, usually made of silicon nitride. The AFM creates a map of force as a function of position of the tip. The position of the tip relative to the sample is altered using piezoelectric translation stages which provides control over the sample position with sub-nanometer precision.²⁰ The changes in the force experienced by the cantilever probe are recorded are determined from the deflection of a laser beam from the cantilever. To effect efficient reflection, the back of the AFM cantilever is often coated with reflective material such as a layer of gold. A laser beam is reflected from the back of the cantilever to a four-quadrant photodiode. The photo-diode responds to the laser beam position with a change in voltage which measures the deflection of the cantilever. The deflection of the cantilever is converted into force using the measured spring constant. The schematic of the instrument is presented in Figure 1.3.

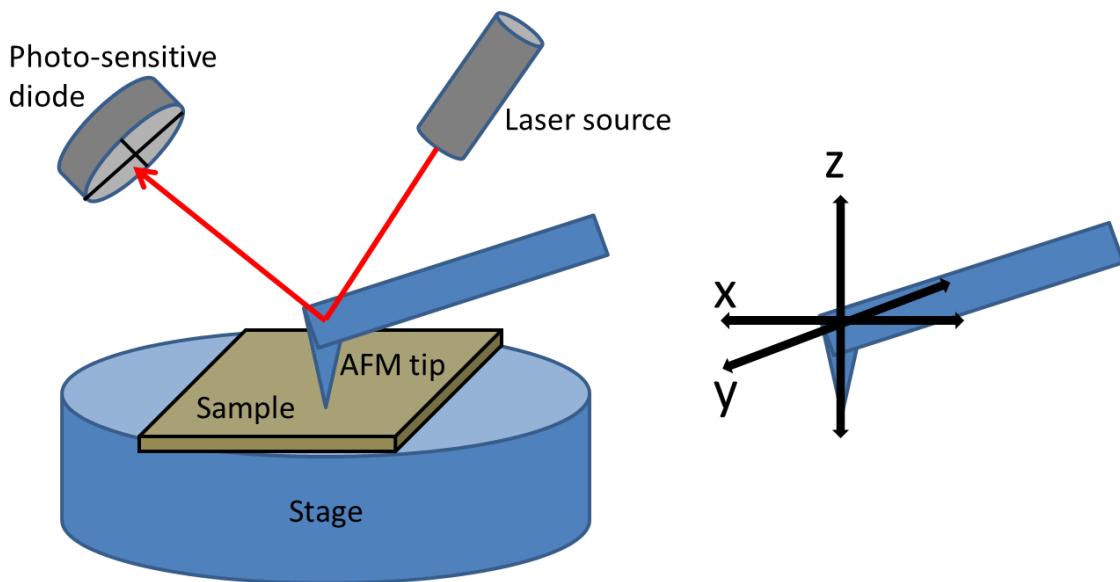


Figure 1.3 Schematic illustration of the AFM tip, piezoelectric translation stage, and the force detection assembly.

AFM has several distinct advantages when compared with other microscopy types. It provides a much higher resolution than an optical microscope, since its resolution is not limited by the wavelength of light, and is capable of imaging in liquids. Under appropriate conditions it is even possible to map distributions of single molecules.²¹ In contrast, scanning electron microscope (SEM) usually requires a conducting solid under high vacuum. These conditions are not always possible to achieve without disturbing the structure of soft materials. AFM can be used to measure surface forces, surface roughness, and mechanical properties of materials and to produce genuine 3D images in buffer solutions and other liquid media. For example, the AFM also allows imaging of live bacterial organisms such as bacteria *in situ*.²²

1.5 Surface imaging

When performing surface imaging with the AFM, there are several approaches available. The sample surface may be imaged either in “contact mode” with the AFM tip in contact with the sample at a constant applied force, or in “tapping mode” with the tip continuously oscillating so as to intermittently touch the sample during each oscillation.

Contact mode AFM can be performed in one of two modes, (a) constant force or (b) variable force. If we assume that the sample is chemically homogeneous, a constant force means a constant height above the sample, so this mode is often called “height mode”. To achieve height mode, the sample is scanned while a feedback loop is activated to maintain a constant deflection on the cantilever by altering the height of a piezoelectric transducer (z -piezo). In this mode the position of z -piezo traces the height of the sample, and is recorded as a function of x - y position to yield a “height image” that represents the height of the sample if the feedback loop is able to maintain constant deflection of the cantilever.

If the gain or frequency of the feedback loop is turned down, then the z -piezo does not track the topography, and the force on the cantilever is a function of position. A record of the deflection as a function of x - y position is called a “deflection image”, and at low gain this deflection image represents the topography. The deflection image is very useful for recording high frequency signals.²⁰ That is, when the topography has high gradients or the image must be collected quickly. Another application is edge detection.

Because the AFM tip is in contact with the sample while it translates sideways, there is friction on the surface, and wear is possible. This is particularly significant for soft and delicate samples such as adsorbed polymers or biological tissue where in contact mode the tip can easily move molecules around the surface, preventing accurate imaging. “Tapping” mode AFM was developed to minimize this “wear”. In tapping mode, the clamped end of the cantilever is driven sinusoidally while the amplitude and the phase of the free end is monitored. The cantilever is positioned such that the tip is only in contact for part of each cycle, and thus it does not scrape along the surface, moving molecules as it goes.²⁰

1.6 Force measurements

In addition to surface images, it is interesting to measure the forces acting in the normal direction between the tip and the sample (a force-distance curve). These force-distance curves are collected by recording (at a given sample location) the cantilever deflection as a function of the vertical displacement of the z -piezo. The atomic force microscopy (AFM) was originally designed with an extremely sharp tip to obtain high lateral resolution while scanning a sample surface. To facilitate comparison with theory, AFM force–distance measurements are often performed with a “tip” of known geometry. This has been achieved through attachment of a silica microsphere (5 to 20 μm) to the free end of the cantilever. Because most surface forces scale with the radius of the object, the larger radius of the sphere compared to a sharp tip also increases the resolution of forces for constant deflection resolution. The measurements performed with a colloidal sphere instead of a regular tip are referred to as the “colloidal probe” technique. This way it is possible to measure forces in the colloidal regime, i.e. between a colloidal particle and a surface, a geometry that is important for colloidal interactions, and has

been extensively studied in the field of fluid mechanics and surface forces. It is also possible to modify the colloidal probe chemically.

The analysis of force–distance curves proceeds as follows: the “raw” photodiode voltage as a function of z -piezo position is captured (Figure 1.4). The voltage is converted to deflection using the measured sensitivity of the so-called constant compliance region. In the constant compliance region the motion of the z -piezo is assumed to be equal to the cantilever deflection. The surface force depends on the separation between the sample and the probe, and not in general on the z -piezo separation. Because the separation changes with deflection, the deflection at each time must be subtracted from the z -piezo position. Further, a constant must be subtracted to determine the absolute separation.

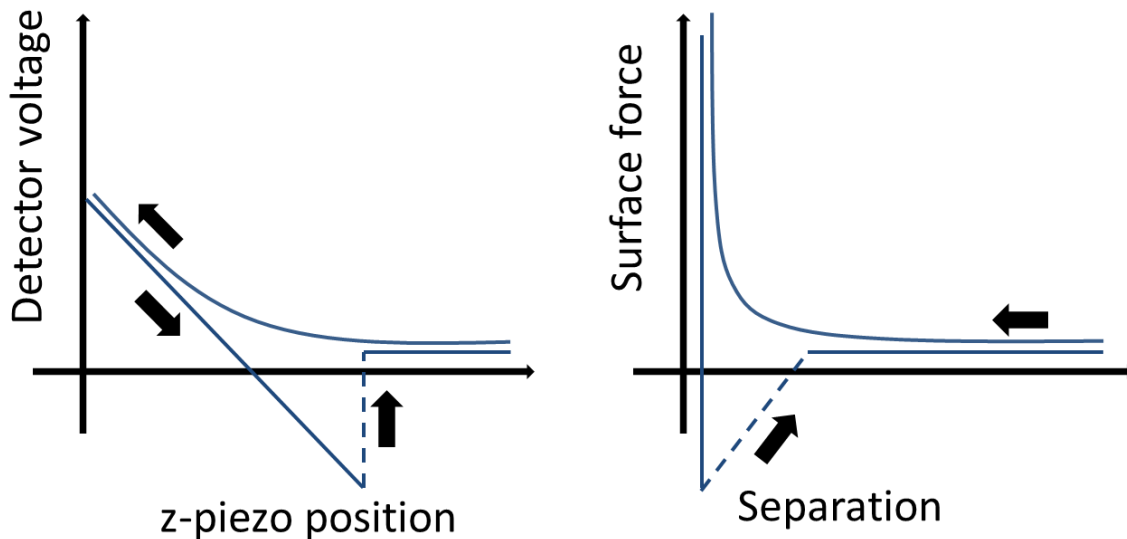


Figure 1.4. Photo-diode response as a function of the z -piezo position (left), and the corresponding surface force-separation plot (right). The sensitivity is obtained from the constant compliance (contact) region and the zero-distance is established relative to the contact regime.

In order to better understand the force-distance curves discussed in this thesis, several examples with explanations are provided in Figure 1.5. By definition at large separations there is no surface force and any residual force due to gravity etc. is subtracted so that the force is set to zero. As the AFM probe approaches the surface, the probe experiences surface forces. For example, in water, there is often a repulsive double-layer force (Figure 1.5a). Sometimes there are attractive forces (Figure 1.5b). When the gradient of an attractive force exceeds the spring constant, the position of the free end of the cantilever is unstable, and the cantilever moves rapidly to the next equilibrium position. This is often called a “jump”. Frequently the next stable equilibrium is with the probe in contact with the sample, which is called a “jump to contact”. After the probe has contacted the sample, the direction of travel of the z -piezo is reversed to pull the probe off the sample. The retract portion contains (a) some of the equilibrium data that was missed during the jump on approach and potentially (b) some metastable local equilibrium positions that can be of great interest. An example of (a) is given in (Figure 1.5c) where a net negative force must be applied to overcome the adhesion that occurs due to strong van der Waals forces at separations of less than a nanometer. An example of (b) is given in Figure 5d. Sometimes polymer molecules stick to the sample, but when the tip or colloid probe touch this layer, the polymer also sticks to the tip or probe. The polymer may then bridge between the two solids. As the probe is moved away from the solid sample, the bridging polymer is stretched and there is an additional attractive force due to stretching of the polymer.²⁰ At some tensile load applied by the cantilever, the bond between the polymer and one of the solids ruptures, and the attractive force is lost, at which time the force due to the polymer drops to zero, which is indicated by the vertical line on Figure 5d. If several polymers of differing

contour lengths between attachment sites are present, then there will be a series of loading and rupture events, as shown in Figure 5d. Therefore the force distance curve provides information about the free lengths of polymer chains bound to the surface, information which is used in the chapter on antimicrobial covalently-bound poly (allylamine) (Chapter 5).

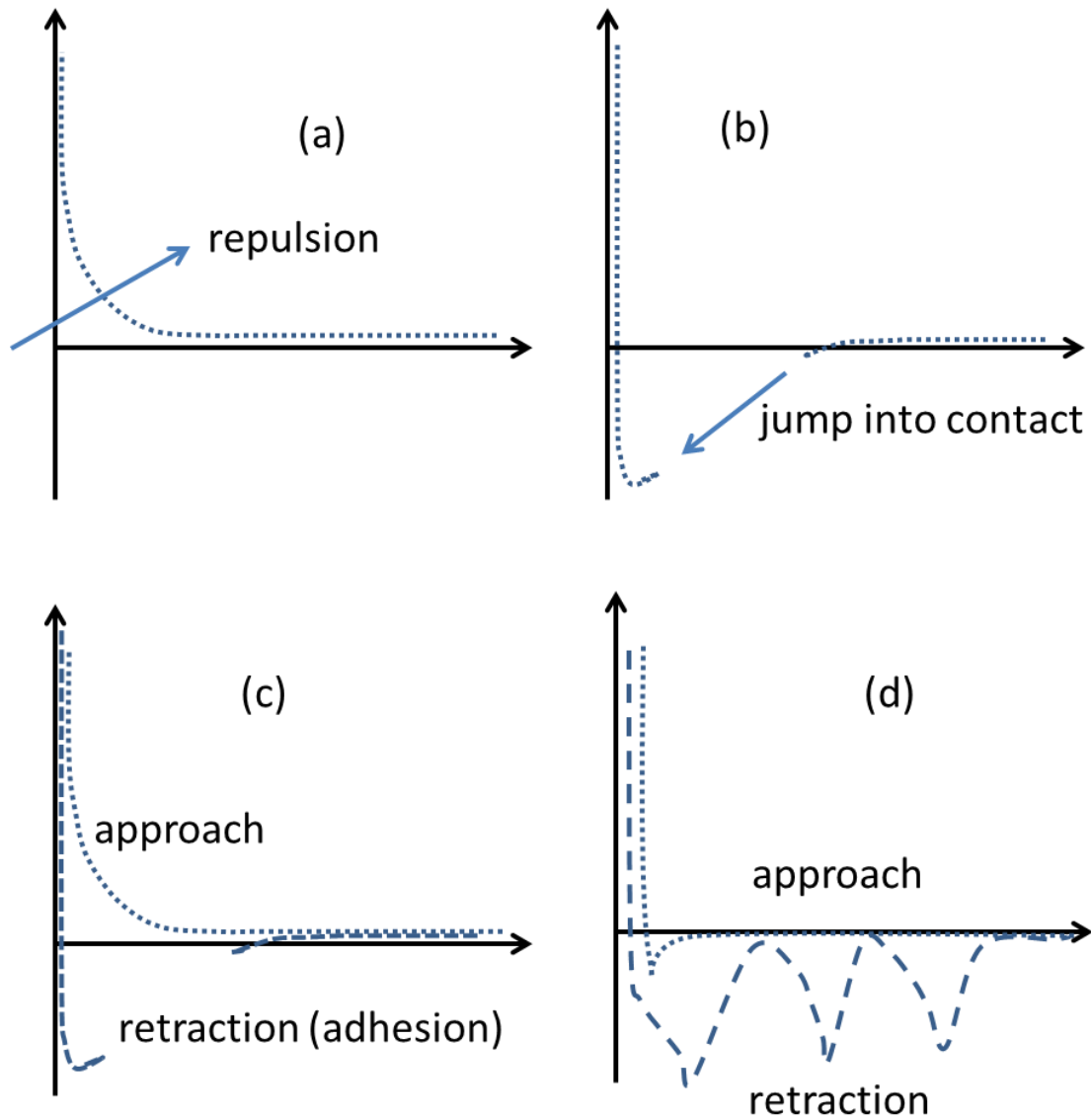


Figure 1.5 Examples of surface force versus separation plots. (a) Repulsive interaction with the sample surface on approach; (b) a mechanical instability and “jump into contact” on approach in the cantilever when the change in the attractive force is bigger than the force constant of the

cantilever; (c) hysteresis when the probe “sticks” to the surface on retraction; (d) an example of “breaking” or detaching of polymer chains from the AFM probe on retraction.

In Chapter 3 of this work we will describe how oligopeptide surfaces can be used to control and modify surface friction measured using lateral force microscopy (LFM) described in Chapter 2. Different types of oligopeptides were used to better understanding of aqueous friction phenomena. Chapter 5 deals with new antimicrobial coatings made of polyallylamine (PA) films bound to epoxide-functionalized surfaces. The coatings were shown to be effective against both Gram-positive and Gram-negative bacteria. The properties of the surface-bound polymer were investigated and the killing efficiency was related to surface charge density and thickness of free polymer chains. Finally Chapter 6 deals with the introductory investigations of interactions of bacteria with antimicrobial coatings using AFM.

References

- (1) Dedinaite, A. *Soft Matter* **2012**, *8*, 273.
- (2) Landherr, L. J. T.; Cohen, C.; Agarwal, P.; Archer, L. A. *Langmuir* **2011**, *27*, 9387.
- (3) Bell, C. J.; Carrick, L. M.; Katta, J.; Jin, Z.; Ingham, E.; Aggeli, A.; Boden, N.; Waigh, T. A.; Fisher, J. *Journal of Biomedical Materials Research Part A* **2006**, *78A*, 236.
- (4) Tiller, J. C.; Liao, C. J.; Lewis, K.; Klibanov, A. M. *P Natl Acad Sci USA* **2001**, *98*, 5981.
- (5) Lode, H. M. *Clinical Microbiology and Infection* **2009**, *15*, 212.
- (6) Klevens R, M. M. A. N. J.; et al. *JAMA* **2007**, *298*, 1763.
- (7) Zilberman, M.; Elsner, J. J. *Journal of Controlled Release* **2008**, *130*, 202.
- (8) Sagiv, J. *Journal of the American Chemical Society* **1980**, *102*, 92.
- (9) Arslan, G.; Ozmen, M.; Gunduz, B.; Zhang, X.; Ersoz, M. *Turk J Chem* **2006**, *30*, 203.
- (10) Aswal, D. K.; Lenfant, S.; Guerin, D.; Yakhmi, J. V.; Vuillaume, D. *Analytica Chimica Acta* **2006**, *568*, 84.
- (11) Pignataro, B.; Licciardello, A.; Cataldo, S.; Marletta, G. *Materials Science and Engineering: C* **2003**, *23*, 7.
- (12) Chaki, N. K.; Vijayamohan, K. *Biosensors and Bioelectronics* **2002**, *17*, 1.
- (13) Butt, H.-J.; Cappella, B.; Kappl, M. *Surface Science Reports* **2005**, *59*, 1.
- (14) Vig, J. R. *Journal of Vacuum Science & Technology A: Vacuum, Surfaces, and Films* **1985**, *3*, 1027.
- (15) Isabell, T. C.; Fischione, P. E.; O'Keefe, C.; Guruz, M. U.; Dravid, V. P. *Microscopy and Microanalysis* **1999**, *5*, 126.
- (16) Pavia, D. L.; Lampman, G. M.; Kriz, G. S. *Introduction to Spectroscopy*; 3rd ed.; Brooks/Cole: United States of America, 2001.
- (17) Tompkins, H. G. *A Users's Guide to Ellipsometry*; Academic Press Inc.: London, 1993.
- (18) Vickerman, J. C.; Briggs, D. *ToF-SIMS: Surface Analysis by Mass Spectrometry*; IM Publications: Chichester, UK, 2001.
- (19) Rodahl, M.; Hook, F.; Fredriksson, C.; A. Keller, C.; Krozer, A.; Brzezinski, P.; Voinova, M.; Kasemo, B. *Faraday Discussions* **1997**, *107*, 229.
- (20) Dufrene, Y. F. *Journal of Bacteriology* **2002**, *184*, 5205.
- (21) Engel, A.; Muller, D. J. *Nat Struct Mol Biol* **2000**, *7*, 715.
- (22) Liu, S.; Wang, Y. *Scanning* **2010**, *32*, 61.

Chapter 2

Measurements of friction using lateral force microscopy

2.1 Introduction

While frictional behavior was first described by Leonardo da Vinci, the development of the original experimentally-based frictional laws was attributed to Guillaume Amontons and Charles-Augustin de Coulomb. Amontons' first and second laws state that the force of friction is directly proportional to the applied load and is independent of the contact surface area.

Coulomb's friction law states that the friction is also independent of the sliding velocity. Most recently, a significant attempt to explain the empirical phenomena behind Amontons' laws was made by Bowden and Tabor in the middle of the 20th century.¹ According to the Tabor and Bowden model, the frictional force depends on the product of the shear stress between the two surfaces and the real area of contact which is much smaller than the apparent contact area.

Validation of Tabor and Bowden's ideas is difficult because the true contact area is difficult to estimate experimentally.

Understanding of the tribological behavior at the nanoscale level is important for the development of technologies in the area of biological and biophysical processes because in both nature and industry, surfaces that slide past each other are lubricated via thin interfacial films.

The focus of this work is friction in aqueous solutions. In articular joints, for example the knee,

are an example of a water-based lubrication system. Healthy cartilage surfaces can slide on each other with extremely low friction coefficients for many years. Cartilage tissue is made up primarily of water with high molecular weight hyaluronic acid (HA), glycosolated proteins and various lipids.² Different models for the mechanism by which this low friction is achieved have been proposed³ and the excellent lubrication between living joints is ascribed to the presence of brush-like macromolecules that are able to sustain sliding and provide separation between surfaces. For example, hyaluronic acid is a charged linear polymeric carbohydrate and the main component of healthy synovial fluid. Osteoarthritic joints contain reduced concentrations of HA resulting in wear and tear of the cartilage. The current method for short-term pain relief in osteoarthritis consists of regular injections of HA or its derivatives. HA is an effective lubricant with healthy or slightly damaged cartilage, but does not reduce cartilage friction for cases of more severe damage. Short synthetic linear amino acid sequences (peptides) were proposed as a potential replacement for HA as a way to restore stability to the joints, relieve pain, and delay surgery.⁴ It is interesting to determine whether the reduction or control of frictional properties can be possible when the peptides are “grafted from” the surface. Grafting holds the polymers in place, but diminishes the conformational freedom of the molecules.

At the end of the 20th century, the study of friction was revolutionized with the invention of atomic force microscopy (AFM), and the surface forces apparatus (SFA)^{5,6} as these devices allowed for precise characterization of friction forces. The principal advantages of SFA are the ability to use molecularly smooth mica, the ability to determine the shape of the contact area and the ability to determine the absolute separation. AFM has the advantage of being amenable to many different materials, particularly glass and silica, which allow easy chemical grafting. To

determine friction forces, the AFM must measure the force normal to both the surface and the direction of motion. Such measurements are called lateral force microscopy (LFM) and rely on measurement of deflection of a microcantilever. In the microscopes in the Ducker Lab this lateral deflection of the cantilever is sensed by a photodiode (See Figure 2.1). The lateral force on the cantilever results in the lateral (torsional) deflection, and the signal can be recorded using the photo-sensitive diode (PSD) detector assembly. A laser beam is aimed at the end of the cantilever and the beam is then deflected onto the PSD using a mirror. The position of the laser spot on the PSD can be used to determine deflection of the cantilever by analyzing the magnitude of the resulting voltage. This is represented schematically in Figure 2.2 where the four quadrants of the PSD are labeled A1, A2, B1, and B2.⁷ The voltage signal obtained with the PSD has to be converted into the units of deflection. The normal and lateral voltage signals can be described by the following two equations:

$$V_{\text{normal}} = (V_{A1} + V_{A2}) - (V_{B1} + V_{B2}) \quad (2.1)$$

$$V_{\text{lateral}} = (V_{A1} + V_{B1}) - (V_{A2} + V_{B2}) \quad (2.2)$$

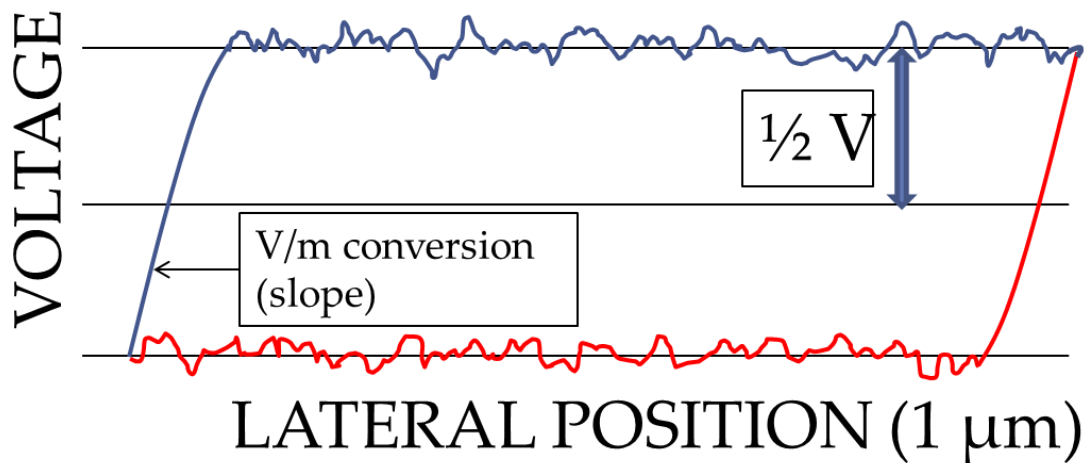


Figure 2.1. Friction loop measured with lateral force microscopy. The dynamic friction is proportional to $1/2V$. Calibration of friction requires the V/m calibration (shown) and the lateral force constant of the cantilever.

Therefore, both normal and lateral surface forces can be investigated simultaneously with the one photodiode. As described above, colloidal probe AFM was first developed by Ducker⁸ and allowed measurements of surface forces with a controlled geometry and increased magnitude force magnitude by attachment of a colloidal sphere to the AFM cantilever. LFM can also be performed with a colloidal probe, which then allows use of a variety of solids.^{9,10} Furthermore, the torsional or the lateral spring constant of the cantilever must be known in order to calculate the force that the cantilever probe is experiencing.

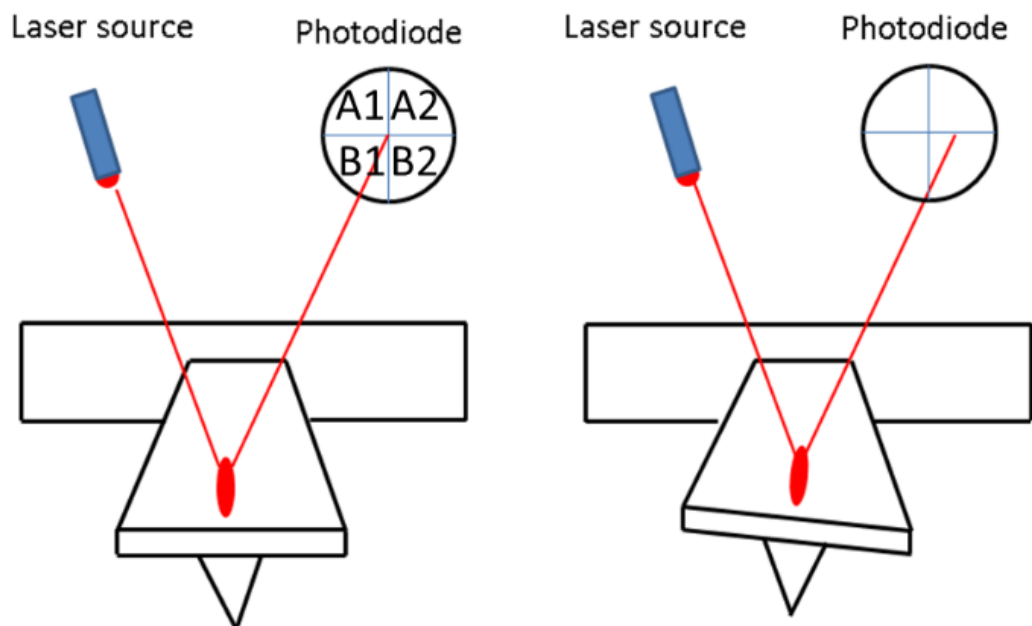


Figure 2.2 Schematic of the torsional rotation of a rectangular AFM cantilever.

2.2 Calibration methods for lateral force microscopy

In LFM, the cantilever is scanned in contact with the solid in the direction normal to both the solid and axis of the cantilever. The resulting friction between the tip and sample applies a force laterally to the end of the tip, which applies a torque to the free end of the cantilever, distorting the shape of the cantilever and causing the reflected laser beam to translate to from side 1 to side 2 (Figure 2.2). Starting from zero velocity, a finite force must be applied to the tip to exceed the static friction and commence motion. During this portion, the cantilever is being loaded proportional to the travel of the piezo, which appears as a linear trace in a plot of photodiode response as a function of lateral position. This is analogous to the constant compliance regime in normal force microscopy. Once the static friction is exceeded, the cantilever starts at the same

velocity as the translation stage, the friction reaches a constant value, the dynamic friction, and the diode response is constant (See Figure 2.1). In some cases stick-slip motion occurs, but this is not considered in this thesis because it was not observed in the measurements. In the absence of stick-slip, the friction is characterized by the dynamic friction.

When the direction of motion of the x-piezo is reversed, the lateral loading on the tip decreases, and the joint between the tip and sample becomes stuck. A second linear regime is encountered (see Figure 2.1). The load drops to zero and then increases in magnitude with the opposite direction to the initial load. Ultimately, the static friction is exceeded and the tip again begins to move in a direction opposite to the initial direction of motion, but in the same direction as the y-piezo stage. Note that friction always opposes the direction of motion. Because the friction is symmetrical with respect to velocity, the kinetic friction is proportional to one half of the difference between the two friction traces shown in Figure 2.1.

2.2.1 LFM torsional sensitivity

The laser beam is deflected by the torsional motion of the cantilever as it slides along the sample surface and the motion is registered by the photodiode and is recorded in the units of lateral voltage. It is possible to define the “torsional sensitivity” of the lateral force microscope as a ratio of the lateral voltage output and the torsional moment applied to the cantilever.¹¹ In this case the lateral friction force can be defined as

$$F_L = \frac{\Delta V_L}{S_T h} \quad (2.3)$$

where ΔV_L is the lateral voltage signal, S_T is the torsional sensitivity which is defined as the ratio of the lateral voltage output to the torsional moment applied to the cantilever, and h is the arm length across which the torque is applied. For our purposes the torsional arm length corresponds to the diameter of the glass sphere attached to the tip of the AFM cantilever. In this case the torsional deflection of the cantilever (ϕ) can be equated to the lateral displacement (Δy) if the ϕ is small. Therefore, $\phi = \Delta y/h$ where the h is the diameter of the colloidal sphere (or the length of the moment arm).¹¹ Therefore, if we know the torsional stiffness of the cantilever, we can then determine the frictional force:⁷

$$F_y = \frac{k_\phi \phi}{h} \quad (2.4)$$

where h is the moment arm which in this case is equal to the colloidal sphere diameter. The calibration of the photo-diode was performed using a simple method first developed by Ducker¹² where it is assumed that the linear part at the start of the friction loop represents the region where the tip is fixed on the sample, so the deflection voltage is proportional to the lateral deflection of the cantilever. The proportionality constant, C_t , is in units of deflection per volt.

To calculate the frictional force we measured and analyzed sets of friction loops at different applied normal loads. The voltage difference between the two flat (dynamic) parts of the friction loop is directly proportional to the magnitude of the friction force. We can further obtain the relationship between the lateral movement of the piezoelectric motor (in volts) and the lateral deflection of the cantilever from the slope of the static friction region. The friction force can then be calculated according to the following equation:

$$F_f = \frac{\Delta V}{2} C_t \frac{k_\phi}{h^2} \quad (2.5)$$

where ΔV is the voltage difference from the dynamic friction loop portion, k_ϕ is the torsional spring constant, C_t is the volts to deflection conversion factor, and h is the moment arm. The voltage difference has to be divided by two to account for the fact that the friction loop shows the cantilever direction as it goes both ways across the sample surface.

The terms “torsional” and “lateral” spring constant are oftentimes used interchangeably but they are not the same, e.g. $F_f = k_{lat} d_{lat} = \frac{k_\phi \phi}{h}$. The torsional spring constant (k_ϕ) can be converted to the lateral spring constant (k_{lat}) if the moment arm length of the cantilever is known and the torsional deflection angle is small using the following equation. The torsional spring constant has the units of [N m] and the lateral spring constant has the units of [N/m].

$$k_{lat} = \frac{k_\phi}{h^2} \quad (2.6)$$

In the above equation, h is the height of the moment arm of the AFM cantilever, i.e. the diameter of the colloidal sphere.

The friction loop can be thought of a “force curve” in the lateral direction. We need similar type of information to extract the frictional force from the friction loop it as we do to extract the normal force from the normal force-distance curve. The stiffness of the spring (in this case lateral or torsional) and the voltage to deflection conversion factor (calibration of the

photodiode) are required. The cantilever calibration in the normal direction has been well researched, and includes such methods as finite element analysis,¹³ method of added mass,¹⁴ reference cantilever method,¹⁵ method of thermal vibrations¹⁴ and others. The photodiode calibration is also fairly straightforward in the normal direction and the most common method uses the “constant compliance” region to determine the voltage to deflection conversion. On the other hand, lateral/torsional calibration is more complex and requires considerable ingenuity. This chapter will describe different methods of how these properties can be obtained in order to perform LFM measurements. Over the past two decades, numerous methods of LFM calibration were proposed and can be roughly divided into two types:

- (1) two-part calibration (spring constant is determined separately from the photodiode calibration)
- (2) combined calibration (spring constant and PSD sensitivity determined together)

In (1) it is necessary to individually determine the lateral or the torsional spring constant and then perform the photodiode calibration. In (2) the stiffness of the cantilever is determined simultaneously with the photodiode calibration, or the mechanical calibration of the cantilever is not necessary at all. This first part of this chapter will serve as an overview of several ways to calibrate the lateral spring constant. The lateral or torsional spring constants can be determined using different methods, such as finite element analysis,¹⁶ direct calculation from the normal spring constant,¹⁷ estimation based on analysis of thermal lateral vibrations in air,¹⁴ method of added mass,¹⁸ stiffness determined by pressing the cantilever against another of known stiffness,¹⁹ wedge calibration method,²⁰ and applying known lateral torque to the cantilever.¹⁵ The second part of this chapter will deal with the photodiode calibration methods. The photodiode can be calibrated using different methods such measuring the deflection of a beam

attached to the reference cantilever,²¹ calibration by using a grating with two known slopes (“wedge method”),²² calibration against a vertical wall,⁷ using a stiffness reference cantilever,¹⁹ friction measurement in the long axis direction,²³ by moving the PSD assembly,²⁴ using the static portion of the friction loop,¹³ and by moving a mirror in place of the cantilever.¹⁵

2.2.2 Sader’s method: analysis of thermally stimulated deflection

In the Sader’s method, the torsional spring constant is calculated using the physical dimensions of the cantilever, its vibrational frequency and the quality factor. This calculation method is derived from the assumption that an AFM cantilever is a beam immersed in a fluid.¹⁴ The main advantages of this method are that it is not destructive, and that the measurement can be performed *in situ* for a rectangular cantilever as long as the cantilever thickness (t) is much smaller than its width (b), and the width is smaller than the length (L). Therefore, the Sader’s calibration does not explicitly rely on the thickness of the cantilever which is difficult to determine experimentally.

If the quality factor of the resonant frequency peak of the cantilever is much greater than one, the torsional spring constant can then be calculated using the following equation:²⁵

$$k_{\phi} = 0.1592\rho b^4 L Q_t \omega_t^2 \Gamma_i^t(\omega_t) \quad (2.7)$$

Where k_{ϕ} is the torsional spring constant, ρ is the density of the fluid, b and L correspond to the cantilever width and length, Q_t is the quality factor, ω_t is the cantilever torsional resonance

frequency, and Γ_i^i is the imaginary component of the hydrodynamic function. The values for the hydrodynamic function are tabulated and depend only on the Reynolds number of the system.

Once k_ϕ has been determined, k_{lat} can be determined as well via $k_{lat} = \frac{k_\phi}{h^2}$ using the known height of the tip or colloidal sphere. The friction force can then be calculated by multiplication by the lateral deflection, which is determined from the friction loop. This requires a calibration of the voltage as described in section 2.3. These two methods combined were used to calibrate the cantilevers for friction measurements in this thesis.

2.2.3 Finite elements method

If the knowledge of the mechanical properties of the cantilever and its precise dimensions are available, it is possible to estimate the spring stiffness by using the finite elements analysis (FEA) of the beam structure.^{13,24} The major drawback to this method is the cubic dependency of the cantilever stiffness on the value of cantilever thickness. It is a difficult property to be measured precisely unless SEM measurements are performed on each cantilever in question. When performing the FEA there must be assumptions made on the nature of the material in order to determine its mass, moment of inertia, etc. As mentioned above, the gold coating changes the mechanical properties of the cantilever in ways that are hard to predict. Therefore, it is preferable to use an experimental method to estimate the spring constant of the individual cantilever before each experiment.

2.2.4 Calibration using a known off-set

Cantilever stiffness can be calibrated by bringing the probe into contact with another cantilever that was vertically glued to a substrate¹⁵. The lateral deflection of one cantilever is then equal to the known normal deflection of the other cantilever. The lateral force constant was calculated by measuring the lateral constant compliance slope at the center of the cantilever and at a known off-set. This method is quite laborious and requires (1) a preparation of a special substrate, (2) accurate calibration of the piezo-motor to be able to obtain an accurate measure of the offset from the center line of the AFM cantilever, and (3) independent calibration of the photodiode with respect to the torsional angle to voltage conversion.

2.2.5 Method of added mass

The method of cantilever stiffness estimation using addition of known mass was first proposed by Cleveland et al. to determine the normal spring constant.¹⁸ In his original paper a series of particles of known mass were attached to the tip of the cantilever which the resonant flexural frequency of the cantilever spring was related to. The normal spring constant was determined from the slope of the plot of added mass versus the inverse square of the spring resonant frequency. This method was then extended to determine the torsional spring constant.¹⁴ The torsional spring constant was related to the square of the torsional resonant frequency and the moment of inertia of the cantilever spring. With the addition of known mass to the tip, the moment of inertia changes and so does the torsional spring constant. The moment of inertia of the added mass can be estimated for a spherical weight using the following equation:¹⁴

$$\omega_t^2 = \frac{k_\phi}{J+J_e} \quad (2.8)$$

In the above equation ω_t is the fundamental torsional resonant frequency of vibration, J is the moment of inertia associated with the added mass, and J_e is the moment of inertia of the unloaded cantilever. It is then possible to calculate the moments of inertia around the moment arm of the cantilever. It is assumed that the added mass is perfectly centered along the major axis of the cantilever at the point of the free end. If the diameter of the sphere is much larger than the thickness of the cantilever, the total added mass moment of inertia can be calculated using the parallel axis theorem. The torsional spring constant can then be related to the torsional resonant frequency using the equation below.

$$\omega_t^2 = \frac{k_\phi}{\frac{7}{5}M_s r^2 + J_e} \quad (2.9)$$

In the equation above M_s is the mass of the sphere attached to the end of the cantilever and r is its radius. Although the calculations used in this approach are fairly straight-forward, the critical drawback is in the difficulty associated with the attachment and removal of a series of spherical particles from the cantilever tip.

2.3 Photodiode calibration methods

The photodiode array provides the measure of the cantilever normal and lateral motion. In order to extract meaningful data from the LFM measurements, it is necessary to determine the appropriate calibration of the photodiode voltage response. The measurement of lateral or torsional spring constants may introduce additional systematic errors into the calculations. It is

possible to use a calibration method that directly relates the lateral force experienced by the cantilever to the lateral voltage signal from the photodiode. In this case it is not necessary to estimate the cantilever stiffness separately. This method ideally would be preferred, particularly if the photodiode calibration was performed using the experimental cantilever. The logical way to achieve this calibration is to apply a known force to the AFM cantilever and to measure the lateral response. Other approaches to lateral photo-diode calibration include determining the slope of the static portion of the friction loop,^{12,26} tilting the AFM head,²⁷ and tilting a reflective sample using a stepper-motor.¹⁵

2.3.1 Photodiode calibration by attachment of a beam to the target cantilever

The photodiode can be calibrated by attaching a beam with a colloidal probe perpendicular to the end of the AFM cantilever and then measuring the torsional signal as the beam is twisted around the spring.²¹ This method calibrates the spring constant and the PSD response to the angular deflection simultaneously. In this arrangement the voltage signal of the PSD is proportional to deflection.²⁸ By measuring the lateral and the normal deflection of the cantilever with the sphere attached it is possible to calculate the calibration factor that relates the lateral voltage signal with the applied torque. The critical disadvantage of this method is that the attachment of a beam it is a delicate and a time-consuming process. This method would work best with a series of cantilevers that have consistent mechanical properties and where the torsional spring constant would not change dramatically from one probe to the next. This way, one representative cantilever could be calibrated, and the other ones could be assumed to have similar torsional

spring constants. This would obviously introduce additional error into the experimental measurements calculations.

2.3.2 Wedge calibration method

The wedge calibration method for LFM was originally proposed by Ogletree et al.²² It has been the most commonly employed standard for LFM calibration used by different researchers as a means to validate their work. The elegance of the wedge method is that it simultaneously calibrates both the lateral spring constant and the photodiode response. It was the first proposed method of this kind where LFM calibration did not rely on the separate determination of the cantilever stiffness.¹⁰ This method was originally designed for regular AFM tips and then extended to colloidal surface probes.²⁰ The wedge method relies on sliding the cantilever probe over a calibration grating of two well-defined slopes such as (101) and (103) planes on SrTiO₃.¹⁰ Using the wedge method the detection system is calibrated for each specific cantilever and the information on the tip geometry can also be obtained. The response of the cantilever to the incline in the surface can be described using a force balance. When the measurement is performed with different normal loads the lateral signal can be calculated. This technique relies on two assumptions that (1) the slopes of the tilted surfaces are precisely known and (2) that the piezo is accurately calibrated in the lateral direction. When the probe moves across a tilted surface, the normal and frictional forces acting on the tip couple into the lateral and normal signals. These signals can be resolved since the known geometry of the inclined surfaces provides additional information. The normal to lateral signal can be compared to the expected normal to lateral force ratios to calibrate the lateral response.⁷

2.3.3 PSD calibration by moving the colloidal sphere against a vertical wall

In a paper by Cannara et al.,⁷ the lateral signal deflection sensitivity was calculated by attaching a colloidal sphere to a reference cantilever of the same width but different length and material than the cantilever of interest. A colloidal sphere was glued to the tip of a test cantilever with the same width and coating as the target. The test cantilever was loaded against a vertical wall and the lateral sensitivity of the PSD was obtained. The lateral force was measured at the equator of the sphere against a vertical surface. The signal sensitivity from the reference cantilever was then corrected to account for the difference in width, signal strength, and the in-plane bending of the cantilever. In this calibration technique the lateral deflection sensitivity was determined to depend on the geometry of the laser beam path, the torsional moment arm, and the total signal on the PSD but did not depend on the width of the cantilever. The resulting slope in the contact region resulted in the calibration of the lateral deflection sensitivity which depended on the beam laser path, the torsional moment arm, and the photodiode response.⁷ The sensitivity of the target cantilever was related to the sensitivity of the test cantilever when accounting for the moment arm length and the total lateral voltage signal. A correction was performed to account for the differences in the cantilever material and dimension. The lateral force experienced by the two cantilevers was related, and the sensitivity of the cantilever of interest was estimated. This method was found to agree very well with the “wedge” calibration method described above.

2.3.4 Calibration using a stiffness reference cantilever

The lateral sensitivity of the detector can be determined by pressing a calibrated reference cantilever with a known normal stiffness against the cantilever of interest inducing a twisting motion.¹⁹ The reference cantilever was then pressed against a hard surface to obtain a relationship between deflection and voltage values. These two sets of data can be compared to determine the sensitivity parameter necessary to convert lateral voltage into force. This method works best for colloidal probes because it is fairly straight-forward to estimate the location of the sphere equator. Since a known force is applied to the cantilever laterally to estimate the lateral voltage/lateral force conversion on the cantilever of interest, it is not necessary to separately determine the cantilever stiffness.

2.3.5 Friction measurements in direction parallel to cantilever long axis

A very interesting method of measuring the frictional AFM response was proposed by Roan and Bhushan.²³ The authors took advantage of the downward tilt of the AFM cantilevers (typically between 7° and 20°) that is a common feature of all AFM instruments. The purpose behind tilting the cantilever downwards was to ensure that the tip of the cantilever came in contact with the sample before the rest of the cantilever holder assembly. This way the colloidal probe attached to the end of the cantilever spring slides in the direction parallel to the cantilever long axis along the sample surface. This motion results in friction parallel to the cantilever's long axis. The direction of the friction changes depending on whether the cantilever was moving upward or downward and the total force acting on the cantilever is a combination of the normal and frictional forces (acting in the same direction). The vertical deflection of the cantilever is

kept constant during scanning. Therefore, the friction measured in the direction parallel to the long axis of the cantilever was assumed to be equal to the vertical spring constant times the vertical piezo displacement. Since the frictional force acts in the direction opposite to which the cantilever is moving, the normal force was adjusted when the sample direction was reversed. The force measured using this method was used to calibrate the frictional force²¹ using a known coefficient of friction. The underlying assumption that the frictional deformation is compensated for by adjusting the normal force is not entirely true because the friction force applies a different moment to the end of the cantilever than the piezo adjustment.¹³ The bending moment of the cantilever is ignored in this calibration therefore it cannot be used quantitatively.

2.3.6 Method of moving the photosensitive-diode assembly

It is possible to estimate the lateral voltage to the lateral deflection calibration when the photodiode position is mechanically adjusted. This way the detector signal can be measured as a function of its manual displacement. The force calculation relies on this calibration, the normal and lateral stiffness of the cantilever, and the width of the friction loop among other parameters. In a paper by Liu et al., the lateral photodiode response was originally calibrated in this way. It was assumed that the angle between the lateral displacement of the PSD and the centers of gravity of the two laser spots on the PSD were approximately twice the cantilever torsional angle.²⁴ It was also assumed that the lateral sensitivity is proportional to the normal sensitivity that can be measured readily. The resulting sensitivity factor was related to the lateral force measured by the cantilever using its torsional stiffness and the apparatus geometry. This method requires the precise knowledge of the geometry of the particular AFM photodiode assembly, and

the ability to mechanically adjust the photodiode position. This was the first method that provided a direct measurement of lateral sensitivity of the AFM photodiode.¹³ It requires an independent calculation of the cantilever torsional spring constant which was then used to convert the cantilever angle (determined by photodiode calibration) into torque.

2.3.7 PSD calibration using the slope of the static portion of the friction loop

The slope of the static region of a friction loop can be used to estimate the conversion between the lateral deflection and the PSD signal. When the force is first laterally applied to the cantilever, the tip and the surface remain in rigid contact while the tip twists to generate a lateral voltage signal. This method can be used when with colloidal probes because the glue joint stiffness can be neglected, and the contact stiffness is much higher than with the standard silicon nitride tip due to the increased contact area. This calibration method was used previously by Ducker,²⁹ Liu,²⁶ and Cain.¹³ Cain et al determined that the results obtained with this calibration method are comparable with the wedge method.¹⁰ As the normal loading increases, the deflection to voltage conversion would approach an asymptote and give the most accurate calibration value at higher normal load. This was confirmed in our experimental results thus additionally validating the use of this method (Figure 2.3). The V/nm conversion for the lateral forces approached a steady value as the normal load was increased. We also compared the results with measurements of friction between two bare silica surfaces to verify that our results were consistent with those reported previously in the literature.

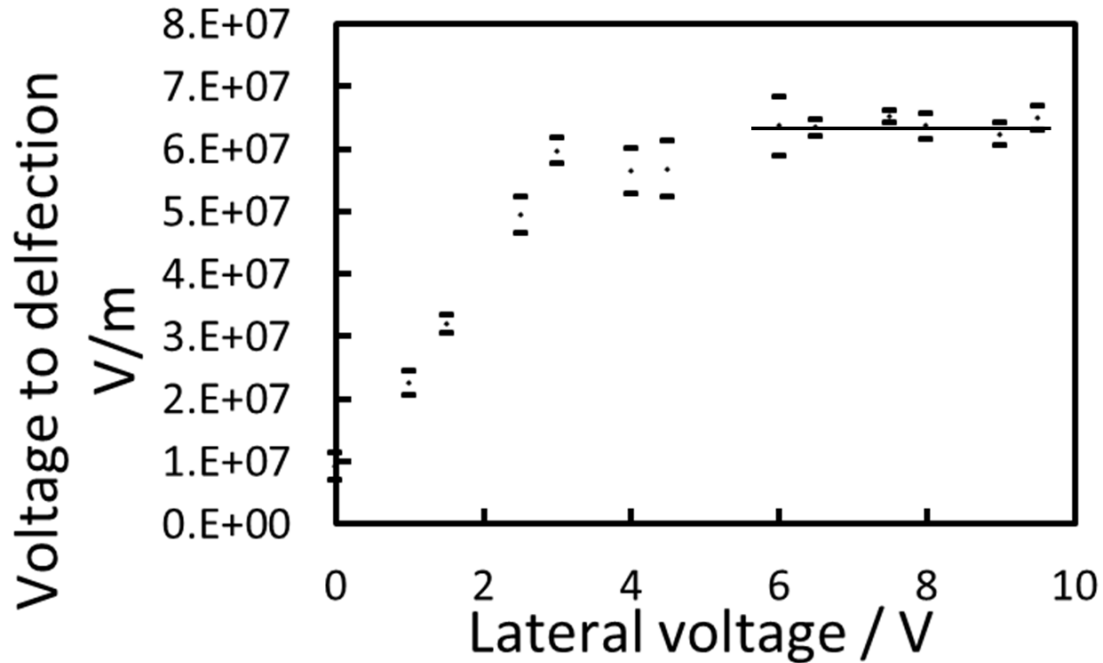


Figure 2.3 Voltage to displacement conversion for a lateral cantilever (error bars represent the standard deviation).

2.3.8 Calibrating the photodiode by moving a mirror in place of the AFM cantilever

The photodiode detector can be calibrated for a range of torsional angles using a mirror mounted in place of the cantilever to reflect the laser beam.¹⁵ The mirror was tilted at known angles using the stepper motor and the lateral voltage signal was detected at each angle. Note that the torsional angle of the cantilever varied by up to 0.001 radians to span the entire range of the PSD. This agrees with the assumption that the torsional angle used in these studies is very small. This calibration of the PSD would provide a very precise relationship between the torsional angle and the detector response but requires the installation of an additional device below the AFM head.

2.4 Contact compliance and in-plane deflection

In a paper by Cannara, the authors analyzed different regions of contact compliance in the case of the colloidal sphere and the sample contact.⁷ There are three areas where mechanical deformation can occur: deformation of the sample-sphere contact, deformation of the glue with which the colloidal sphere is attached, and finally the deformation of the cantilever itself. In an ideal measurement, we should only be recording the cantilever deformation which can then be related to surface forces. In colloidal probe AFM, the compliance of the glue joint is approximately three orders of magnitude smaller than the compliance of the cantilever, therefore it can be ignored.¹³ As suggested by Cain et al. for colloidal probes,¹³ the probe-surface contact is noncompliant compared to the cantilever spring, so practically all deflection occurs in the cantilever.

The difference between the torsional bending and the in-plane bending is illustrated in Figure 2.4. The in-plane bending must be taken into account because it has the potential of reducing the frictional force values. It is possible to establish a criteria for an LFM cantilever that would be acceptable to use without significant in-plane deformation during lateral loading. In the paper by Sader and Green³⁰ the authors investigated how much the in-plane deformation of the AFM cantilever would affect the LFM measurements. The authors emphasized that in the case of perpendicular cantilevers the in-plane deformation could have a significant effect and therefore affect the measurement of the frictional force. Certain types of cantilevers would have a negligible in-plane deformation depending on their physical dimensions as shown with FEA. It was shown that the in-plane spring constant approaches the maximum value when the ratio of the cantilever length to its width is low. A criterion was established to determine if a particular

cantilever is acceptable for LFM measurements. This calculation is given below and it expresses the ratio of the lateral to in-plane spring constants to the ratio of the lateral to normal spring constant.

$$\varepsilon \equiv \frac{k_{lat}}{k_{in-plane}} = \frac{2}{3(1+\nu)} \left(\frac{t}{h}\right)^2 \left(\frac{L}{w}\right)^2 = \frac{k_{lat}}{k_{norm}} \left(\frac{t}{w}\right)^2 \ll 1 \quad (2.8)$$

In the case of the cantilevers used in this study, this ratio is indeed much smaller than one and therefore the in-plane bending of these cantilevers can be disregarded. Additionally, Chung et al. suggested that in certain cases the PSD is practically insensitive to the in-plane bending. In equatorial loading of the colloidal sphere the ratio of in-plane deflection to torsional deflection can be % 4-5 whereas in frictional loading it is 1 %.¹¹

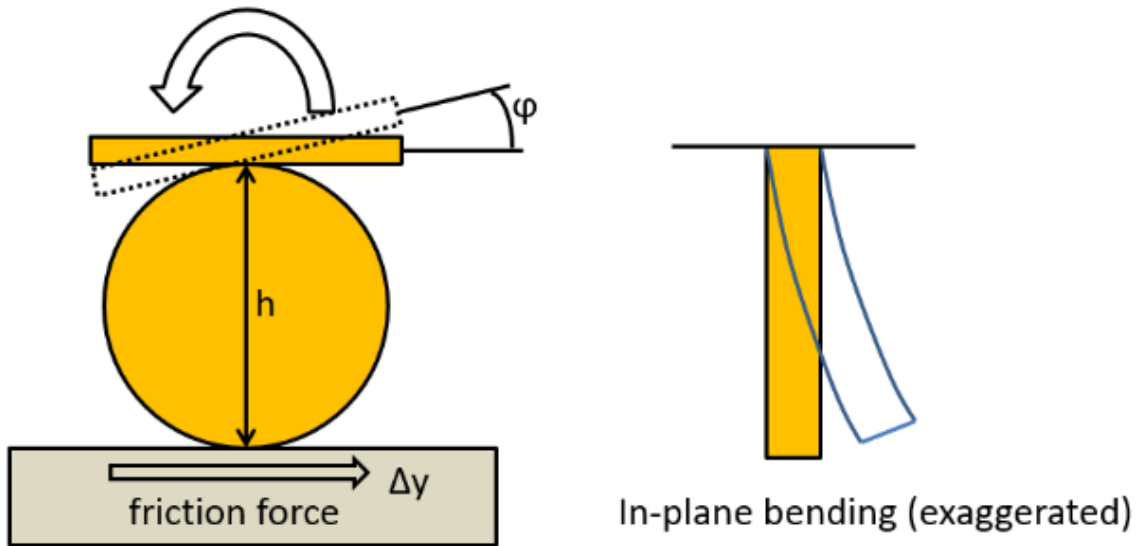


Figure 2.4 Schematic of the torsional (left) and in-plane (right) displacement of the AFM cantilever.

2.5 Hydration lubrication

The extracellular fluid present in articular joints can be mimicked by the PBS buffer medium. PBS salt solutions have a two-fold effect on the frictional forces when compared with the pure water medium. On one hand, the hydrated salt ions provide support for a molecular layer of water that separates the surfaces. On the other hand, the salt ions have an electrostatic effect on the long-range interactions between the substrate and the probe. The electrostatic repulsion is reduced, which leads to reduction in both attractive and repulsive forces. Since the friction in aqueous systems (hydration lubrication) is the object of investigation in the next chapter, it is important to establish the basic principles here. Israelachvili and Pashley studied the hydration forces on mica surfaces in monovalent electrolyte solutions³¹ using the SFA.³² They found a short-ranged repulsive force that was attributed to the presence of hydrated ions adsorbed to the interface. Work performed by Vakarelski et al. also demonstrated that hydrated cations affected frictional properties between surfaces when measured in an electrolyte solution.¹⁷ Their hypothesis was that adsorbed cations, hydrated by the surrounding water, maintained a fluid-filled gap between the surfaces, which acted as a boundary lubricant.¹⁷ Higashitani and coworkers performed a number of studies on how different hydrated ions affect friction between silica surfaces and found that the frictional force differs with the diameter of the hydrated salt ions.^{17,31,33-36} Friction was reduced significantly in aqueous solutions of high salt concentrations.^{17,37}

The next chapter will describe how frictional properties are affected by thin films of oligopeptides. Oligopeptides are interesting because (a) they use the same monomer units as

proteins that are present in the body, and (b) it is possible to create a wide range of sequences with distinct chemistry to test the correlation between chemistry and friction. To create the oligopeptide surface coatings we used a very well-known and established process of solid phase peptide synthesis (SPPS) assisted with a microwave reactor. The synthesis procedure that was originally developed by Bruce Merrifield (and won him a Nobel Prize in 1984) is much more efficient than the traditional solution-based techniques because the solid immobilizes the peptide so that unreacted material can be separated simply by washing. The SPPS employs the so-called orthogonal protection scheme which allows the use of protective groups to prevent unwanted reactions, followed by the selective removal of these protective groups, without damaging the peptide.

2.6 Friction control using polymer films

Adsorbed or chemically grafted polymers can be used to control and reduce interfacial friction. The primary mechanism of friction reduction by polymers is to keep the solids separated, and thus to reduce the magnitude of normal forces between the surfaces. Polymers with a sufficient grafting density stretch away from the surface and form a polymer “brush”. The brush keeps the solids separated. The factors that influence friction in the presence of brushes include polymer brush density, solvent quality, and surface charge. Polymer brushes produce friction by different energy dissipative mechanisms such as: (1) breaking and reforming of intermolecular bonds, (2) sliding of polymer chains against each other and through the solvent, and (3) breaking of polymer–surface attachment points.³⁸ Lubrication is explained by the mobility of the polymer chains due to the layer of solvent between the two polymer brushes. If the polymer chain from two solids interpenetrate, then the chains from one solid must move through the chains of the

other solid, causing the breaking and reforming of many polymer-polymer contacts, and breaking of entanglements resulting in increased sliding friction.³⁹ Therefore, repulsion between the two polymer brushes due to osmotic pressure or entropic effects is important when sliding friction reduction is the goal. If the two surfaces are similarly charged there is a natural electrostatic repulsion which results in reduction in sliding friction. If the two surfaces are oppositely charged, there is an electrostatic attraction that may result in interpenetration of polymer chains and an increase in friction. Neutral polymer brushes can lead to a reduction in sliding friction between surfaces and hydrated ions can act as lubricants.⁴⁰ Increased grafting density reduces the coefficient of friction by creating a uniform surface of stretched chains with decreased surface viscosity.⁴¹ Generally speaking, the coefficient of friction decreases with increasing film thickness and increased polymer grafting density. A high coefficient of friction is associated with the collapsed conformation of polymer chains on the surface, while extended conformations with a high fraction of solvent significantly reduces the frictional force.⁴² A more efficient reduction of the frictional forces is achieved when both surfaces are coated with friction-reducing polymers (symmetrical system) as opposed to coating only one of the surfaces (asymmetrical system).⁴³

References

- (1) Bowden, F. P.; Tabor, D. *Friction and Lubrication of Solids*; Clarendon: Oxford, 1950.
- (2) Yu, J.; Banquy, X.; Greene, G. W.; Lowrey, D. D.; Israelachvili, J. N. *Langmuir* **2011**.
- (3) Klein, J. *Proceedings of the Institution of Mechanical Engineers -- Part J -- Journal of Engineering Tribology (Professional Engineering Publishing)* **2006**, 220, 691.
- (4) Bell, C. J.; Carrick, L. M.; Katta, J.; Jin, Z.; Ingham, E.; Aggeli, A.; Boden, N.; Waigh, T. A.; Fisher, J. *Journal of Biomedical Materials Research Part A* **2006**, 78A, 236.
- (5) Sinnott, S. B. In *Handbook of Nanostructured Materials and Nanotechnology*; Nalwa, H. S., Ed.; Academic: 1999; Vol. 2.
- (6) Dedkov, G. V. *Physics - Uspekhi* **2000**, 43, 541.
- (7) Cannara, R. J.; Eglin, M.; Carpick, R. W. *REVIEW OF SCIENTIFIC INSTRUMENTS* **2006**, 77, 053701.
- (8) Ducker, W. A.; Senden, T. J.; Pashley, R. M. *Nature* **1991**, 353, 239.
- (9) Butt, H.-J.; Cappella, B.; Kappl, M. *Surface Science Reports* **2005**, 59, 1.
- (10) Cain, R. G.; Reitsma, M. G.; Biggs, S.; Page, N. W. *REVIEW OF SCIENTIFIC INSTRUMENTS* **2001**, 72, 3304.
- (11) Chung, K.-H.; Pratt, J. R.; Reitsma, M. G. *Langmuir* **2009**, 26, 1386.
- (12) Ducker, W. A. *Colloids and surfaces. A, Physicochemical and engineering aspects* **1994**, 93, 275.
- (13) Cain, R. G.; Biggs, S.; Page, N. W. *Journal of Colloid and Interface Science* **2000**, 227, 55.
- (14) Green, C. P.; Lioue, H.; Cleveland, J. P.; Proksch, R.; Mulvaney, P.; Sader, J. E. *REVIEW OF SCIENTIFIC INSTRUMENTS* **2004**, 75, 1988.
- (15) Bogdanovic, G.; Meurk, A.; Rutland, M. W. *Colloid Surf. B-Biointerfaces* **2000**, 19, 397.
- (16) Neumeister, J. M.; Ducker, W. A. *REVIEW OF SCIENTIFIC INSTRUMENTS* **1994**, 65, 2527.
- (17) Donose, B. C.; Vakarelski, I. U.; Higashitani, K. *Langmuir* **2005**, 21, 1834.
- (18) Cleveland, J. P.; Manne, S.; Bocek, D.; Hansma, P. K. *REVIEW OF SCIENTIFIC INSTRUMENTS* **1993**, 64, 403.
- (19) Ecke, S.; Raiteri, R.; Bonaccorso, E.; Reiner, C.; Deiseroth, H.-J.; Butt, H.-J. *REVIEW OF SCIENTIFIC INSTRUMENTS* **2001**, 72, 4164.
- (20) Varenberg, M.; Etsion, I.; Halperin, G. *REVIEW OF SCIENTIFIC INSTRUMENTS* **2003**, 74, 3362.
- (21) Feiler, A.; Attard, P.; Larson, I. *REVIEW OF SCIENTIFIC INSTRUMENTS* **2000**, 71, 2746.
- (22) Ogletree, D. F.; Carpick, R. W.; Salmeron, M. *REVIEW OF SCIENTIFIC INSTRUMENTS* **1996**, 67, 3298.
- (23) Palacio, M. L. B.; Bhushan, B. *Critical Reviews in Solid State and Materials Sciences* **2010**, 35, 73
- (24) Liu, E.; Blanpain, B.; Celis, J. P. *Wear* **1996**, 192, 141.
- (25) Green, C. P.; Sader, J. E. *Journal of Applied Physics* **2002**, 92, 6262.
- (26) Liu, Y.; Wu, T.; Evans, D. F. *Langmuir* **1994**, 10, 2241.

- (27) Pettersson, T.; Nordgren, N.; Rutland, M. W.; Feiler, A. *REVIEW OF SCIENTIFIC INSTRUMENTS* **2007**, *78*, 093702.
- (28) Reitsma, M. G. *Review of Scientific Instruments* **2007**, *78*, 106102.
- (29) Ducker, W. A.; Clarke, D. R. *Colloids Surfaces A* **1994**, *93*, 275.
- (30) Sader, J. E.; Green, C. P. *Review of Scientific Instruments* **2004**, *75*, 878.
- (31) Donose, B. C.; Vakarelski, I. U.; Taran, E.; Shinto, H.; Higashitani, K. *Industrial & Engineering Chemistry Research* **2006**, *45*, 7035.
- (32) Pashley, R. M. *Journal of Colloid and Interface Science* **1981**, *80*, 153.
- (33) Taran, E.; Kanda, Y.; Vakarelski, I. U.; Higashitani, K. *Journal of Colloid and Interface Science* **2007**, *307*, 425.
- (34) Taran, E.; Donose, B. C.; Vakarelski, I. U.; Higashitani, K. *Journal of Colloid and Interface Science* **2006**, *297*, 199.
- (35) Vakarelski, I. U.; Higashitani, K. *Journal of Colloid and Interface Science* **2001**, *242*, 110.
- (36) Vakarelski, I. U.; Ishimura, K.; Higashitani, K. *Journal of Colloid and Interface Science* **2000**, *227*, 111.
- (37) Raviv, U.; Klein, J. *Science* **2002**, *297*, 1540.
- (38) Dedinaite, A.; Thormann, E.; Olanya, G.; Claesson, P. M.; Nystrom, B.; Kjoniksen, A.-L.; Zhu, K. *Soft Matter* **2010**, *6*, 2489.
- (39) Schorr, P. A.; Kwan, T. C. B.; Kilbey, S. M.; Shaqfeh, E. S. G.; Tirrell, M. *Macromolecules* **2003**, *36*, 389.
- (40) Raviv, U.; Giasson, S.; Kampf, N.; Gohy, J.; Jerome, R.; Klein, J. *Nature* **2003**, *425*, 163.
- (41) Landherr, L. J. T.; Cohen, C.; Agarwal, P.; Archer, L. A. *Langmuir* **2011**, *27*, 9387.
- (42) Zhang, Z.; Morse, A. J.; Armes, S. P.; Lewis, A. L.; Geoghegan, M.; Leggett, G. J. *Langmuir* **2011**, *27*, 2514.
- (43) Pettersson, T.; Naderi, A.; Makuska, R. a.; Claesson, P. M. *Langmuir* **2008**, *24*, 3336.

Chapter 3

Effects of grafted oligopeptides on friction measured with lateral force microscopy

Abstract

Frictional and normal forces were measured between a glass particle and grafted polypeptide films in aqueous solution at 25°C. Homopolypeptide molecules consisting of 11 monomers of either glutamine, leucine, glutamic acid, lysine, or phenylalanine and one heteropolymer were each “grafted from” an oxidized silicon wafer using microwave-assisted solid phase peptide synthesis. The peptide films were characterized using x-ray photoelectron spectroscopy and secondary ion mass spectrometry. Friction force measurements showed that the polypeptides increased the magnitude of friction compared to a bare hydrophilic silicon wafer, but that the friction was a strong function of the nature of the monomer unit. The most hydrophobic monomer, leucine, exhibited the highest friction while the hydrophilic monomer, poly-glutamic acid exhibited the lowest friction. When the two surfaces had opposite charges, there was a strong attraction, adhesion, and high friction between the surfaces. Friction for all polymers was lower in phosphate buffered saline than in pure water, which was attributed to lubrication via hydrated salt ions.

3.1 Introduction

Understanding, predicting and controlling of friction is important in both natural and engineered systems. Friction and associated wear are usually modulated using a lubricant, which can either be a liquid, or a thin interfacial film. Here our particular interest is control of friction in biological systems (such as artificial joints¹ and engineered tissue)² that are immersed in aqueous solution and require a degree of biocompatibility. Control of friction is achieved through control of surface chemistry³ that in turn mediates the role of water in the film between surfaces. Our goal is to increase the understanding and control of friction by using well-characterized oligopeptide films with distinct variation in hydrophobicity and charge. Although the monomers are “natural”, we utilize artificial peptides, mainly homopolymers so that the friction properties can be ascribed to a single chemical species.

Low friction arises from repulsive forces between surfaces and the mobility of molecules in thin films. In aqueous systems lubrication is produced by hydrated ion shells trapped between charged surfaces⁴⁻⁷ or confined in charged polymer brushes.⁸ Low friction systems also occur when there is high fluidity of the film between the two contacting surfaces.⁹ Recent reports in the literature describe efforts to reduce friction through the use of surfactants¹⁰⁻¹⁶ or polymers at interfaces.^{3,10,17-30} Surfactant bilayers exhibit good lubricating properties when their bilayers are intact.^{6,31} However, surfactant molecules can be “squeezed out” at the interface which increases friction.^{3,8} On the other hand, polymers, with their multiple attachment points, are more difficult to desorb, and therefore are more robust as surface lubricants.³ The overall rationale for addition of polymers to reduce friction is to produce repulsion between the sliding surfaces. This repulsion can be entropic, due to confinement of the polymer chains,²⁸ due to electrostatic

interactions,^{18,32} or due to the energy required to remove the water of hydration of hydrophilic groups.²⁹ The osmotic pressure between the mobile ions surrounding zwitterionic chains also provides a very strong repulsive force.³⁰ On the other hand, bridging between polymer chains on either surface,³³ and interpenetration of polymer chains increases friction.⁹ Therefore, denser polymeric layers can support more efficient lubrication because of reduced interpenetration of the brushes.⁸ Low frictional forces are generally associated with interfacial layers with high fluidity and attractive forces between interfacial layers result in a higher frictional response.³ For example in one study it was shown that repulsion between adsorbed layered polyelectrolytes resulted in low friction, but entanglements between polymer chains increased the friction by an order of magnitude.¹⁸ It also has been shown that the coefficient of friction decreases with the thickness of the brush layer¹⁹ which changes depending on the interaction between the polymer brush and the solvent.^{19,34} Polymer brushes in good solvents adopt an extended conformation¹⁹ which leads to low friction, whereas poor solvent conditions result in attraction between the two interfaces and a higher frictional force.^{3,17,19}

Polymers attached to surfaces can be classified into two categories, “grafted to” and “grafted from”. The “grafted to” polymers are first synthesized and later grafted or physisorbed to the surface with subsequent losses in yield. Additionally, the polymer design is constrained by the necessity of incorporating a chemical group or a monomer sequence that can spontaneously adsorb and stay adsorbed to the surface under lateral and normal loads. For example, the monomers that are supposed to provide low friction may also bind to the solid so that the polymer does not have the desired conformation. Here we explore friction of “grafted from” polymer films, where the polymer is grown directly from a covalent linkage to the solid so that

there is separation in the design of final polymer structure and initial attachment to the solid.^{35,36} Another significant advantage of the “grafting from” technique is that the density of the adsorbed polymer can be programmed from the density of grafting sites rather than being dependent on the thermodynamics and kinetics of adsorption from solution. The major disadvantage of the “grafting from” strategy lies in the inability to separate unwanted polymer products, i.e. for the peptide synthesis used here, incomplete sequences or the sequences that are missing one or more amino acids. In this study we focused our attention on modifying friction by grafting polymer molecules (oligopeptides) from the interface. The use of peptides rather than synthetic polymers has the following advantages: (1) The ability to precisely control the sequence through solid-phase synthesis; (2) The diverse range of monomer chemistry (hydrophilic, hydrophobic, hydrogen bonding and charged), see Table 3.1; (3) The huge number of different polymers that can be made ($20^{11} \approx 2 \times 10^{14}$ combinations for an 11-mer); (4) The ability to prepare naturally occurring sequences with known function. We have focused on 11-mers to keep a low rate of errors in the sequence. There is a constant error of less than about 1.2% for each monomer,³⁷ so by keeping a short sequence we obtain a high degree of monodispersity in the grafted polymer (see results).

The side chains for the homopolymers are shown in Table 3.1, and the grafted polymer structure is shown in Figure 3.1. We have chosen two hydrophobic peptides, one cationic, one anionic and one hydrophilic but neutral. In addition, we have examined a short heteropeptide sequence, P₁₁₋₉ (Figure 3.1) which was previously proposed as a replacement for hyaluronic acid to restore stability to the joints, relieve pain, and delay surgery and was shown to reduce friction when added to solution.³⁸ It is interesting to determine whether friction is reduced when the P₁₁₋₉ is “grafted

from” the surface, rather than free in solution. We have also examined the effect of buffer, phosphate buffered saline (PBS), which approximates physiological conditions. Friction forces were measured using Lateral Force Microscopy (LFM) with a colloidal probe.³⁹ Colloid probe LFM was found to be superior to using standard silicon or silicon nitride cantilever tips because of a much larger and more well-defined contact area of the spherical probe.⁴⁰

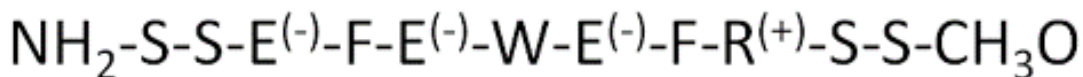
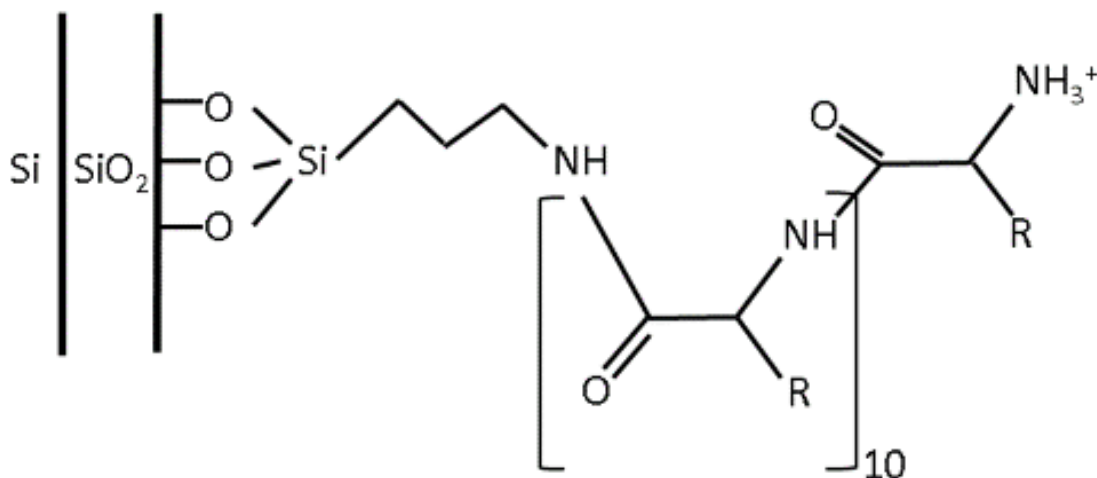


Figure 3.1 Schematic of grafted peptide (top) and sequence of the P₁₁₋₉ peptide (bottom).

3.2 Materials and methods

3.2.1 Reagents

The following chemicals were purchased from Sigma-Aldrich: (3-aminopropyl) triethoxysilane (APTES), piperidine, N,N-diisopropylethyleneamine 99%, and trifluoroacetic acid (TFA). Other chemicals used were: toluene (Fisher Chemical), sulfuric acid 18M (Fisher Chemical), hydrogen peroxide 30% in water (LabChem Inc.), N-Methyl-2-pyrrolidone or NMP (Fisher Bioreagents), methanol (Fisher Chemicals), ethanol 200 proof (Decon Laboratories, USP grade), triethylsilane (TES) 97% (Aldrich), phosphate buffered saline or PBS with pH=7.4 (Sigma). The PBS solution consisted of 0.137 mmol/L of NaCl, 2.7 mmol/L of KCl, 10 mmol/L of Na₂HPO₄•H₂O, and 2.0 mmol/L of KH₂PO₄. The Fmoc-protected amino acids, O-Benzotriazole-N,N,N',N'-tetramethyluronium-hexafluoro-phosphate (HBTU) and the Rink Amide Linker were purchased from Anaspec Inc.

3.2.2 Silicon wafer preparation

Polished silicon wafers with a 3.5 μm oxide layer (“silica wafers”) were purchased from University Wafers. Before synthesizing the peptide on the surface, the silica wafers were treated with the highly corrosive “piranha solution” (3 parts of 18 M sulfuric acid to 1 part of 30% hydrogen peroxide in water) for 40 minutes, then washed in copious amounts of water, rinsed with ethanol and dried with ultrahigh purity (UHP) nitrogen gas. In order to add the amine functionality to the surface for reaction with peptides, the wafers were placed in a 1% w/v solution of 3-aminopropyltriethoxysilane (APTES) in dry toluene at 60° for 4 minutes, washed in

toluene, methanol, then ethanol, and dried under a stream of UHP nitrogen gas. The silica wafers were then treated with a snow-cleaner (dry ice sprayer) to remove polymerized silane.

3.2.3 Peptide synthesis

Peptides films were synthesized using the well-established procedure of solid phase peptide synthesis,⁴¹ in which the peptide is built from an amine-functionalized surface one amino acid at a time by a series of “coupling steps” (adding an H-protected amino acid) and “deprotecting steps” (where the amine of the added amino acid is regenerated so that it can react with the next amino acid). APTES-silica wafers were placed inside a microwave reactor (Discover SPS, CEM, Inc.) and washed with NMP. Coupling solution (an Fmoc-protected amino acid dissolved in 19:1 NMP and DIEA with the HBTU activator) was added to the reactor at 25 W at 75°C. All of the coupling steps were performed for 5 minutes except for the first amino acid, which was in the reactor for 10 minutes to ensure a complete coupling. After the coupling of each amino acid, the wafer was washed three times in NMP and the Fmoc groups were removed with the deprotection solution (20% v/v piperidine in NMP) for 3 minutes in the microwave reactor at 45 W at 75°C. The coupling and deprotection steps were then repeated to attach the entire amino acid sequence. After the last amino acid in the sequence was added and deprotected the surfaces were washed in NMP three times, then in ethanol, and dried under a stream of nitrogen gas. Finally, the side chain protective groups were removed by placing the surfaces into a solution of TFA with deionized water and triethyl silane (95:2.5:2.5) for two hours. Afterwards the surfaces were washed with methanol, ethanol, and dried in a stream of nitrogen.

3.2.4 Colloidal probe preparation

Glass spheres (10 μm in diameter, Duke Scientific Corp.) were mounted onto the cantilevers with thermal epoxy on a heating stage using two translational stages, and a video camera with a 50 x objective lens. The location of the mounted sphere was verified with an optical microscope. Colloid probes were cleaned prior to each experiment using a UV lamp.

3.2.5 Calibration of the photodiode and the lateral spring constant

In order to calibrate the AFM to perform frictional measurements, we obtained two pieces of information: (1) the spring constant of the cantilever and (2) the conversion of the photo-diode response from arbitrary units of volts into physical units of cantilever deflection in both normal and lateral modes. We measured both the torsional and normal spring constants of the AFM cantilevers using the method developed by Sader et al,⁴² which is based on measurements of the thermal vibrations of the cantilever in air. This method was selected because it was simple to implement in our system, did not rely on the cantilever thickness (which is difficult to determine accurately), and the measured spring constant has been found to be similar to other methods.⁴³

The torsional spring constant, k_ϕ (units of Nm), was calculated as follows:

$$k_\phi = 0.1592\rho b^4 L Q_t \omega_t^2 \Gamma_i^t(\omega_t) \quad (3.1)$$

where b and L are the cantilever width and length, Q_t and ω_t are the resonant torsional quality factor and the torsional resonant frequency for the cantilever (determined experimentally), and Γ_i^t is the imaginary component of the hydrodynamic function. The hydrodynamic function does not have an analytical solution for a rectangular cantilever undergoing a torsional oscillation, but if the

cantilever thickness is smaller than its width, the hydrodynamic function can be evaluated numerically.⁴⁴ The normal spring constant was calculated using a similar approach.

The torsional spring constant with units of N-m was then converted into the lateral spring constant (units of N/m) using:⁴⁵

$$k_l = \frac{k_\phi}{h^2} \quad (3.2)$$

where h is the moment arm which in this case is equal to the colloidal sphere diameter.

The calibration of the photo-diode voltage was performed by assuming that the linearly increasing part at the start of the friction loop represents the region where the tip is fixed on the sample (static friction). In this region the diode lateral voltage corresponds to lateral deflection of the cantilever, so the voltage can be converted to a distance.⁵ This distance is then multiplied by the lateral spring constant to obtain the lateral force. For each friction loop, the dynamic friction was calculated as half of the difference between the friction forces in each direction. We validated this method by comparing our results for friction of a bare glass particle on a silicon wafer to those of earlier researchers.^{46,47} Typical measured spring constants were $k_n = 0.60$ N/m, and $k_\phi = 5.0 \times 10^{-9}$ N m, $k_l = 50$ N/m.

3.2.6 Friction measurements

The lateral (frictional) forces were measured using an Asylum Research Cypher AFM with the wafers in aqueous solution at $23 \pm 2^\circ\text{C}$. The frictional forces were measured as a function of normal load ranging from 0 to 250 nN. The upper range was limited by the normal spring

constant of the AFM cantilever. Because the friction force increases with applied load and there is a roughly fixed absolute error in measuring the torsional deflection, experiments at low load have a higher relative error. The lateral signal was measured between ten and thirty times at each normal load. The frictional forces were measured with increasing normal load and then with decreasing normal load on the same sample position. This was done to verify that the colloidal probe did not damage the film. The experiment with each oligopeptide was repeated several times on different locations of the same sample silicon wafer and also repeated on different wafers on different days. The friction versus normal load results were averaged for repeat experiments on the same oligopeptide. The normal force measurements were repeated at least ten times on each sample location to verify that the results were reproducible. The friction did not change over the period of about one hour that it took record a set of measurements. The rms roughness of peptide surfaces was less than 1 nm over a $(20 \mu\text{m})^2$ scan area so the surfaces were very smooth.

3.2.7 X-ray photoelectron spectroscopy (XPS)

The XPS measurements were performed on a Phi Quanterra machine with a monochromated Al $K\alpha$ source at 50W over 200 μm at a 45° angle. The overall scan was acquired at 280 eV pass energy in 15 sweeps at 1 eV step size and individual element scans were acquired at 26 eV with 10 to 40 sweeps depending on the element at 0.1 eV step size.

3.2.8 Secondary ion mass spectrometry (SIMS)

The molecular weight of the synthesized peptide sequence was verified using the 4800 Matrix Assisted Laser Desorption Ionization Time of Flight (MALDI TOF) analyzer. The matrix used was the 4 mg/mL α -cyano-4-hydroxy-cinnamic acid (99%) in 50% acetonitrile, 0.1% TFA and 20mM ammonium citrate. Data was collected in reflecto-positive ion mode and the instrument was calibrated to 1 kV using standards. The peptide sequence was synthesized on 1 mm glass beads using the amide Rink linker, which was cleaved in TFA prior to the measurement. The sample was centrifuged under vacuum to remove the excess TFA and the resultant solution was deposited onto the SIMS grid for analysis.

3.3 Results and discussion

3.3.1 Characterization of the peptide

The validity of the peptide synthesis method was tested by measuring the atomic mass of a sample peptide. A sample peptide of 21 amino acids with sequence GIGKFLKKAKKFGKAFVKIKK was synthesized and the mass measured by Secondary Ion Mass Spectrometry (SIMS). The synthesis was altered to introduce a trifluoroacetic acid (TFA)-cleavable Rink linker between the solid and the peptide so that the peptide could be removed and then analyzed by SIMS, and the solid support was glass beads rather than a silica wafer. The SIMS analysis was consistent with the target sequence because the dominant peak in the mass spectrum (2363.5 g/mol) is the expected mass (2363.5 g/mol) for the sequence. The area of the 2363.5 g/mol peak is 58% of the total area. Note that the laser desorption often cleaves the molecules so the low mass features in the spectrum may be decomposition products, rather than undesired products in the actual film. Thus the final yield of desired chains is likely much greater than 58%.

We also examined the film using X-ray Photoelectron Spectroscopy (XPS) to verify that there were indeed peptide bonds in the “peptide film”. The broad range spectrum showed that the peptide synthesis reduced the area of the silicon and oxygen peaks, commensurate with a layer over the oxidized silicon wafer, and that there was a nitrogen peak after reaction with APTES. The nitrogen and carbon peaks grew after synthesis of the peptide. All these features are consistent with grafting of a peptide. More detail is visible in the high resolution carbon and nitrogen scans (Figure 3.2).³⁶ The C1s carbon spectrum shows a shoulder just under 288 eV

which is consistent with the formation of an amide bond. The N1s spectrum after grafting the peptide shows a new and pronounced peak at 399.5 eV, which is consistent with a nitrogen atom in an amide (peptide bond), and the two amine peaks are diminished relative to the APTES-wafer signal,³⁶ as expected when a surface amine reacts with a carboxylic acid to form a peptide.

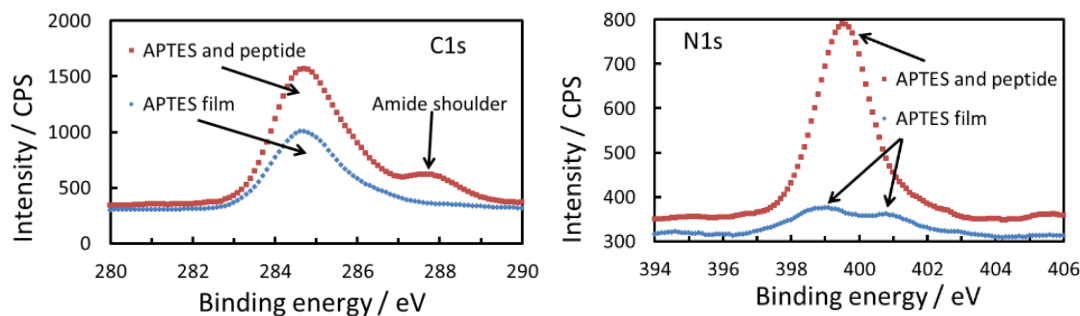


Figure 3.2 X-ray photoelectron spectroscopy analysis of the APTES and APTES-peptide surfaces. The intensity of the carbon peak (C1s) increased dramatically after the peptide was synthesized and the characteristic amide shoulder appeared at 288 eV. The nitrogen peak (N1s) on the APTES film displays the characteristic double peak of an amine, whereas the peptide film shows a single and large peak typical of amides.

3.3.2 Normal and frictional forces on the bare silicon wafer

Normal and friction forces between a clean silica particle and clean silica wafers were measured using AFM to verify that forces were consistent with previous results.^{47,48} The normal forces between a glass particle and a clean (piranha-treated) wafer and the silica probe were monotonically repulsive as expected because silica and glass are negatively charged at neutral pH, which produces a repulsive double-layer force. The range of the repulsive force was reduced in phosphate buffered saline (PBS) solution, again as expected because the ionic

strength is 154 mM, which corresponds to a Debye-length of ~ 0.7 nm. The friction results that were obtained on a clean silica surface were consistent with existing reports in the literature:⁴⁸ the friction force increases linearly with load, with a friction co-efficient of 0.25 in water and 0.37 in PBS. Table 3.2 summarizes the friction coefficients, μ , of all tested films.

3.3.3 Normal and lateral forces acting on polylysine films

For the polylysine grafted silica wafers there is a strong attraction between the wafer and the glass sphere, as shown in Figure 3.3A. This is evident from the missing data caused by mechanical instability at separations smaller than 20 nm in water and smaller than 30 nm in PBS. The mechanical instability occurs when the gradient of the attractive force exceeds the cantilever spring constant. After the sphere contacts the plate, a net pull-off force is required to separate the sphere from the plate. These attractive forces occur because the glass particle is negatively charged and thus opposite in charge to the lysine film: in contact, the opposite charges attract and at a distance there are attractive double-layer forces.

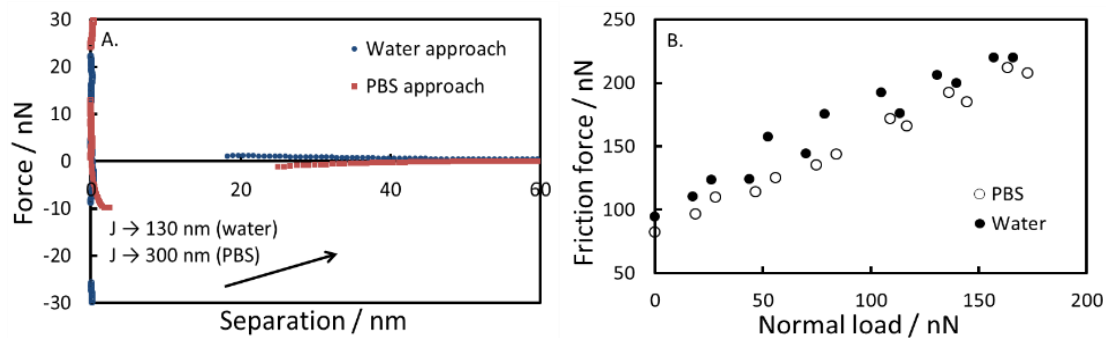


Figure 3.3 A. Normal forces and B. frictional forces between a glass probe and the polylysine-grafted silica wafer. PBS caused a slight reduction in friction. A net force (85 nN in water and 170 nN in PBS) is required to separate the surfaces. The standard deviation for each point on the friction plot was 12 nN in water and 15 nN in PBS.

Examining now the friction as a function of load (Figure 3.3B) it is clear that there is a large value of friction at zero *applied* load. This is because the attractive forces between oppositely charged surfaces applies an “internal” load, even in the absence of an applied load. The adhesion force, F_a , and the friction at zero load, β , are summarized in Table 3.2. It is not clear why the addition of PBS increases the adhesion: our expectation is that binding of ions to each charged solid would have diminished the attraction of the charged groups between solids. But PBS reduces the friction, in line with the expectation that hydrated ions will act as a lubricant.⁴⁻⁷ The friction force for the peptide films (including the polylysine film) is a linear function of load, and therefore follows the modified version of the Amonton’s law proposed by Derjaguin:^{49,50}

$$F_f = \mu N + \beta \quad (3.3)$$

where F_f is the friction force, μ is the coefficient of friction, N is the applied normal load, and β is the extrapolated friction force at zero normal load.

3.3.4 Normal and lateral forces acting on poly(glutamic acid) films

Normal force versus distance profiles on the poly(glutamic acid) wafer were similar to those acting on the clean silicon wafer, which is not surprising since glutamic acid is also negatively charged. The addition of PBS produces a similar effect of reducing the range of the repulsion on the poly(glutamic acid) films (Figure 3.4A). PBS also reduces the friction. This is interesting, because repulsive forces usually cause a reduction in friction, yet the opposite occurs here. The explanation is found in comparing figures 3.4A&B where we see that the reduction in friction can only be resolved at loads exceeding ~ 50 nN, which is in the range where the normal force in water and PBS are indistinguishable in our measurement and the separation is very small. At this load, the double-layer force is not important; PBS acts to reduce friction by providing more ions to hold the water in the thin layer. The many charges on the polyglutamic acid may also aid in holding the non-covalently-bound ions and their hydration near the solid, thereby lowering friction. At the load loads (< 50 nN) where the normal force is greater in water, the friction is so low that we cannot resolve a difference in friction in water and PBS solution.

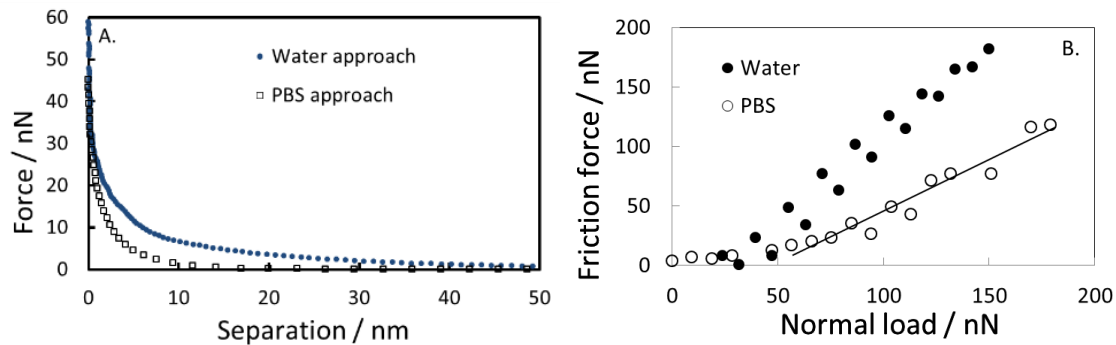


Figure 3.4 A. Normal forces and B. typical frictional forces between a glass probe and the poly(glutamic acid)-grafted silica wafer. The standard deviation for each point on the friction plot was 12 nN in water and 15 nN in PBS. The parameters shown in Table 3.2 were obtained from the fits line shown here, which includes only data at normal loads greater than 50 nN.

3.3.5 Normal and lateral forces acting on the hydrophobic films: polyleucine and polyphenylalanine

The normal forces acting on the polyleucine film displayed a short range attraction on approach and a strong adhesion (Figure 3.5A). Long range attractive normal forces between hydrophilic and hydrophobic asymmetrical systems have been documented in the literature,^{51,52} but their origin is unclear. It is likely that this small attractive force with a range of about 15 nm is electrostatic, and arises from attraction between the negatively-charged glass particle and the positive charges on both the terminal ammonium on the peptide or unreacted amine groups on APTES. Adhesion decreases with increasing salt concentration (PBS). The addition of PBS should both screen electrostatics and make the surfaces more hydrophilic by ion adsorption, both of which will decrease adhesion.

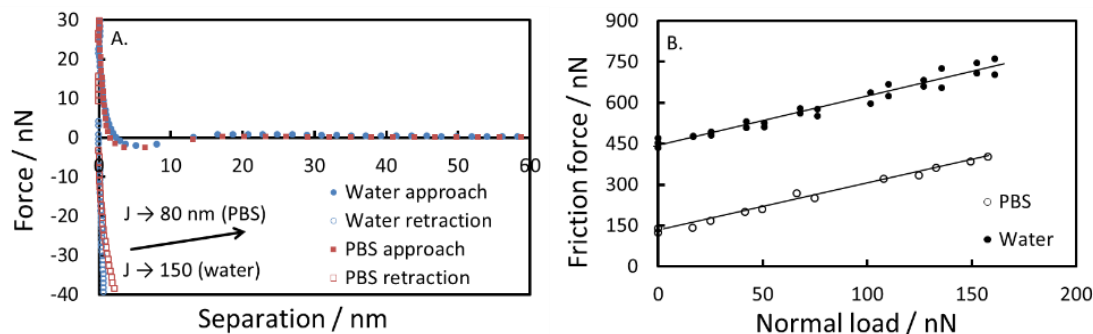


Figure 3.5 A. Normal forces and B. frictional forces between a glass probe and the polyileucine grafted silica wafer. There is a strong adhesive force between the two interfaces evident on colloidal probe retraction. The standard deviation for each point on the friction plot was 20 nN.

The most striking feature of the friction plots is the exceptionally high friction on the polyileucine film (Figure 3.5B): there is both high friction at zero applied load and a high friction coefficient. We consider two possible explanations for the high zero-load friction. First there is the large adhesion for the polyileucine film. As discussed originally by Derjaguin (see equation Equation 10 in the review by Gao et al),⁴⁹ the intermolecular forces apply a load, which also produces the effect of adhesion. This internal load acts similarly to an applied load, and causes friction. This correlation is also evident for polylysine, which shows both a high adhesion and high zero load friction. However, the effect of PBS is telling. PBS causes a dramatic decrease in the friction for polyileucine (by 70%) with a more modest drop in adhesion (by 30%). Clearly the internal loading (as evidenced by the adhesion) is not the primary issue. We postulate that the explanation is that the hydrophobicity of the polyileucine excludes the lubricating effect of hydrated water. The addition of PBS brings the water back to the thin film, reducing the friction. In contrast, the polylysine is intrinsically hydrophilic so the addition of PBS causes only a modest decrease in friction even with large changes in adhesion.

Normal forces on the polyphenylalanine film were similar to those on polyleucine (Figure 3.6A): a weak attraction with a range of about 15 nm, and an adhesion which is not as strong as for polyleucine. However, the friction forces (Figure 3.6B) for the aromatic polyphenylalanine are much weaker than for polyleucine. In fact, the friction forces are similar to other, more hydrophilic polymers such as glutamine. Phenylalanine is a less hydrophobic amino acid than leucine according to previous studies,^{53,54} which may explain the reduction in adhesion. The dramatic difference in friction between the two surfaces is much greater than the difference in adhesion. We propose that the difference is again caused by ion hydration. Cations have a much greater interaction with aromatic groups than aliphatic groups,⁵⁵ thus friction in the aromatic film is lubricated by the presence of a greater density of hydrated ions.

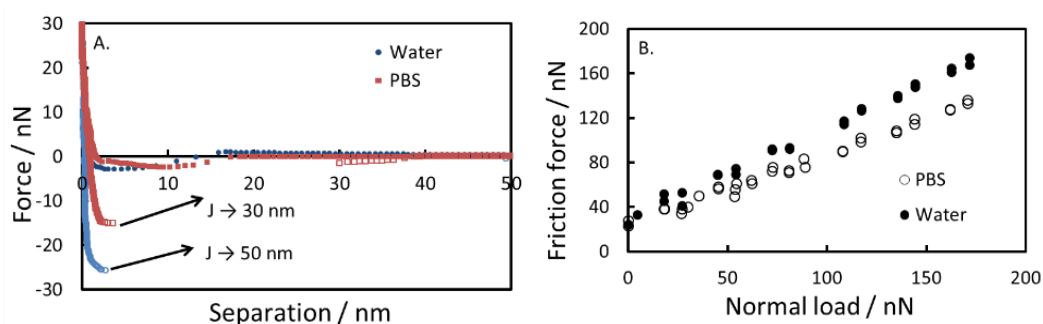


Figure 3.6 A. Normal forces and B. frictional forces between a glass probe and the polyphenylalanine-grafted silica wafer. There is a strong adhesive force between the two interfaces during the retraction. The standard deviation for each point on the friction plot was 14 nN in water and 7 nN in PBS.

3.3.6 Normal and lateral forces acting on polyglutamine films

The normal and frictional responses of the polyglutamine film (Figure 3.7), which has an uncharged and hydrophilic monomer, are different from the polyglutamic acid films. First there is adhesion between the surface and the probe that is greatly reduced in PBS (Figure 3.7A). The small adhesion can be explained by the electrostatic force between the terminal amine groups on the peptide molecule, which is screened in salt solution. Polyglutamine was the only oligopeptide chain that did not show a strong reduction in the frictional response when in salt solution compared to water. It has been reported previously that when the polymers grafted from the surface are lacking charged groups, the addition of salt to the solution does not have a strong effect on the friction.^{9,56} We observed a similar effect here, but not for the hydrophobic peptides.

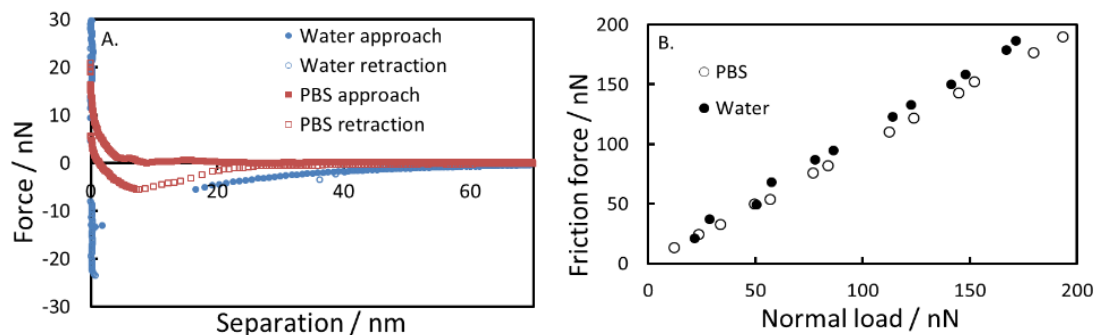


Figure 3.7 A. Normal forces and B. frictional forces between a glass probe and the polyglutamine-grafted silica wafer. The standard deviation for each point on the friction plot was 17 nN for the measurement in water and 5 nN for the measurement in PBS solution.

3.3.7 Effect of P₁₁₋₉

Previously the addition of the heteropeptide, P₁₁₋₉, to solution was found to produce a significant reduction in friction.³⁸ Here we find that the same polymer grafted from the solid produces

unremarkable friction (Figure 3.8B). The mechanism of friction reduction proposed previously was lubrication by self-assembled fibrils. Clearly, we have hindered fibril formation by grafting from the solid so this mechanism is lost. Thus our results are consistent with those observed previously.

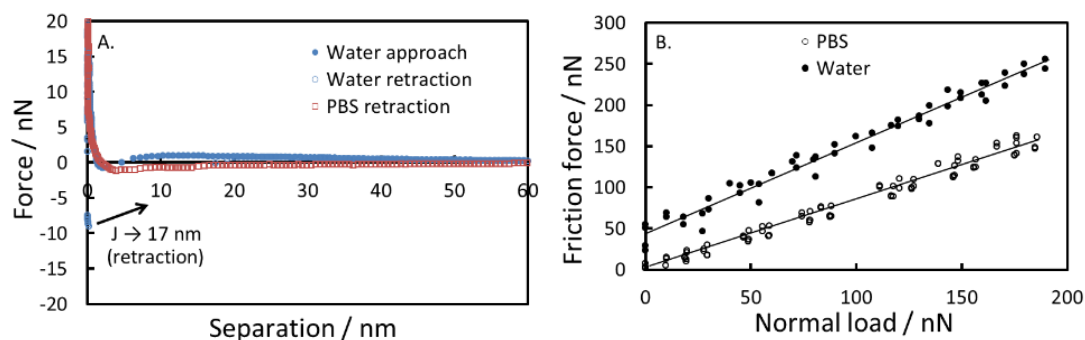


Figure 3.8 A. Normal forces and B. frictional forces between a glass probe and the P₁₁-9-grafted silica wafer. There was some attraction in deionized water between the film and the silica probe that was screened in PBS. The standard deviation for each point on the friction plot was 20 nN.

3.3.7 Effect of peptide length

Since it has been suggested in previous studies that the lubrication depends on the fluidity of the aqueous layer between the two interfaces,⁵⁷ longer peptide chains should result in a reduced friction. We confirmed this in an experiment using two different lengths of the glutamic acid peptide chain. The friction in water decreased by a factor of 1.6 at the higher applied loads when the length of the peptide chain was increased two-fold.

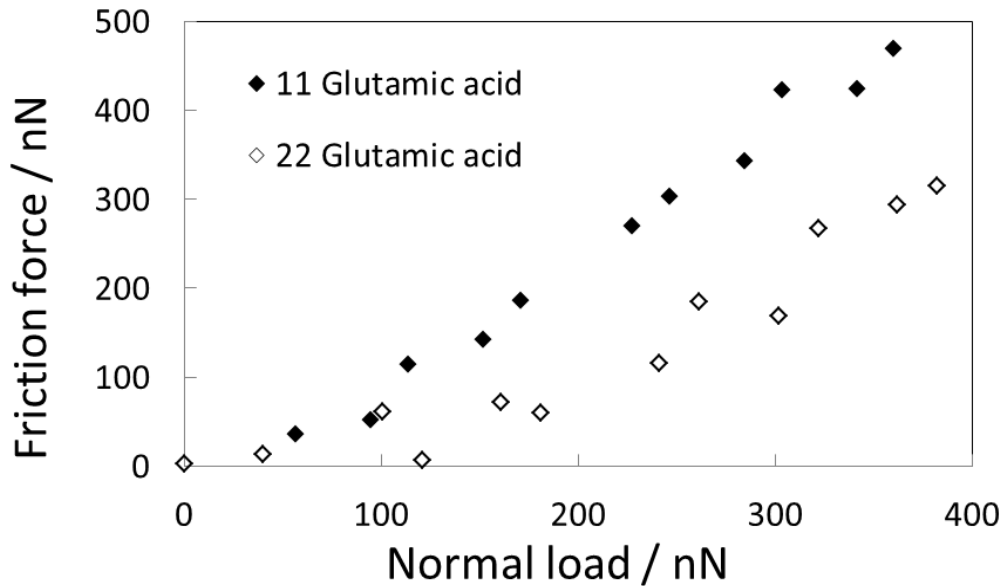


Figure 3.9 Frictional force versus normal load for two poly-glutamic acid films, 11 amino acid long (a) and 22 amino acid long (b) in water. The friction reduced dramatically when the longer peptide chain was used.

3.3.8 Effect of hydrophobicity on friction

In general, friction has been found to correlate with adhesion hysteresis,⁵⁸ which we cannot measure accurately in our experiments. However, considering all the different peptide films measured here, there was a correlation between the measured normal adhesion and the friction at zero applied load (Figure 3.10) which was explicable in terms of the extra load applied by the intermolecular forces. For example poly(glutamic acid) has zero adhesion (a large repulsion at zero separation) and zero friction at zero applied load whereas the films with the largest intermolecular force load (as evidenced by the measured adhesion) had the greatest friction at zero load. The correlation between friction and adhesion does not apply in every case measured

here, and in detail, the friction is mainly determined by the hydrophilicity of the film, which also controls the adhesion. The hydrophilic peptides produced the lower friction. This is similar to the concept, discussed previously, that a better solvent for the polymer produces lower friction.^{27,28} In this case, the polymer chains are short, so the effect of extending the polymers from the surface is not expected to dominate, the main effect is retention of the water of hydration under the applied load. The repulsive normal forces from polyglutamic acid produced the lowest friction, which is partly because the polymer is very hydrophilic, but also because of the repulsive force caused by the electrostatic interaction. The polyglutamic acid film has the interesting behavior that the extrapolated friction at zero applied loads is negative. There is a strong electrostatic repulsion between the two surfaces, and a hydration force is expected. These combine to give a large “internal repulsion” which gives a negative total load at zero applied loads. The applied load has to be increased to about 30 nN to overcome this repulsion before we are able to resolve friction forces. Once this repulsive force is overcome, there is a high friction coefficient, so that polyglutamic acid actually has a higher friction than even polyphenylalanine at high load. This high friction coefficient is lost when hydrated ions are introduced from PBS.

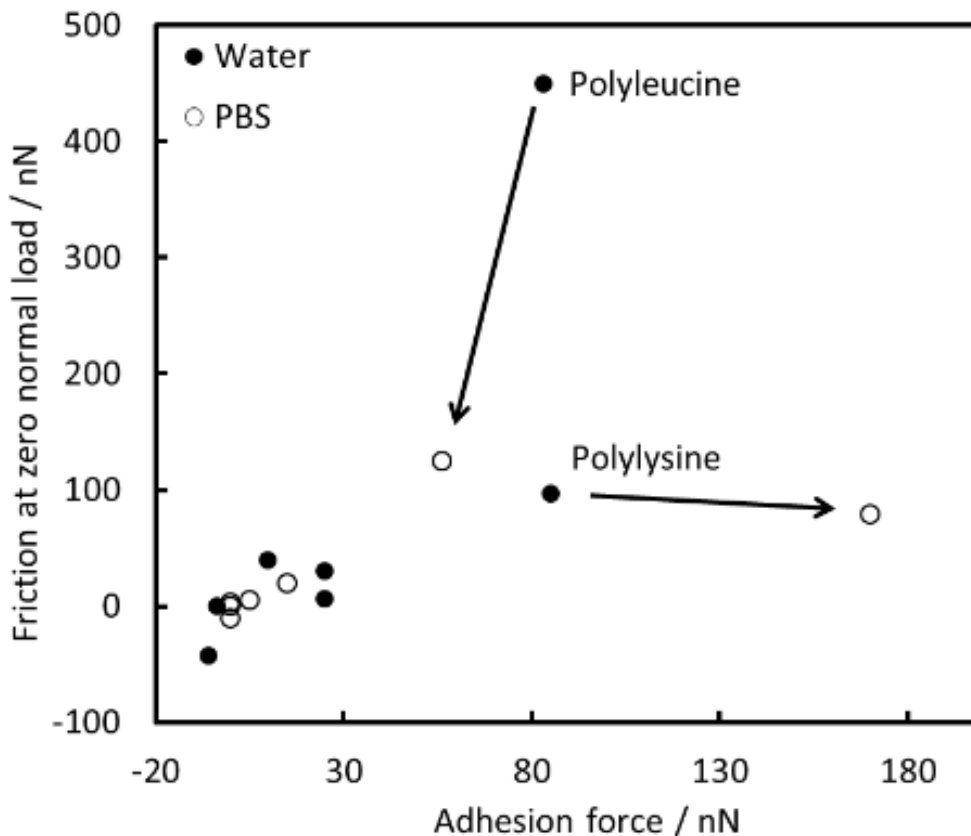


Figure 3.10 Relationship between measured adhesion and friction.

Friction forces on the oligopeptide films in PBS are lower than in water (Table 3.2). Previously, low friction in the presence of hydrated ions was described by Homola,⁷ Raviv,⁴ and Higashitani.^{46,48,59,60} It is postulated that lubrication occurs via a water hydration layer which is held by adsorbed cations. Several studies have shown that an extra normal force is required to bring two surfaces together in order to remove water and the hydrated ions on both mica⁶¹ and silica surfaces.^{39,62-64} The additional repulsive force keeps the surfaces separated at the same applied load, allowing for a layer of mobile lubricating ions or water so friction is reduced in concentrated aqueous salt solutions.^{4,46} Therefore, the PBS salt solution had a two-fold effect on frictional forces when compared to a pure water medium. First, the hydrated salt ions provided

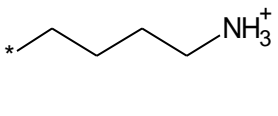
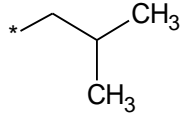
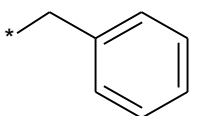
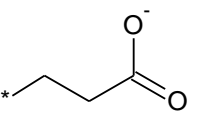
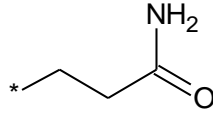
support for a molecular layer of water that separated the surfaces. Second, the salt ions have an electrostatic effect on the long-range interactions between the substrate and the probe. The electrostatic double layer was screened out which led to reduction in both attractive and repulsive forces.

The relative importance of hydrophobicity and change in determining friction can be assessed by considering polyleucine and polylysine in Figure 3.9. As stated previously, the addition of PBS has a dramatic effect on the polyleucine friction at zero load (with only a modest change in adhesion) whereas PBS causes only a small change in friction at zero load for polylysine. The polylysine is already hydrophilic so there is little change in friction, whereas the polyleucine film is made more hydrophilic by the PBS ions so there is a large reduction in friction. In contrast, the dramatic change in adhesion for polylysine has little effect on the friction: the layer is already hydrated so the friction does not change greatly. Despite the overall correlation between zero load friction and adhesion, the hydrophilicity is more important than the adhesion.

3.4 Conclusions

Friction measurements showed a linear relationship between normal load and friction (Amonton behavior) for a sphere interacting with a homo-oligopeptide-coated plate. The friction at zero loads was correlated with the adhesion between the sphere and the plate. Changes in this adhesion and the friction depended on the hydrophobicity and electrostatic forces: hydrophobic films and oppositely charged films produced high friction, whereas hydrophilic and like-charges produced low friction. However, the most important determinant of friction is the hydrophilicity: more hydrophilic films produce lower friction. The frictional forces in PBS were lower than in water, which was attributed to screening of the double layer attraction for oppositely charged surfaces, and additional separation created between surfaces due to the presence of hydrated salt ions. Friction in the presence of the grafted films was greater than for a clean silica wafer: the grafted chains did not act as lubricants. Longer peptides produced lower friction, which suggests that conformational freedom is important for a grafted polymer lubricant.

Table 3.1 Amino acid R-groups used in the synthesis of peptide films with charges at pH 7.

Lysine	Leucine	Phenylalanine	Glutamic acid	Glutamine
				
Hydrophilic (+) charge	Hydrophobic neutral aliphatic	Hydrophobic neutral aromatic	Hydrophilic (-) charge	Hydrophilic neutral

* represents the amino acid backbone,

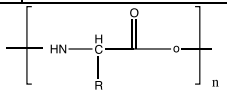


Table 3.2 Friction coefficients and adhesive forces at zero load.

Amino acid	Water				Phosphate buffered saline			
	μ	β nN	F_a nN	N nN	μ	β nN	F_a nN	N nN
Bare wafer (-)	0.25±0.03	0±5	-*		0.36±0.03	-10±5	0	29
P11-9 (-)	1.1±0.04	40±10	10	-52	0.85±0.02	3±10	0	-3.5
Phenylalanine (0)	0.78±0.03	30±10	25	-54	0.68±0.02	20±10	15	-31
Lysine (+)	0.9±0.1	97±10	85	-130	0.73±0.06	79±10	170	-120
Leucine (0)	1.8±0.1	450±20	83	-240	1.7±0.2	125±10	56	-72
Glutamic acid (-)	1.5±0.2	-42±5	-*	28	0.9±0.1	0±5	0	2.5
Glutamine (0)	0.94±0.04	6±5	25	-7	0.89±0.02	5±5	5	-4.2

Errors: The friction coefficients were estimated using linear regression of the friction force versus normal load measurements. The error in the friction coefficients is the 95% confidence interval. The standard deviation on the attractive force measurements (F_a) was under 5%.

Legend: μ - friction coefficient = slope of friction-load plot, β – extrapolated frictional force at zero normal load, F_a - attractive force experienced by the probe in the normal direction on retraction, i.e. adhesion force (negative indicates repulsion), N - extrapolated normal load at zero friction. * No adhesion; negative sign symbolizes repulsive force at small separation.

References

- (1) Moro, T.; Takatori, Y.; Ishihara, K.; Konno, T.; Takigawa, Y.; Matsushita, T.; Chung, U. I.; Nakamura, K.; Kawaguchi, H. *Nat Mater.* **2004**, *3*, 829.
- (2) Klein, J. *Science* **2009**, *323*, 47.
- (3) Dedinaite, A.; Pettersson, T.; Mohanty, B.; Claesson, P. M. *Soft Matter* **2010**, *6*, 1520.
- (4) Raviv, U.; Klein, J. *Science* **2002**, *297*, 1540.
- (5) Ducker, W. A. *Colloids and surfaces. A, Physicochemical and engineering aspects* **1994**, *93*, 275.
- (6) Ducker, W. A.; Luther, E. P.; Clarke, D. R.; Lange, F. E. *Journal of the American Ceramic Society* **1997**, *80*, 575.
- (7) Homola, A. M.; Israelachvili, J. N.; Gee, M. L.; McGuiggan, P. M. *J. Tribol.-Trans. ASME* **1989**, *111*, 675.
- (8) Gaisinskaya, A.; Ma, L.; Silbert, G.; Sorkin, R.; Tairy, O.; Goldberg, R.; Kampf, N.; Klein, J. *Faraday Discussions* **2012**, *156*, 217.
- (9) Dedinaite, A. *Soft Matter* **2012**, *8*, 273.
- (10) Zhang, Q.; Archer, L. A. *Langmuir* **2005**, *21*, 5405.
- (11) Vakarelski, I. U.; Brown, S. C.; Rabinovich, Y. I.; Moudgil, B. M. *Langmuir* **2004**, *20*, 1724.
- (12) Tariq, M.; Serro, A. P.; Colaço, R.; Saramago, B.; Lopes, J. N. C.; Rebelo, L. P. N. *Colloids and Surfaces A: Physicochemical and Engineering Aspects* **2011**, *377*, 361.
- (13) McNamee, C. E.; Yamamoto, S.; Kappl, M.; Butt, H.-J.; Higashitani, K.; Dédinaite, A.; Claesson, P. M. *Journal of Colloid and Interface Science* **2011**, *364*, 351.
- (14) Sulek, M. W.; Zieba, M.; Wasilewski, T.; Sas, W. *SCIENTIFIC PROBLEMS OF MACHINES OPERATION AND MAINTENANCE* **2010**, *3*, 19.
- (15) Liu, X.; Song, J.; Wu, D.; Genzer, J.; Theyson, T.; Rojas, O. J. *Industrial & Engineering Chemistry Research* **2010**, *49*, 8550.
- (16) Dekkiche, F.; Corneci, M. C.; Trunfio-Sfarghiu, A. M.; Munteanu, B.; Berthier, Y.; Kaabar, W.; Rieu, J. P. *Colloids and Surfaces B: Biointerfaces* **2010**, *80*, 232.
- (17) Dedinaite, A.; Thormann, E.; Olanya, G.; Claesson, P. M.; Nystrom, B.; Kjoniksen, A.-L.; Zhu, K. *Soft Matter* **2010**, *6*, 2489.
- (18) Pettersson, T.; Dedinaite, A. *Journal of Colloid and Interface Science* **2008**, *324*, 246.
- (19) Zhang, Z.; Morse, A. J.; Armes, S. P.; Lewis, A. L.; Geoghegan, M.; Leggett, G. J. *Langmuir* **2011**, *27*, 2514.
- (20) Yu, J.; Banquy, X.; Greene, G. W.; Lowrey, D. D.; Israelachvili, J. N. *Langmuir* **2011**, *28*, 14609.
- (21) Pettersson, T.; Naderi, A.; Makuska, R. a.; Claesson, P. M. *Langmuir* **2008**, *24*, 3336.
- (22) Nordgren, N.; Rutland, M. W. *Nano Letters* **2009**, *9*, 2984.
- (23) Nordgren, N.; Eklöf, J.; Zhou, Q.; Brumer, H.; Rutland, M. W. *Biomacromolecules* **2008**, *9*, 942.
- (24) Stiernstedt, J.; Brumer, H.; Zhou, Q.; Teeri, T. T.; Rutland, M. W. *Biomacromolecules* **2006**, *7*, 2147.

- (25) Muller, M. T.; Yan, X.; Lee, S.; Perry, S. S.; Spencer, N. D. *Macromolecules* **2005**, *38*, 5706.
- (26) Feiler, A.; Plunkett, M. A.; Rutland, M. W. *Langmuir* **2003**, *19*, 4173.
- (27) Schorr, P. A.; Kwan, T. C. B.; Kilbey, S. M.; Shaqfeh, E. S. G.; Tirrell, M. *Macromolecules* **2003**, *36*, 389.
- (28) Klein, J.; Kumacheva, E.; Mahalu, D.; Perahia, D.; Fetters, L. J. *Nature* **1994**, *370*, 634.
- (29) Chen, M.; Briscoe, W. H.; Armes, S. P.; Cohen, H.; Klein, J. *European Polymer Journal* **2011**, *47*, 511.
- (30) Raviv, U.; Giasson, S.; Kampf, N.; Gohy, J.; Jerome, R.; Klein, J. *Nature* **2003**, *425*, 163.
- (31) Ducker, W. A.; Clarke, D. R. *Colloids Surfaces A* **1994**, *93*, 275.
- (32) Abraham, T.; Giasson, S.; Gohy, J. F.; Jerome, R. *Langmuir* **2000**, *16*, 4286.
- (33) Dunlop, I. E.; Briscoe, W. H.; Titmuss, S.; Jacobs, R. M. J.; Osborne, V. L.; Edmondson, S.; Huck, W. T. S.; Klein, J. *Journal of Physical Chemistry B* **2009**, *113*, 3947.
- (34) Klein, J.; Kamiyama, Y.; Yoshizawa, H.; Israelachvili, J. N.; Fredrickson, G. H.; Pincus, P.; Fetters, L. J. *Macromolecules* **1993**, *26*, 5552.
- (35) Mosse, W. K. J.; Koppens, M. L.; Gras, S. L.; Ducker, W. A. *Langmuir* **2009**, *26*, 1013.
- (36) Mosse, W. K. J.; Koppens, M. L.; Gengenbach, T. R.; Scanlon, D. B.; Gras, S. L.; Ducker, W. A. *Langmuir* **2009**, *25*, 1488.
- (37) CEM, Ed.; CEM: Matthews, 2009; Vol. Application Note BIO-0008, p 2.
- (38) Bell, C. J.; Carrick, L. M.; Katta, J.; Jin, Z.; Ingham, E.; Aggeli, A.; Boden, N.; Waigh, T. A.; Fisher, J. *Journal of Biomedical Materials Research Part A* **2006**, *78A*, 236.
- (39) Ducker, W. A.; Senden, T. J.; Pashley, R. M. *Langmuir* **1992**, *8*, 1831.
- (40) Chung, K.-H.; Pratt, J. R.; Reitsma, M. G. *Langmuir* **2009**, *26*, 1386.
- (41) Bodanszky, M. *Principles of peptide synthesis*; Second, revised edition ed.; Springer-Verlag: Berlin, 1993.
- (42) Green, C. P.; Lioue, H.; Cleveland, J. P.; Proksch, R.; Mulvaney, P.; Sader, J. E. *REVIEW OF SCIENTIFIC INSTRUMENTS* **2004**, *75*, 1988.
- (43) Pettersson, T.; Nordgren, N.; Rutland, M. W.; Feiler, A. *REVIEW OF SCIENTIFIC INSTRUMENTS* **2007**, *78*, 093702.
- (44) Green, C. P.; Sader, J. E. *Journal of Applied Physics* **2002**, *92*, 6262.
- (45) Cannara, R. J.; Eglin, M.; Carpick, R. W. *REVIEW OF SCIENTIFIC INSTRUMENTS* **2006**, *77*, 053701.
- (46) Donose, B. C.; Vakarelski, I. U.; Higashitani, K. *Langmuir* **2005**, *21*, 1834.
- (47) Plunkett, M. A.; Feiler, A.; Rutland, M. W. *Langmuir* **2003**, *19*, 4180.
- (48) Taran, E.; Donose, B. C.; Vakarelski, I. U.; Higashitani, K. *Journal of Colloid and Interface Science* **2006**, *297*, 199.
- (49) Gao, J.; Luedtke, W. D.; Gourdon, D.; Ruths, M.; Israelachvili, J.; Landman, U. *J. Phys. Chem. B* **2004**, *108*, 3410.
- (50) Derjaguin, B. Z. *Phys.* **1934**, *88*, 661.
- (51) Tsao, Y. H.; Evans, D. F.; Wennerstroem, H. *Langmuir* **1993**, *9*, 779.
- (52) Christenson, H.; Claesson, P. M. *Advances in Colloid and Interface Science* **2001**, *91*, 391.
- (53) Kyte, J.; Doolittle, R. F. *Journal of Molecular Biology* **1982**, *157*, 105.

- (54) Hessa, T.; Kim, H.; Bihlmaier, K.; Lundin, C.; Boekel, J.; Andersson, H.; Nilsson, I.; White, S. H.; von Heijne, G. *Nature* **2005**, *433*, 377.
- (55) Mecozzi, S.; West Jr., A. P.; Dougherty, D. A. *Proc. Natl. Acad. Sci. USA* **1996**, *93*, 10566.
- (56) Nomura, A.; Goto, A.; Ohno, K.; Kayahara, E.; Yamago, S.; Tsujii, Y. *Journal of Polymer Science Part A: Polymer Chemistry* **2011**, *49*, 5284.
- (57) Ohmae, N.; Martin, J. M.; Mori, S. *Micro and nanotribology*; The American Society of Mechanical Engineers: New York, 2005.
- (58) Yoshizawa, H.; Chen, Y. L.; Israelachvili, J. *Journal of Physical Chemistry* **1993**, *97*, 4128.
- (59) Taran, E.; Kanda, Y.; Vakarelski, I. U.; Higashitani, K. *Journal of Colloid and Interface Science* **2007**, *307*, 425.
- (60) Donose, B. C.; Vakarelski, I. U.; Taran, E.; Shinto, H.; Higashitani, K. *Industrial & Engineering Chemistry Research* **2006**, *45*, 7035.
- (61) Pashley, R. M. *Journal of Colloid and Interface Science* **1981**, *80*, 153.
- (62) Adler, J. J.; Rabinovich, Y. I.; Moudgil, B. M. *Journal of Colloid and Interface Science* **2001**, *237*, 249.
- (63) Tadros, T. F.; Lyklema, J. *Journal of Electroanalytical Chemistry and Interfacial Electrochemistry* **1968**, *17*, 267.
- (64) Ducker, W. A.; Senden, T. J.; Pashley, R. M. *Nature* **1991**, *353*, 239.

Chapter 4

Introduction to antimicrobial films and atomic force microscopy

4.1 Introduction

There is a strong motivation to design surfaces that kill harmful microorganisms on contact and prevent transmission of infectious diseases. Examples of applications include catheters, implants, and other medical devices, ventilation and air ducts, hospital supplies and equipment.^{1,2} Catheter contamination is a serious source of infections that occurs in 10-50% of catheterized patients. For every day of catheterization the risk of infection increases by as much as 10%.³ Catheter-related infections are a significant source of morbidity and mortality and increase medical expenses by prolonging hospitalization.⁴ Consequently, bacterial contamination of catheters and other medical devices that leads to serious infections is a reason behind more than half of all nosocomial infections.⁵ Creating a simple and straightforward way to make catheters resistant to bacteria would reduce both the rates of infections and the use of antibiotics.

Infection is the most prominent reason for biomaterial implant failure in the US.⁶ Therefore, antimicrobial coatings of artificial joints or pacemakers could prevent life-threatening diseases. Other applications for surface coatings include intravenous lines which when colonized by bacteria often become a source of fever. IV line infections are generally not associated with the usual signs of infections and therefore may go undiagnosed. Common pathogens in these

infections are *S. epidermidis* or *S. aureus*.⁷ Tracheal intubation almost always results in an infection which long-term patients are more susceptible to. These infections eventually develop into pneumonia if left untreated.⁸ Therefore, application of antimicrobial films on tracheostomy tubes could reduce the risk. For more information on the anti-microbial coatings, particularly in the hospital environment, one is referred to an excellent review by Parkin et al.⁹

The original goal of this project was to attach antimicrobial oligopeptide molecules to a surface to render it antimicrobial. The naturally occurring antimicrobial peptides have been under an intense investigation for many years.¹⁰ The polyallylamine (PA) coating was originally designed as a tether molecule used as a point of attachment of oligopeptides. We discovered that the PA had very strong antimicrobial properties by itself and so it was used as the antimicrobial coating without further attachment of peptide molecules. A major advantage of cationic polymers and peptides over traditional antibiotics is that their action is thought to be physical, rather than the chemical action of antibiotics. Whereas antibiotic resistance is commonplace, antimicrobial resistance would require bacteria to change the way that they compartmentalize the exterior of phospholipid membranes. Such radical change is much less likely than a small modification to bacterial chemistry required to develop antibiotic resistance. Therefore it has been recognized that unlike traditional antibiotics, the anti-microbial peptides do not produce resistance in bacteria. For example, nisin which is a 34-residue peptide produced by *Lactococcus lacti*, has been used for over 50 years as a food preservative without causing significant bacterial resistance.¹¹ Another example is mersacidin which is a tetracyclic peptide effective against methicillin-resistant *Staphylococcus aureus* (MRSA). Since peptides generally

target fundamental structures, such as bacterial cell membranes, the development of resistance is significantly reduced as confirmed by several studies.¹²

4.2 Bacterial organisms used in this study

The bacterial cell envelope is a multilayer structure that serves a purpose of protecting the organism from the environment. Historically, bacteria were characterized in two categories: Gram-positive and Gram-negative. A Gram-positive bacterial cell is characterized by a thick peptidoglycan layer that typically lacks the outer membrane. The Gram-negative bacterial cells have a more compact cell wall with two phospholipid bilayers. The Gram-negative bacteria cell wall contains a cytoplasmic membrane and an outer membrane. There is a space between the two membranes that contains one or two layers of peptidoglycan. The Gram-positive bacteria lack the outer membrane but instead possess a much thicker (10-20 layers) peptidoglycan constituent.¹³ Importantly, the outer membrane in Gram-negative bacteria is not a phospholipid membrane. It contains phospholipids in the inner but not the outer leaflet. In contrast, the outer leaflet contains glycolipids, in particular lipopolysaccharide. The Gram-negative cell wall can be described as a gel-like matrix that is composed of cross-linked saccharide strands that are oriented perpendicularly to the plasma membrane while the peptide bridges adopt a parallel configuration.¹⁴ The peptidoglycan layer is the stress-bearing structure and is responsible for the cell shape. In both Gram-positive and Gram-negative bacteria the peptidoglycan layer consists of long strands of polysaccharide molecules that are cross-linked by stretchable peptides. The layers of peptidoglycan are threaded with anionic polymers (the so-called teichoic acids).¹⁵ The

bacterial cell shape has been shown to play a critical role in the regulation of various bacterial functions such as attachment and motility.¹⁶

Pseudomonas aeruginosa (*P. aeruginosa*) is a gram-negative opportunistic pathogen that is able to colonize various environments. It can be found in soil, water, or on human skin and thrives in oxygen-deficient environments despite being an aerobic organism under normal growth conditions. *P. aeruginosa* may cause serious diseases and infections, particularly in individuals with compromised immunity. Infections and subsequent colonizations of this bacterium in kidneys, lungs and other vital organs can be fatal.¹⁷ The most common types of infection with this organism include burn injuries, infections of the outer ear, and post-operative infections. *P. aeruginosa* is found on medical surfaces, such as catheters and is a major cause of hospital infections.¹⁸ It is estimated that one in ten hospital-acquired infections in the US are due to *P. aeruginosa*. *P. aeruginosa* is known for its low antibiotic susceptibility which is attributed at least in part to the low permeability of the bacterial cell envelope. Its intrinsic resistance is exacerbated by the acquired resistance through mutation and horizontal gene transfer. *P. aeruginosa* possesses a large genome size, which allows it to adapt to different environments and it secretes virulence factors.^{19,20} These bacteria have the ability to attach to different surfaces due to the presence of adhesion molecules on the bacterial cell wall. In Gram-negative bacteria the fimbriae (proteins) act as adhesins and in Gram-positive bacteria it is the surface proteins or the polysaccharide surface layer.²¹ These cell wall structures allow *P. aeruginosa* to avoid the natural immune response of its host. This organism was chosen because it is known to cause disease, and is particularly likely to colonize medical devices. The inherent antibiotic resistance

of *P. aeruginosa* was attractive since it provided a challenge to the antimicrobial films that we synthesized.

Escherichia coli (*E. coli*) is a Gram-negative, facultative anaerobic, rod-shaped bacterium most commonly found in the lower intestine. Although most *E. coli* strains are harmless, some serotypes may cause food poisoning.²² There exists an environmentally persistent *E. coli* that is able to survive outside of the host for extended periods of time.²³ The cells are between 0.5 and 2.0 μm in size and these bacteria can survive on a variety of substrates. Some strains of *E. coli* possess flagella and are motile.²⁴ Infectious strains of *E. coli* can cause a variety of diseases such as gastroenteritis, urinary tract infections, meningitis and others. *E. coli* was selected for this study because it is the most widely studied prokaryotic model organism that is easy to culture and to work with since the risk of infection is rather low.

Staphylococcus aureus (*S. aureus*) is a bacterium commonly found in the respiratory system and on the skin. It turns out that 20% of humans carry *S. aureus*.²⁵ This bacteria is not always pathogenic but may result in skin infections, respiratory infections, and food poisoning. The illnesses associated with this organism include meningitis, folliculitis, abscesses, bacteremia, osteomyelitis, skin infections, pneumonia, toxic shock syndrome, endocarditis, and sepsis. *S. aureus* is one of the most common causes of hospital-acquired infections and is often the cause of post-surgical infections as well. These infections are especially prevalent in people that have just received a prosthetic joint replacement as they are more vulnerable to heart valve infections, sepsis, and pneumonia. The virulent strains produce toxins and synthesize cell-surface proteins

which disrupt the normal immune response. Moreover, the antibiotic-resistant *S. aureus* strains, such as MRSA, are a serious problem in modern medicine often requiring intense antibiotic treatments and surgery and often resulting in death. MRSA is particularly feared among practitioners of wrestling, Brazilian Jiu Jitsu, Luta Livre and other grappling martial arts as skin infections spread rapidly through skin-to-skin contact and may result in significant training downtime and in worst cases surgery or death. Making matters worse, certain strains of *S. aureus* can survive on dry environmental surfaces up to several months.²⁶ *S. aureus* was chosen for this study as the Gram-positive representative of a dangerous and potentially harmful organism which is known for its resistance to traditional antibiotics and the prevalence of infection in hospital environments.

Staphylococcus epidermidis (*S. epidermidis*) is a Gram-positive bacterium found in the human skin flora. This organism is composed of nonmotile cocci arranged in grape-like structures. The size of individual organisms varies between 0.5 and 1 μm . It is not usually pathogenic but presents a risk of developing an infection for people with compromised immune systems and is therefore prevalent in hospital environments. *S. epidermidis* is of particular concern to people exposed to catheters or other surgical implants as it has the ability to form biofilms on these devices which is a major virulence factor.²⁷ The outside of the organism is made up of sulfated polysaccharide which allows the bacteria to bind to already existing biofilm. The decreased metabolism of the bacteria inside the biofilm combined with the impaired diffusion of antibiotics leads to the reduction of antibiotic effectiveness.²⁷ The biofilms mentioned above have the potential to grow on plastic devices that are placed inside the human body such as intravenous catheters, prostheses, implants and so on.²⁸ This may be a cause for infection and cause diseases

such as endocarditis and in other cases may lead to sepsis. Since antibiotics are often inefficient against biofilms, the only recourse may be to remove or replace the infected device or implant which can lead to more complications and infections. *S. epidermidis* was chosen for this study because it is a known pathogen that has the propensity of colonizing medical devices and surgical implants.

4.3 Proposed mechanism of action of antimicrobial compounds

It was proposed that the antimicrobial immobilized cationic polymers disrupt the integrity of the bacterial membrane, which results in cell death.²⁹ Their action is thought to be physical as opposed to the chemical inhibition caused by traditional antibiotics. Development of resistance to polycationic antimicrobials would thus require a fundamental change to their cell wall and membrane and is therefore considered unlikely. The structures of the bacterial cell wall and the outer membrane are open networks of macromolecules and do not offer a perfect barrier against penetration of foreign molecules.³⁰ The bacterial cell envelope can be thought of as a large two-dimensional polyelectrolyte which carries an overall negative charge which is stabilized by divalent ions such as Mg^{2+} and Ca^{2+} . The negative charge comes from the teichoic or lipoteichoic acid molecules in Gram-positive bacteria and the lipopolysaccharides and phospholipids of Gram-negative bacteria.³⁰ Kugler et al. proposed that bacteria interacted with charged surfaces during the adsorption stage, and the removal of divalent counterions in the cell envelope led to bacterial death.³¹

There were several studies performed using the AFM to evaluate the action of antimicrobials dissolved in solution on bacterial cells. The details of these investigations as well as the major

conclusions are summarized in Table 4.1. It is obvious that there may be differences in how the bacterial cell wall would react to a dissolved chemical compound as opposed to a surface-bound polymer. However, membrane degradation associated with the exposure to antimicrobial compounds would likely occur in both scenarios.

The majority of the antimicrobial experiments with the AFM were performed with Gram-negative organisms and with *E. coli* in particular. *E. coli* is a very well-studied Gram-negative bacterium that is a low health risk and presents a challenge to microbicidal compounds because of the double-membrane structure of its cell wall. The antimicrobial compounds that were used in prior AFM studies were predominantly peptide molecules. Peptide antimicrobials are molecules produced by living organisms that have an antimicrobial effect when dissolved in solution. They are composed of hydrophilic, hydrophobic, and cationic amino acids that allow them to interact with different parts of the bacterial cell.¹⁰ Besides the antimicrobial peptides, other antimicrobial compounds included a nitric oxide surface³² and a study involving more traditional quaternary ammonium compounds.³³ The exact mechanism of action of these compounds is still under investigation.

In order to induce bacterial cell death the antimicrobial compounds must first penetrate the bacterial cell wall and particularly the cell membrane. Naturally, the interaction between the cell membrane and antimicrobial compounds has been the subject of investigation. The AFM allows imaging of the bacterial membranes *in situ*. With sufficient imaging speed, it is even possible to create real-time images of the membrane disruption.³⁴ The overall conclusion from the studies surveyed here was that the membrane degradation was a significant contributing factor to cell

death when bacteria are exposed to toxic materials.³² It was determined that the membrane becomes rough, then fragmented, which eventually leads to cytoplasmic leakage and total cell collapse.³⁵ This process may be accompanied with formation of micelles. It is not always precisely clear whether the bacteria are already “dead” by the time the membrane surface disruption is registered with the AFM. However, there has been one major finding that was confirmed by different research groups, and that is bacterial death happens in distinct stages.

Li et al. studied the effects of Sushi peptides on Gram-negative *E. coli* and *P. aeruginosa* by imaging the bacteria in air using contact-mode AFM.³⁶ They analyzed the bacterial surface morphology and surface roughness and proposed that the antimicrobial peptides killed bacteria in three separate stages. First, the outer membrane of bacteria was damaged, then the inner membrane became permeable to the incoming antimicrobials, and finally both membranes disintegrated.

In a study by de Silva et al. the researchers looked into the effects of an antimicrobial peptide on *E. coli*.³⁷ The bacterial cells were analyzed using tapping mode AFM in air and the elastic modulus of the bacteria as well as their surface roughness were determined. The authors proposed a two-step effect of peptides on bacterial cells. First, the stiffness of the membrane was lost and micelles were formed from the cellular membrane. In the second stage of the process a complete cellular rupture occurred. In this report the authors also noted that peptides displaced magnesium ions present in the lipopolysaccharide (LPS) matrix which resulted in cross-bridging of the negative charges of the LPS lipids and facilitated the cell membrane collapse. The

displacement of cell membrane ions has been proposed previously as the reason for the bacterial cell death.

A similar theory was proposed by Alves et al. where it was found that an antimicrobial peptide induced neutralization of the bacterial surface which resulted in membrane collapse and cell death.³⁸ In a paper by Fantner et al., the *E. coli* cells were imaged using high-speed tapping AFM.³⁴ They determined two distinct stages of bacterial death. In the first (incubation) stage the bacterial surface roughness gradually increased, and the length of time necessary for this process varied. In the second (execution) stage the bacteria rapidly collapsed. These reports point to the conclusion that bacterial death by the action of antimicrobials is a complex process where different distinct stages can be identified and these processes follow different time scales.

4.4 Review of the recent work in antimicrobial films

It would be ideal to design a surface that would kill bacteria through direct contact. Although it is possible to prepare surfaces that kill bacteria by leaching antibacterial species into the environment, these coatings lose their potency over time and could potentially be toxic.³⁹⁻⁴¹ Therefore it is ideal to develop a film that covalently bonds to the surface or is attached using layer-by-layer deposition.²

The following is an overview of the studies performed in the field of antimicrobial coating development in the recent years. In the early 2000s, Klibanov et al. developed a film that killed both Gram-positive and Gram-negative bacteria on contact by amine activation of a polymeric substrate, followed by bromo-alkylation and then derivatization with poly(4-vinylpyridine). The

resultant surfaces were up to 99% effective in killing airborne bacteria.⁴² Klibanov described the use of long-chain hydrophobic cations such as poly(4-vinyl-N-hexylpyridinium) and branched N-hexyl,N-methyl-polyethyleneimine against *S. aureus*.¹ The authors were able to conclude that the antimicrobial polymers had to be hydrophobic in nature and also positively charged in order to be effective against bacterial cells. They also found a minimum molecular weight of the polymer that made it effective against bacteria. In another paper by Klibanov, a layer-by-layer films of N,N-dodecyl,methyl-polyethylenimine (PEI) as the cation and poly(acrylic acid) (PAA) as the anion were shown effective at killing *E. coli* and *S. aureus*.² Under the right combination of application conditions, the films were effective against both Gram-positive and Gram-negative bacteria and against a strain of the influenza virus despite being only 10 nm in thickness. The films were determined to be non-toxic towards mammalian cells and acted through prevention of bacterial attachment to the surface. The authors found that a sufficient number of bilayers had to be applied to a surface under low pH which resulted in the positive charges protruding into the solution and being effective against the bacteria and viruses.

Rubner and co-workers developed a layer-by-layer film with embedded silver ions. The resultant films acted on bacteria through the release of the silver ions and by contact killing of bacterial cells with immobilized quaternary ammonium salts.⁴³ In another paper by Rubner and Lichter, polyelectrolyte multilayers were adsorbed on glass slides under specific pH conditions. It was shown that if deposited under the correct pH and ionic strength conditions, the polyelectrolyte multilayers contained free cationic chain segments which were efficient at disrupting cell membranes of *S. epidermidis* and *E. coli*.⁴⁴ The appropriate deposition conditions

ensured that there was a high density of mobile positive charges on the surface for the films to be effective.^{31,45}

In a study by Tew and others poly(butylmethacrylate)-*co*-poly(Boc-aminoethyl methacrylate) was “grafted from” a glass slide via surface-initiated atom transfer radical polymerization. The resultant films were shown to have 100% killing efficiency against *S. aureus* and *E. coli* when the bacterial suspensions were sprayed onto the activated glass substrates.²⁹ The mechanism of action was described to be insertion of the polymer into the phospholipid membrane of the cell.

In a recent work by Vikram Dhende and others, antimicrobial polyethylenimines that contained hydrophobic N-alkyl and benzonphenone groups were covalently attached to a variety of surfaces. The polymers were then covalently cross-linked with UV radiation and tested with *S. aureus* and *E. coli* with 98% killing efficiency. The thickness of the films was determined to be around 50 nm and the effectiveness of the film was explained based on the interaction of the hydrophobic film with the hydrophobic cell membrane. The electrostatic interaction between the cell membrane and the positively charged polymer backbone was speculated to disrupt the ionic integrity of the membrane resulting in cell death.⁴⁶

Kuroda and his coworkers performed an experiment where they deposited amphiphilic polycations on glass slides by dipping them in a polymer solution and showed effective killing of *E. coli* and *S. aureus*. The quaternary ammonium ions within the films gave the film the antimicrobial functionality while the methoxyethyl groups were used to tune the hydrophobicity of the surface. The bacteria killing capability of the resultant film was attributed to the finely

tuned amphiphilic properties of the polymer which facilitated its interaction with the bacterial cells.⁴⁷

Another example of incorporating the positively charged quaternary ammonium ions into a polymer network can be found in the recent experiments performed by Russel Composto and others at the Institute of Medicine and Engineering at the University of Pennsylvania.

Quaternary ammonium ions were infused into the chitosan network using the Michael reaction with acryl reagent and then bound to the surface with epoxide functionality. The films showed a high positive charge by zeta potential measurements and displayed a strong microbicidal action against *S. aureus*.⁴⁸ The positive charge of the quaternary ammonium ions was sufficient to disrupt the bacterial membrane resulting in cell death.

The next chapter will describe a novel antimicrobial film that was developed in our laboratory and shown to kill both Gram-positive and Gram-negative bacteria. The final chapter will go into the details of AFM investigations of bacterial interactions with antimicrobial compounds.

Bacteria	Antimicrobial agent	AFM imaging mode	Metric	Conclusions
<i>P. aeruginosa</i> , <i>E. coli</i> ³²	Nitric oxide (NO)	Tapping mode in air	Bacterial surface roughness, morphology, cell height/length	Membrane degradation is a significant contributing factor to NO's bacterial cytotoxicity
<i>E. coli</i> ⁴⁹	Antibacterial magainin 2, hemolytic bee venom melittin	Tapping mode in air	Surface morphology	Peptides caused different morphological changes, therefore different mechanisms
<i>S. aureus</i> , <i>S. epidermidis</i> , ³³	Quaternary ammonium compound	Contact mode in aqueous buffer		Surface must be positively charged for the bacteria to remain attached
<i>E. coli</i> , <i>P. aeruginosa</i> ³⁶	Endotoxin-binding Sushi peptide	In air using contact mode	Surface morphology and roughness	peptide perturbs the GNB membrane via the "carpet-model", peptides appear to act in three stages: damage of the bacterial outer membrane, permeabilization of the inner membrane and disintegration of both membranes
<i>E. coli</i> ³⁷	PGLa, an antimicrobial peptide isolated from hemocytes of frog skin	Contact mode, liquid and air	Elastic modulus, surface roughness	Two stage effect – (1) loss of stiffness, formation of micelles, (2) was further damaged resulting in total cell rupture. The peptide action resulted in the removal of bacterial pili. In second stage there PGLa interacts with the outer membrane by displacing Mg ²⁺ from LPS, cross-bridging negative charges of LPS lipids.
<i>E. coli</i> ³⁴	Antimicrobial peptide CM15	High speed tapping AFM in liquid	Surface roughness	Killing is combination of time-variable incubation phase (seconds to minutes) and a more rapid execution phase (less than 1 minute)
<i>P. aeruginosa</i> ³⁵	Tetrameric antimicrobial peptide SB006	Noncontact amplitude modulation mode	Bacterial height and fragmentization of membrane, parameter P – bacterial surface irregularity	Fragmentation of bacterial membrane and volume decrease (leakage of cytoplasmic material) membrane permeability disruption while the cell wall remains rigid
<i>E. coli</i> ³⁸	Antimicrobial Peptides BP100 and pepR	Intermittent contact mode	Surface roughness and surface morphology	surface neutralization occurs close to MIC values.

Table 4.1 An overview of AFM studies of bacterial cell interactions with antimicrobial compounds.

References

- (1) Klibanov, A. M. *J. Mater. Chem.* **2007**, *17*, 2479.
- (2) Wong, S. Y.; Li, Q.; Veselinovic, J.; Kim, B.-S.; Klibanov, A. M.; Hammond, P. T. *Biomaterials* **2010**, *31*, 4079.
- (3) Donlan, R. M.; Costerton, J. W. *CLINICAL MICROBIOLOGY REVIEWS* **2002**, *15*, 167.
- (4) Shah, A.; Mond, J.; Walsh, S. *Antimicrob Agents Ch* **2004**, *48*, 2704.
- (5) Bowersock, T. L.; Woodyard, L.; Hamilton, A. J.; DeFord, J. A. *Journal of Controlled Release* **1994**, *31*, 237.
- (6) Kenawy, E.-R.; Worley, S. D.; Broughton, R. *Biomacromolecules* **2007**, *8*, 1359.
- (7) Cunha, B. A. *Critical care clinics* **1998**, *14*, 263.
- (8) Brook, I. *Annals of Ontology, Rhinology and Laryngology* **2004**, *113*, 830.
- (9) Page, K.; Wilson, M.; Parkin, I. P. *Journal of Materials Chemistry* **2009**, *19*, 3819.
- (10) Zasloff, M. *Nature* **2002**, *415*, 389.
- (11) Jenssen, H.; Hammil, P.; Hancock, R. E. W. *Clin. Microbiol. Rev.* **2006**, *19*, 491.
- (12) Ge, Y.; MacDonald, D. L.; Holroyd, K. J.; Thornsberry, C.; Wexler, H.; Zasloff, M. *Antimicrob. Agents Chemother.* **1999**, *43*, 782.
- (13) Sekiguchi, J.; Yamamoto, H. In *Escherichia coli and Bacillus subtilis : The Frontiers of Molecular Microbiology Revisited*; Sadaie, Y., Matsumoto, K., Eds. 2012, p 115.
- (14) Dmitriev, B. A.; Toukach, F. V.; Schaper, K.-J.; Holst, O.; Rietschel, E. T.; Ehlers, S. *Journal of Bacteriology* **2003**, *185*, 3458.
- (15) Silhavy, T. J.; Kahne, D.; Walker, S. *Cold Spring Harbor Perspectives in Biology* **2010**, *2*.
- (16) Huang, K. C.; Mukhopadhyay, R.; Wen, B.; Gitai, Z.; Wingreen, N. S. *Proceedings of the National Academy of Sciences* **2008**, *105*, 19282.
- (17) Balcht, A.; Smith, R. *Pseudomonas Aeruginosa: Infections and Treatment*; Informa Healthcare, 1994.
- (18) Fine Mj, S. M. A. C. C. A.; et al. *JAMA* **1996**, *275*, 134.
- (19) Cooper, M.; Tavankar, G. R.; Williams, H. D. *Microbiology* **2003**, *149*, 1275.
- (20) Atabek, A.; Camesano, T. A. *Journal of Bacteriology* **2007**, *189*, 8503.
- (21) Klemm, P.; Schembri, M. A. *International Journal of Medical Microbiology* **2000**, *290*, 27.
- (22) Vogt, R. L.; Laura, D. *Public Health Rep.* **2005**, *120*, 174.
- (23) Ishii, S.; Sadowsky, M. J. *Microbes and Environments* **2008**, *23*, 101.
- (24) Darnton, N. C.; Turner, L.; Rojevsky, S.; Berg, H. C. *Journal of Bacteriology* **2007**, *189*, 1756.
- (25) Kluytmans, A.; van Belkum, A.; Verbrugh, H. *CLINICAL MICROBIOLOGY REVIEWS* **1997**, *10*, 505.
- (26) Cimolai, N. *Eur J Clin Microbiol Infect Dis* **2008**, *27*, 481.
- (27) Salyers, A. A.; Whitt, D. D. *Bacterial Pathogenesis: A Molecular Approach*, 2nd ed.; 2nd ed.; ASM Press. : Washington, D.C., 2002.
- (28) Otto, M. *Nat Rev Micro* **2009**, *7*, 555.
- (29) Madkour, A. E.; Dabkowski, J. M.; Nüsslein, K.; Tew, G. N. *Langmuir* **2008**, *25*, 1060.
- (30) Timofeeva, L.; Kleshcheva, N. *Appl Microbiol Biotechnol* **2011**, *89*, 475.

- (31) Kugler, R.; Bouloussa, O.; Rondelez, F. *Microbiology* **2005**, *151*, 1341.
- (32) Deupree, S. M.; Schoenfisch, M. H. *Acta Biomaterialia* **2009**, *5*, 1405.
- (33) Crismaru, M.; Asri, L. A. T. W.; Loontjens, T. J. A.; Krom, B. P.; de Vries, J.; van der Mei, H. C.; Busscher, H. J. *Antimicrob Agents Ch* **2011**, *55*, 5010.
- (34) Fantner, G. E.; Barbero, R. J.; Gray, D. S.; Belcher, A. M. *Nat Nano* **2010**, *5*, 280.
- (35) Rossetto, G.; Bergese, P.; Colombi, P.; Depero, L. E.; Giuliani, A.; Nicoletto, S. F.; Pirri, G. *Nanomedicine: Nanotechnology, Biology and Medicine* **2007**, *3*, 198.
- (36) Li, A.; Lee, P. Y.; Ho, B.; Ding, J. L.; Lim, C. T. *Biochimica et Biophysica Acta (BBA) - Biomembranes* **2007**, *1768*, 411.
- (37) da Silva Jr, A.; Teschke, O. *Biochimica et Biophysica Acta (BBA) - Molecular Cell Research* **2003**, *1643*, 95.
- (38) Alves, C. S.; Melo, M. N.; Franquelim, H. G.; Ferre, R.; Planas, M.; Feliu, L.; Bardají, E.; Kowalczyk, W.; Andreu, D.; Santos, N. C.; Fernandes, M. X.; Castanho, M. A. R. B. *Journal of Biological Chemistry* **2010**, *285*, 27536.
- (39) Agarwal, A.; Weis, T. L.; Schurr, M. J.; Faith, N. G.; Czuprynski, C. J.; McAnulty, J. F.; Murphy, C. J.; Abbott, N. L. *Biomaterials* **2010**, *31*, 680.
- (40) Tiller, J. C.; Liao, C. J.; Lewis, K.; Klibanov, A. M. *P Natl Acad Sci USA* **2001**, *98*, 5981.
- (41) Bagheri, M.; Beyermann, M.; Dathe, M. *Antimicrob Agents Ch* **2009**, *53*, 1132.
- (42) Tiller, J. C.; Lee, S. B.; Lewis, K.; Klibanov, A. M. *Biotechnology and Bioengineering* **2002**, *79*, 465.
- (43) Li, Z.; Lee, D.; Sheng, X.; Cohen, R. E.; Rubner, M. F. *Langmuir* **2006**, *22*, 9820.
- (44) Lichter, J. A.; Rubner, M. F. *Langmuir* **2009**, *25*, 7686.
- (45) Murata, H.; Koepsel, R. R.; Matyjaszewski, K.; Russell, A. J. *Biomaterials* **2007**, *28*, 4870.
- (46) Dhende, V. P.; Samanta, S.; Jones, D. M.; Hardin, I. R.; Locklin, J. *Acs Appl Mater Inter* **2011**, *3*, 2830.
- (47) Han, H.; Wu, J.; Avery, C. W.; Mizutani, M.; Jiang, X.; Kamigaito, M.; Chen, Z.; Xi, C.; Kuroda, K. *Langmuir* **2011**, *27*, 4010.
- (48) Lee, H.-S.; Eckmann, D. M.; Lee, D.; Hickok, N. J.; Composto, R. J. *Langmuir* **2011**, *27*, 12458.
- (49) Mencken, M.; Holroyd, D. L.; Rautenbach, M. *Antimicrob. Agents Chemother.* **2005**, *49*, 4085.

Chapter 5

Antimicrobial surfaces using covalently-bound polyallylamine

Abstract

We investigated the antimicrobial properties of the cationic polymer, polyallylamine (PA), when covalently bonded to glass. The objective was to obtain a robust attachment, yet still allow extension of the polymer chain into solution to enable interaction with the bacteria. The PA film displayed strong antimicrobial activity against *Staphylococcus epidermidis*, *Staphylococcus aureus*, and *Pseudomonas aeruginosa*, which includes both Gram-positive and Gram-negative bacteria. Glass surfaces were prepared by a straightforward two-step procedure of first functionalizing with epoxide groups using 3-glycidoxypropyltrimethoxy silane (GOPTS) and then exposing to PA so that the PA could bind via reaction of a fraction of its amine groups. The surfaces were characterized using X-ray photoelectron spectroscopy and Fourier transform infrared spectroscopy to verify the presence of the polymer on the surface, zeta potential measurements to estimate the surface charge of the films, and atomic force microscopy to determine the extension of the polymer chains into solution. Antimicrobial properties of these coatings were evaluated by spraying aqueous suspensions of bacteria on the functionalized glass slides, incubating them under agar, and counting the number of surviving cell colonies.

5.1 Introduction

Bacterial infections that spread through invasive procedures such as tracheal intubation, cardiovascular lines or urinary catheters are prevalent in hospital environments.¹ Hospital acquired infections alone are the fourth most common cause of death in the US² and bacterial contamination of medical devices is the cause of more than half of all hospital-acquired infections.³ Often the only solution to an infected implant is its removal and replacement, which creates additional health issues and economic costs⁴ because it must be followed by a long-term antibiotic treatment.⁵ In addition to the problems associated with medical devices and implants, the effectiveness of routine disinfection of common hospital surfaces is still being debated.⁶ It has been reported that most Gram-positive bacteria and certain Gram-negative species such as *Pseudomonas Aeruginosa* (*P. aeruginosa*) can survive on dry surfaces for many months.⁷ These all reveal the urgent need for new strategies to prevent microbial infections caused by contaminated surfaces. One such strategy is to coat the surface of a medical device in a material that strongly resists the attachment or growth of bacteria, preventing biofilm formation. Antifouling and antimicrobial surface coating can be used in biomaterial implants, where the bacterial infection is the most common source of failure.^{8,9} A significant advantage of surface antimicrobial treatments over systemic antibiotics and antimicrobials is that systemic treatments require a large dose of the antibiotic and produce side effects distant from the implant or catheter, whereas an irreversible immobilization of antimicrobials on the medical devices is localized to the site where the action is needed. Therefore, this paper focuses on the use of new non-leaching surface coatings for the purpose of preventing bacterial infection on a particular device.

The requirements for a microbicidal coating ideally include: 1) ease of synthesis, 2) stability, 3) insolubility in aqueous environments, 4) potential for regeneration, and 5) biocidal ability towards a wide range of microbes.⁹ These requirements can be satisfied through the use of immobilized polycationic polymers that have many advantages: 1) lack of bacterial resistance, 2) prolonged effectiveness due to immobilization and lack of diffusion, 3) lack of toxicity due to immobilization of active agents, and 4) effectiveness against both Gram-positive and Gram-negative organisms. There are many antimicrobial systems that have been studied in connection with killing bacteria on contact, and these include quaternary ammonium compounds,¹⁰⁻¹² layer-by-layer self-assembled polyelectrolytes,¹³⁻¹⁵ polyamine films,¹⁶ and chitosan.¹² Recent review articles describe both antimicrobial polymers¹⁶⁻¹⁸ and polymeric surface coatings.^{1,19,20}

The proposed mechanism for the antimicrobial action of immobilized cationic polymers is that they disrupt the integrity of the bacterial membrane, which results in cell death.^{21,22} Their action is thought to be physical as opposed to the chemical inhibition caused by traditional antibiotics. Development of resistance to polycationic antimicrobials would thus require a fundamental change to the cell wall and membrane and therefore is considered unlikely. The structures of the bacterial cell wall and the outer membrane are open networks of macromolecules and do not offer a perfect barrier against penetration of foreign molecules.¹⁶ The bacterial cell envelope can be thought of as a large two-dimensional polyelectrolyte which carries an overall negative charge which is stabilized by divalent ions such as Mg^{2+} and Ca^{2+} . The negative charge comes from the teichoic or lipoteichoic acid molecules in Gram-positive bacteria and the lipopolysaccharides and phospholipids of Gram-negative bacteria.¹⁶ Kugler et al. proposed that

bacteria interacted with charged surfaces during the adsorption stage, and the removal of divalent counterions in the cell envelope led to bacterial death.²³

There are three main factors that affect antimicrobial properties of surface coatings and they are:

1) hydrophobicity and degree of alkylation, 2) surface charge density, and 3) polymer molecular weight. Polymer hydrophobicity may affect the antimicrobial functionality of the surface because the interior of the cell membrane is hydrophobic.^{22,24} The alkylation of the polymer alters the hydrophobicity.²⁵ According to a study by Tiller et al., in order to kill bacteria, immobilized polymeric chains must be sufficiently long, polycationic, and hydrophobic but not overly so.²⁴ The positive charge is necessary to induce an electrostatic interaction with the bacterial membrane and to prevent the polymer chains from collapsing onto each other.

Adsorption of extra cationic charge could also disrupt the structure and effect cell signaling.

The surface charge density therefore plays a critical role in determining the microbicidal effect of a polymer system.^{9,16,23,26} In a paper by Murata et al. the authors concluded that quaternary ammonium (QA) divalent cations exchanged with the divalent cations in the cell membrane which resulted in the membrane disruption and cell death.²⁶ The QA surface charge density required to inhibit the growth of *E.coli* bacteria was estimated to be 10^{14} to 10^{15} QA groups per cm^2 . In a study by Kugler et al., the surface charge density necessary to inhibit growth of *E. coli* and *Staphylococcus epidermidis* (*S.epidermidis*) was estimated to be 10^{12} to 10^{13} cations/ cm^2 .²³ In this case, the efficiency of bacterial inhibition was a strong function of the surface charge and did not vary with the polymer length. There have been other studies however that concluded that the antimicrobial activity of surface-bound polymers generally increased with the increasing molecular weight.^{16,24} Klibanov et al. have shown that for two different systems there was a

minimum molecular weight required to exert the antimicrobial effect.²² In a study by Huang and others, polymers with a high molecular weight were found to have nearly 100% efficiency while oligomers did not have the same effect.²⁷ The cell wall thickness for the model bacterial organisms varies between 15 and 40 nm.²⁸⁻³⁰ Therefore, it is likely that the polymer molecules are required to have a certain length to extend sufficiently far from the surface to interact with the bacterial membrane, which would correlate with the molecular weight. For example in a study by Lichter et al., it was determined that the polyelectrolyte multilayers would only be effective against *S. epidermidis* and *E. coli* when synthesized under specific pH conditions that would allow for free cationic chain segments to extend into solution.¹⁴

In this work we evaluated the antimicrobial properties of polyallylamine (PA)-coated glass surfaces against both Gram-positive and Gram-negative bacteria. Our bacterial studies were performed at pH 7.4 where many of the amine groups on PA are protonated, and we use PAH to refer to the partially protonated version of the polymer. PAH incorporated in layer by layer self-assembled films has been used in the past to create antimicrobial coatings.^{14,15,31} Creating a simple two-step application procedure of PA on epoxide-functionalized glass creates a more robust, and easy-to-synthesize film. The PAH surfaces were characterized using surface sensitive techniques to estimate the surface charge and the degree to which polymer chains extended into solution. We assay the number of bacterial cells that are able to reproduce to form colonies on surfaces coated in PAH. Since the mechanism of action of polycationic antimicrobials is thought to be damage to the cell wall or membrane,^{22,32} which leads to death of the bacterium, we use the term “killing” to describe the effect of the antimicrobial polymer film.

5.2 Materials and methods

5.2.1 Materials used

Polyallylamine in freebase form was purchased from Polysciences and polyallylamine hydrochloride was purchased from Sigma Aldrich. Other chemicals used in this study were toluene (Fisher Chemical), sulfuric acid 18M (Fisher Chemical), hydrogen peroxide 30% in water (LabChem Inc.), ethanol 200 proof (Decon Laboratories, USP grade), acetone (Fisher Scientific, HPLC grade), 3-glycidoxypropyl-trimethoxy silane or GOPTS (Aldrich $\geq 98\%$), PBS with pH=7.4 (Sigma). Yeast dextrose broth (YDB) was prepared following the recipe provided by Cunliffe *et al.*³³ Tryptic soy broth (TSB) was prepared by dissolving following materials in deionized (DI) water (resistivity at 25 °C: 18.2 M Ω cm): Bacto tryptone (17 g L⁻¹), bacto soytone (3 g L⁻¹), dextrose (2.5 g L⁻¹), sodium chloride (5 g L⁻¹) and dipotassium phosphate (2.5 g L⁻¹). Bacto tryptone (10 g L⁻¹), yeast Extract (5 g L⁻¹), sodium chloride (10 g L⁻¹) were dissolved in water to make Lysogeny broth (LB). Agar plates were made by adding 1.5% of bacto agar to either of the above described culturing media. The ingredients used to prepare the bacterial growth media were purchased from Fisher scientific.

5.2.2 Preparation of antimicrobial films

Standard VWR microscope slides (soda-lime glass) were cut into 15 mm \times 13 mm pieces using a diamond saw. The slides were immersed into 3M NaOH solution in water for 10 min to create a clean fresh surface, thoroughly rinsed in DI water, and then cleaned in the “Piranha” solution (3:1 solution of 18M H₂SO₄ to 30% H₂O₂ – warning Piranha causes severe burns to tissue) for 40 minutes with occasional stirring to create a clean surface with exposed hydroxyl groups. The slides were again washed in copious amounts of water, then rinsed in ethanol and dried in a

stream of ultra-high purity nitrogen. The slides were further modified with (3-glycidyloxypropyl) trimethoxysilane (GOPTS) by reaction with 100% GOPTS at 37°C for either 6 or 60 minutes.³⁴ Following the GOPTS treatment, the slides were sonicated in dry toluene for 3 minutes, washed in toluene, then in copious amounts of ethanol and dried with a stream of nitrogen gas. The glass slide was covered with a 15% freebase PA in water (pH = 11) and left to react at 75°C for 36 h. The reaction is shown schematically in Figure 5.1. The slides were rinsed in DI water (for about 20 times) and also left in the ultra-sonic bath in water to remove any PA that was not covalently bonded to the surface. When a PA solution at pH 7 was used there was no antimicrobial activity. This control experiment with protonated amine shows that the lone pair of nitrogen was necessary to react with the epoxide to produce a robust film: without a covalent film, there was no activity. Additional sample slides were created in which the PA was attached by simply dipping the glass slides into a PA solution using a procedure adopted from Zucolotto and coworkers (“dipped slides”).³⁵ These samples were used to compare electrostatic rather than covalent attachment. After cleaning in NaOH solution and Piranha, the glass slides were immersed into 0.3 mg/mL of PA, with 0.5 mol/L NaCl in DI water with the pH adjusted to slightly acidic using 4M HCl. The slides were then washed three times in DI water and dried in a laminar flow cabinet.

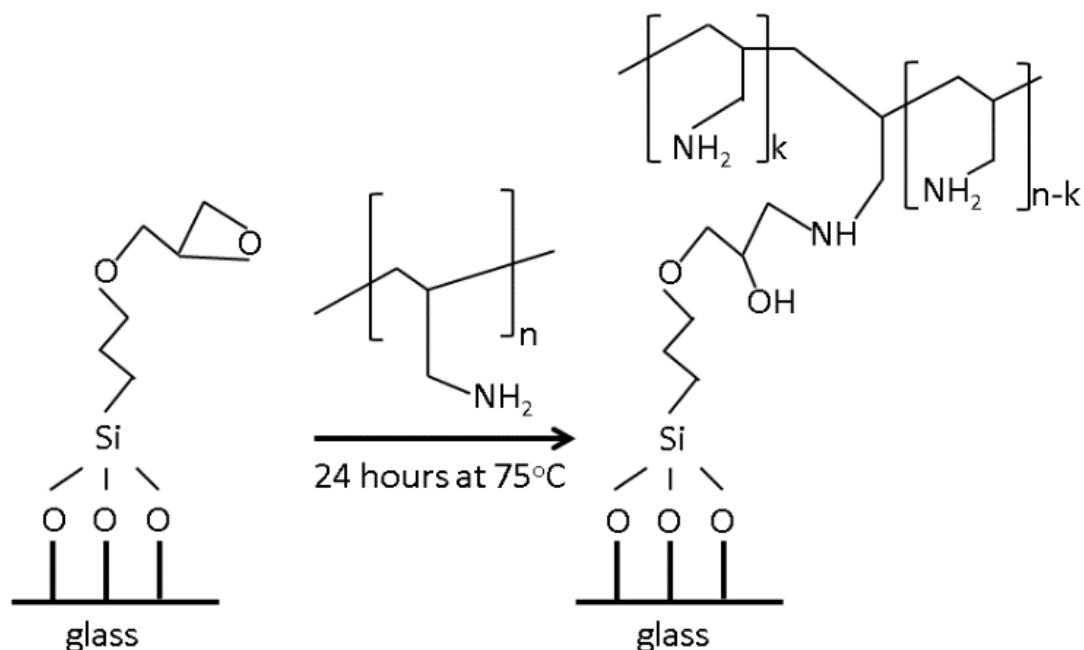


Figure 5.1 Schematic of covalent attachment of PA to glass. The primary amine groups become protonated at neutral pH.

5.2.3 X-ray photoelectron spectroscopy

The X-ray photoelectron spectroscopy (XPS) measurements were performed on a Phi Quanterra machine with a monochromated Al K α source (1486 eV) at 50 W over 200 μm at a 45° angle. Individual element scans were acquired at pass energy 26 eV at 0.1 eV step size with 10 to 40 sweeps (depending on the element).

5.2.4 Attenuated total reflectance Fourier transform infrared spectroscopy

Attenuated total reflectance Fourier transform infrared spectroscopy (ATR-IR) used a Varian-670 IR with an MCT detector combined with Vari-GATR accessory at 60° incident angle and polarizer at 0° with a germanium crystal a to sample films on a *silicon* surface with native oxide. A pressure

clamp was used to enhance the contact between the film and the surface. 64 scans were performed over the region of 4000 to 700 cm^{-1} at 4 cm^{-1} resolution, and each sample surface was tested several times to verify repeatability. The resulting spectra were ATR and baseline corrected using Resolutions Pro software.

5.2.5 Atomic Force Microscopy

An atomic force microscope (Cypher, Asylum Research, Santa Barbara, CA) was used to create images of the PA films deposited on a *silicon* wafer with a native oxide coating in the PBS solution and to determine the extension of the polymer chains into the solution. Rectangular AFM probes (ORC8, Bruker, Camarillo, CA) with a nominal spring constant of 0.7 N/m were cleaned for 20 min with UV/ozone prior to each use. The spring constant was measured before each experiment with the thermal method developed by Sader³⁶ using the Asylum Research software. AFM imaging was conducted in contact mode on surfaces in an aqueous environment, using the same instrument as for the force studies. All images presented have been subjected to a first order line flatten. The extension of the PA chains in solution was found by measuring force curves at 1 $\mu\text{m/s}$ rate and 20-30 force curves were measured at each point on the film.

5.2.6 Zeta potential measurements

The zeta potential of the PA-coated glass surfaces was determined using a SurPASS Electrokinetic Analyzer (Anton Paar GmbH, Graz, Austria). The SurPASS tubing was rinsed using very dilute isopropanol (<1% vol. in water) solution and then with DI water for approximately 10 minutes. The slides were mounted in the SurPASS using the “clamping cell” configuration and 1 mmol NaCl solution in DI water was used as the electrolyte.

5.2.7 Antimicrobial assay

P. aeruginosa (ATCC 27853), *S. epidermidis* (ATCC 14990), and *S. aureus* (ATCC 27217) were used as model organisms to test the antimicrobial performance of the modified surfaces. The spray testing technique was adapted from Tiller *et al*²⁴. A 1.5% agar plate was inoculated using a -80° C stock of each bacteria strain and incubated at 37° C overnight. LB plates were used for *S. epidermidis*, and *P. aeruginosa*, and TSB plates were used for *S. aureus*. In a 125 ml flask, 10 ml of culture media was inoculated with three to four colonies of the bacteria and incubated in a shaker at 37° C and 150 rpm until the bacteria reached the logarithmic growth phase as indicated by the optical density of the suspension. Yeast-dextrose broth was used to grow *S. epidermidis* and TSB was used with *P. aeruginosa* and *S. aureus*. The resulting culture was centrifuged (3000g, 11 minutes, room temperature) and the cells were re-suspended in autoclaved DI water to a final concentration of 10⁷ cells/ml. A 125 ml of the bacteria suspension was transferred to a standard chromatography sprayer (Kontes, TLC sprayer) and used to spray both modified and control samples in a BSL-2 cabinet. The inlet pressure of the sprayer was kept constant and the volumetric flow rate was approximately 10 ml/min. Before spraying, each slide was washed with 70% ethanol followed by three rinses with autoclaved DI water and air-dried in a biological safety cabinet. Triplicates of the control and the modified slides were used in each experiment. After the spraying, the slides were allowed to dry in air for 2 to 5 minutes and the growth agar was then carefully poured on top of the slides and allowed to solidify. After an overnight incubation at 37° C, the surviving bacterial colonies were counted to estimate the antimicrobial properties of the PA films compared with the clean glass control.

5.3 Results and discussion

5.3.1 XPS and ATR-IR show the presence of free amines

After the reaction of GOPTS with a silica surface, XPS showed that C/N ratio increased from 16 to 36 and the C/Si ratio from 0.23 to 0.29. These results were consistent with the results reported previously by Ulijn and coworkers.³⁴ When the PA was added to the surface, the C/N ratio dropped dramatically from 36 to 5.0 due to the large number of nitrogen atoms present in the PA. The binding of PA to the surface was further confirmed by examining the N1s peak (Figure 5.2) where the peaks at 399 and 401 eV indicated the presence of amine bonds. To further verify the presence of free amine groups on the surface, two cysteine Fmoc-protected amino acid residues were bound to the PA surface using solid phase synthesis.^{37,38} The reaction of the amine was verified by (a) the shift of the N1s peak to 400 eV indicated formation of amide bonds on the surface and loss of amine (Figure 5.2) and (b) the production of a sulfur S2p peak at 162 eV (not shown).

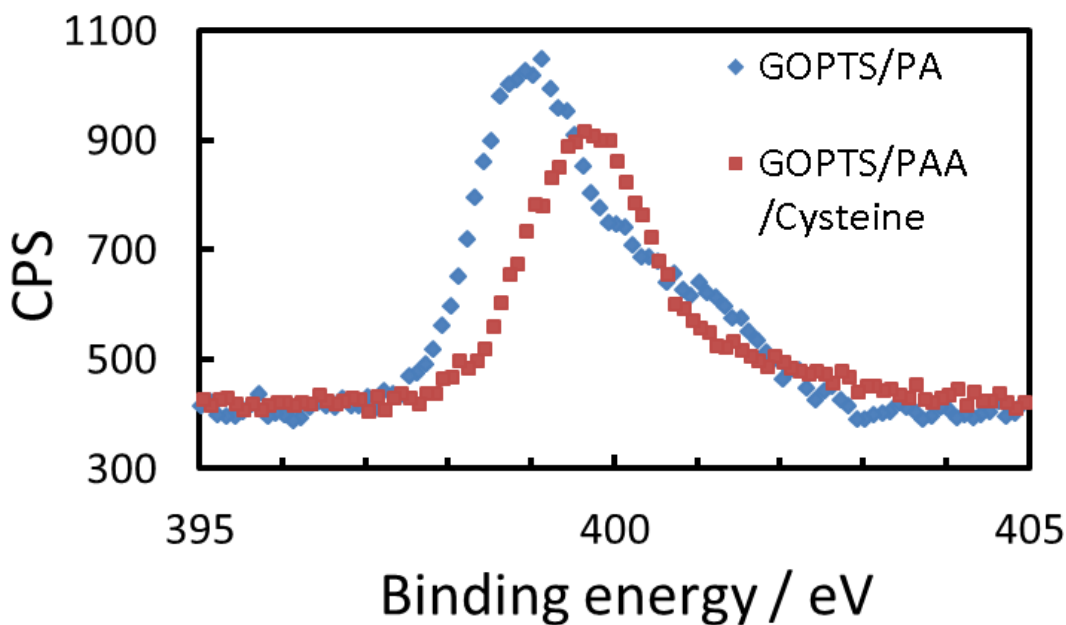


Figure 5.2 N1s peak of the XPS spectrum of a 15,000 MW PAA film. The peak at 399 and the shoulder at 401 eV are consistent with the presence of amine groups. After reaction with cysteine, the amine peaks are replaced with the amine peak at 400 eV. Note the disappearance of the amine shoulder at 401 eV after the reaction with cysteine.

The ATR-IR spectrum of the 15,000 MW PA film on a silicon wafer (Figure 5.3) confirms the XPS results. There is a broad peak between 3000 and 3600 cm^{-1} which includes the expected NH stretch and OH stretch from the alcohol formed by reaction of PA with GOPTS (see Figure 5.1). There is also a strong primary amine bending absorption at around 1660 cm^{-1} and a much weaker secondary amine bending absorption at 1550 cm^{-1} .³⁹ This data is consistent with the formation of a PA film with an abundance of free primary amines present and fewer secondary amines binding the polymer to the glass.

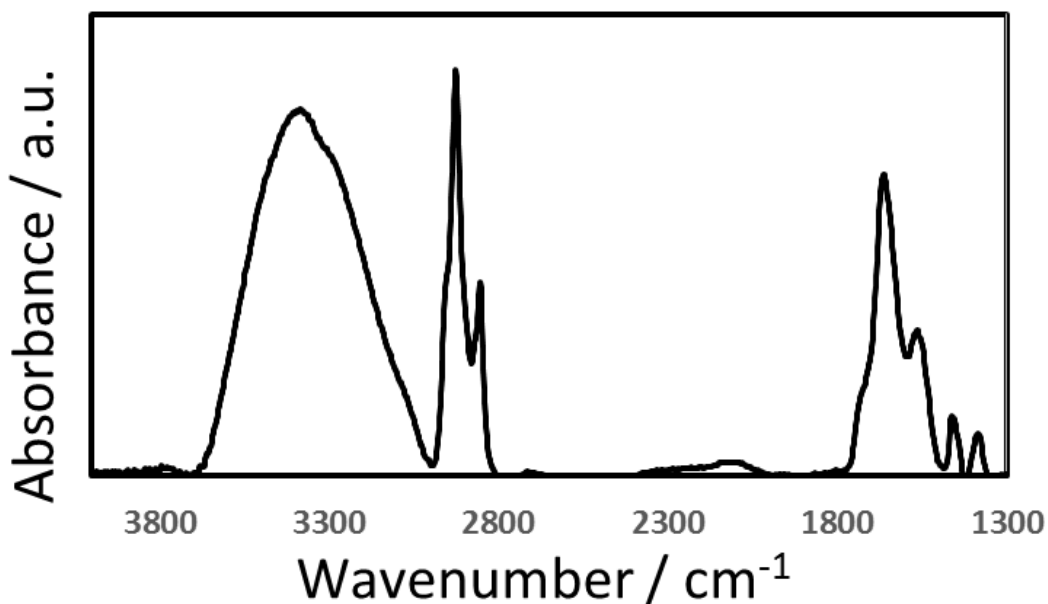


Figure 5.3 ATR-IR spectrum of a 15,000MW PAA/GOPTS film on a silicon wafer.

5.3.2 AFM imaging

AFM contact mode imaging in PBS over an area of $5 \times 5 \mu\text{m}^2$ was used to characterize the surface coatings. The films were synthesized on smooth silicon wafers ($\text{rms roughness } 120 \pm 5 \text{ pm}$), instead of standard microscope glass to facilitate detection of thin films. The GOPTS coating was imaged after a shorter (6 min) and longer (60 min) GOPTS/silicon application time. The film is rougher than the wafer, but still very smooth with an rms roughness of $0.14 \pm 0.01 \text{ nm}$ after 6 min and $0.34 \pm 0.15 \text{ nm}$ after 60 minutes. After 6 minutes of reaction, there are $\sim 0.6 \text{ nm}$ high and $\sim 200 \text{ nm}$ wide dots which we attribute to polymerized clusters of GOPTS. After 60 minutes, there are more clusters and the existing clusters have grown in width and height, so that spacing between clusters of epoxide sites is reduced. There may also be isolated epoxides on the solid that are not resolved.

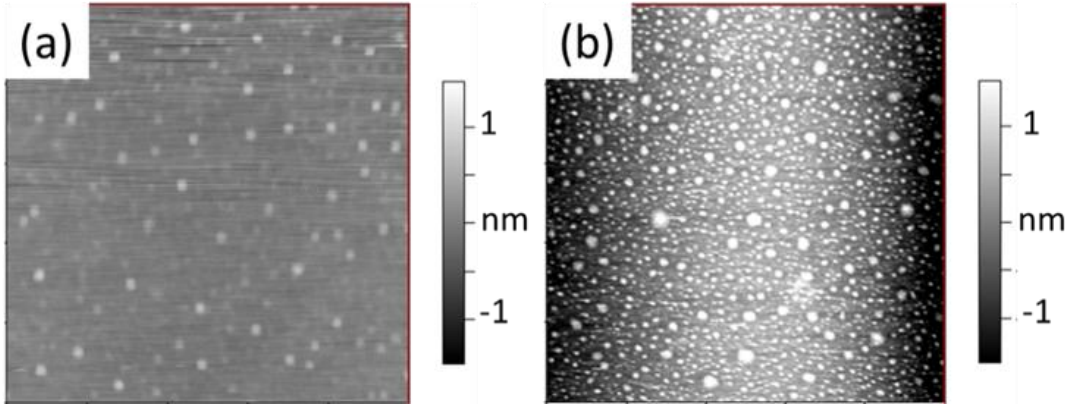


Figure 5.4 The atomic force microscope image of a silicon wafer that was GOPTS treated for 6 min (a) and 60 min (b). The image sizes are $5 \times 5 \text{ } (\mu\text{m})^2$, with the scale bars indicating sample height.

After reaction of the 15,000 MW PA (Figure 5.5c), the film is amorphous and has greater rms roughness ($500 \text{ pm} \pm 100$) than the bare silica, but is still very smooth. After reaction with the 58,000 MW PA the surface morphology is very different: there are fibers and the rms roughness is $18 \text{ nm} \pm 2$ (Figure 5.5d).

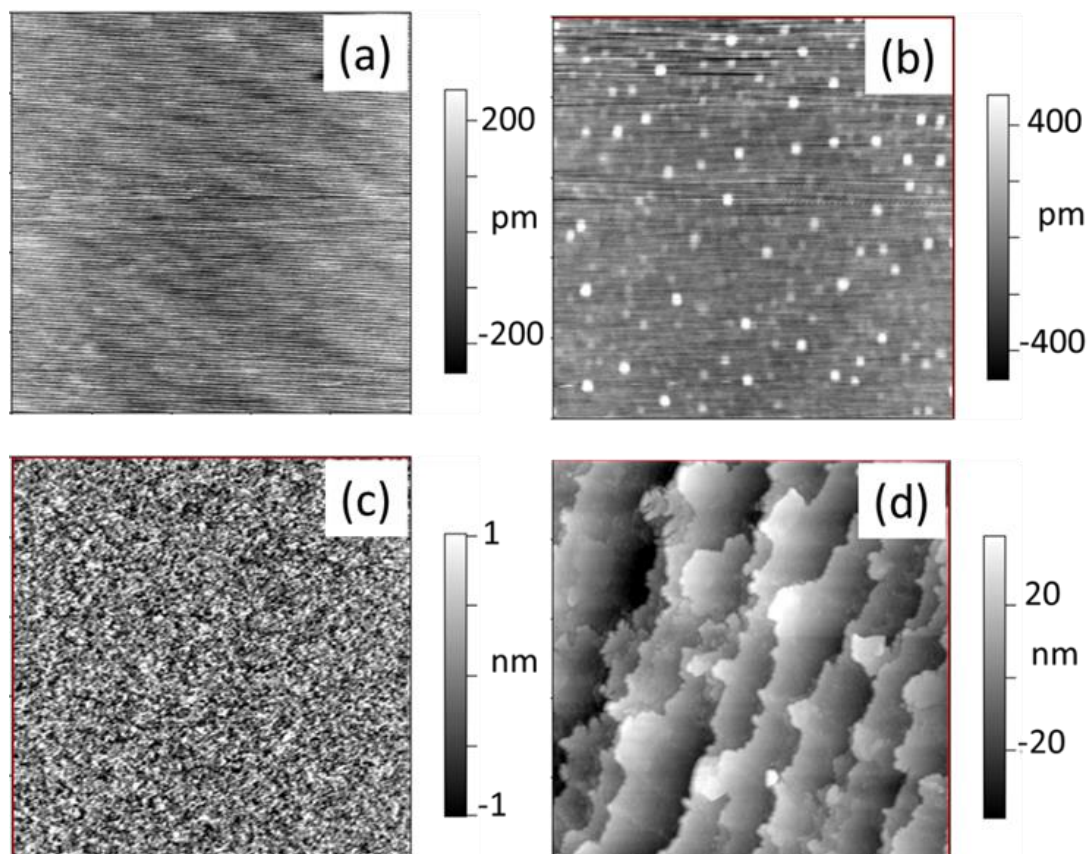


Figure 5.5 Atomic force microscopy images of the bare silicon wafer (a), the GOPTS coated silicon wafer (b), 15,000 MW PAA (c) and 58,000 MW PAA (d). All images are $5 \times 5 (\mu\text{m})^2$ with the scale on the right indicating the height of the sample. The *rms* surface roughness of these samples is as follows: (a) 120 ± 5 pm, (b) 140 ± 10 pm, (c) 500 ± 100 pm, and (d) 18 ± 2 nm.

5.3.3 Measurement of surface charge and potential

Streaming potential measurements were used to calculate the zeta potential of the films using the Fairbrother and Mastin equation.⁴⁰ The zeta potential was determined by first measuring the streaming potential of the flat surface in the current mode with 1 mM NaCl at neutral pH as the electrolyte. The zeta potential for 15,000 MW PA was $+76 \pm 0.5$ mV and $+61 \pm 1$ mV for 58,000 MW PA. This corresponded to the charged amine group density⁴¹ in the order of 10^{12} (+)/ cm^2

which was consistent with the literature predictions of the minimum surface charge density required to kill bacteria on contact.

For the covalently bonded PA, the zeta potential remained constant over many measurements, a fact that attests to the stability of the PA coating (Figure 5.6a). In addition, the zeta potential remained constant after washing with 200 mL of PBS. In contrast, the dipped PA surface had only a mild positive potential at the beginning and the zeta potential decreased steadily over the course of 10 surface scans (Figure 5.6b). This illustrates that the electrostatically adsorbed PA layer was weakly attached to the silicon surface.

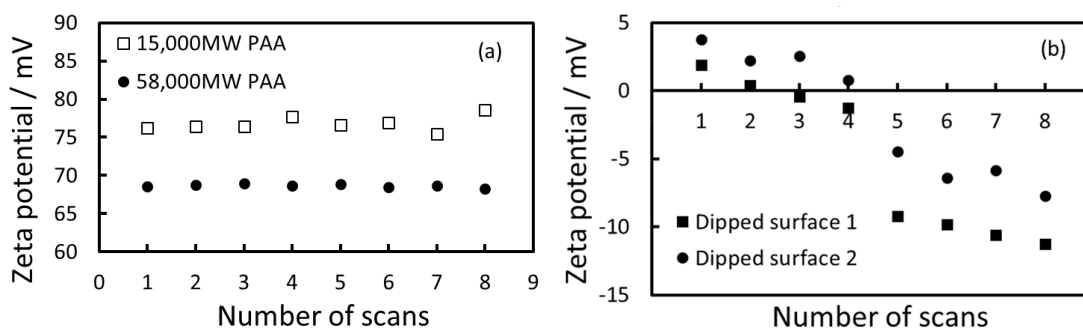


Figure 5.6 Zeta potential of (a) covalently-bound PAA/GOPTS films after an hour-long GOPTS application, and (b) two dipped 15,000MW PAA films. The zeta potential remains stable in the covalently bound samples and decreases with time for the dipped samples.

Our interpretation of the zeta potential measurement is illustrated by the cartoon shown in Figure 5.7. The dipped polymer acts as the counterion to the silanol groups on the glass and therefore lies close to the glass. In contrast, the GOPTS reacts with some silanol groups, and covers other groups so there is much lower electrostatic interaction with the solid. Thus, for GOPTS/PA the

polymer chains extend much further into solution. This hypothesis was further investigated with AFM force measurements as described in the next section.

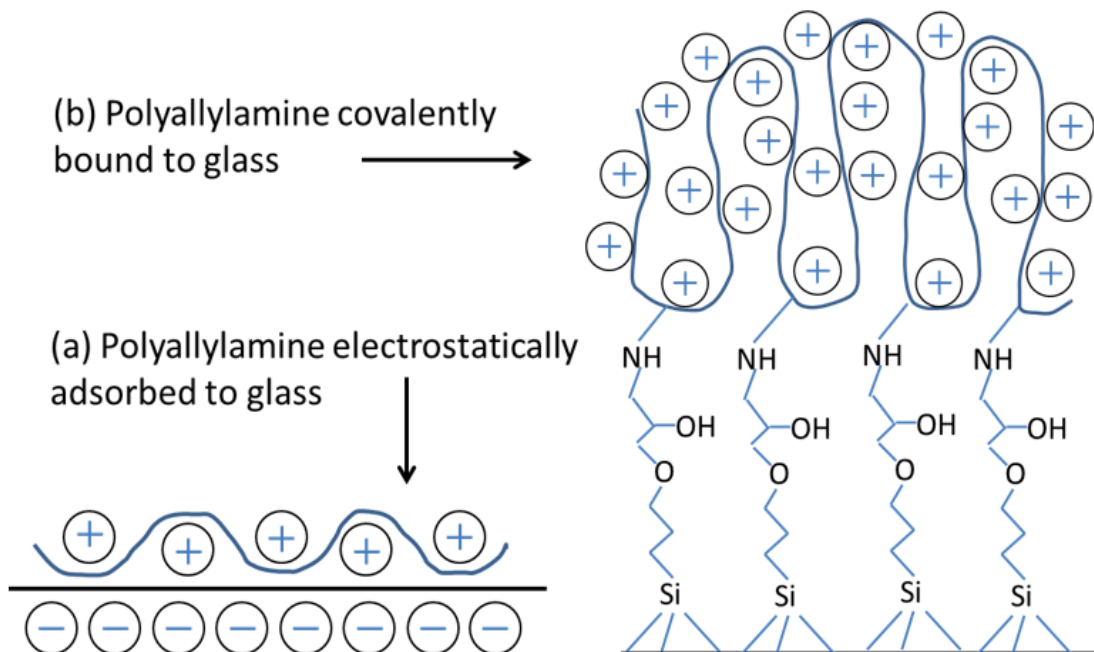


Figure 5.7 Cartoon of the proposed difference in the binding conformation of the electrostatically adsorbed (a) and covalently bound (b) PA.

5.3.4 Measurement of the extended length of PA chains

AFM was used to characterize the chain length of the PA molecules via force measurement between an AFM tip and the PA-coated surfaces in PBS solution. A sample force curve is shown in Figure 5.8 where the tip approach and the polymer chain extension during the retraction of the tip are shown. On approach, the first force is felt at about 10 nm, consistent with an “undisturbed” PA film thickness of about 10 nm. When the AFM cantilever retracted from the surface, the physically adsorbed PA chains remained “stuck” to the tip and gradually desorbed as the separation increased. This measurement relied on the fact that the PA was

positively charged in solution at physiological pH, and the silicon nitride tip is negatively charged (isoelectric point for silicon nitride cantilever is around $\text{pH} = 3$ ⁴²).

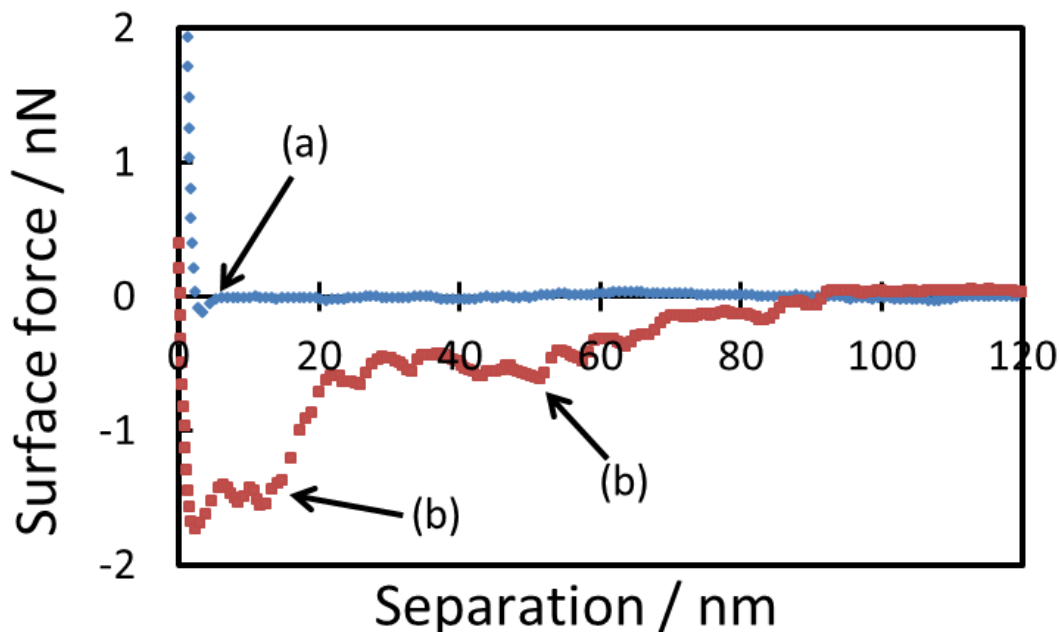


Figure 5.8 Typical force curve between a PA/GOPTS film and a (negatively charged) silicon nitride cantilever (60 min. GOPTS reaction, measurement performed in PBS). Note that (a) is the point where the cantilever tip encounters the PA film on approach (blue curve) and (b) are the representative “jumps” where the individual PA chains detached from the AFM tip on retraction (red curve).

The point on the retraction curve where the attraction between the tip and the surface became zero was termed the extended chain length (ECL) of the polymer. At larger separations, there is no force, so no polymer is bridging the tip and the glass. At smaller separations, there is a series of “jumps” each of which is usually interpreted as desorption of a polymer chain or a segment of polymer chain.⁴³ There was a wide range of “jumps” as illustrated in Figure 5.7, and the longest

chains extend up to 90 nm from the glass. Average ECL values, (Figure 5.9), demonstrate the important point that the PA chains that are attached to GOPTS extend into solution for 50–200 nm, depending on the conditions. This is consistent with the cartoon in Figure 5.6. This extended chain length is comparable to or exceeds the typical bacterial cell wall. Thus, the GOPTS/PA should be able to reach from the silica to the bacterial membrane, if required. In contrast, the dipped-PA had much shorter chains.

In more detail, Figure 5.9 shows that the maximum chain length was greater for (a) shorter reaction time of GOPTS (6 min vs. 60 min) and (b) lower molecular mass. It is surprising that longer ECL values correspond to the shorter reaction time of GOPTS. We expected that a longer reaction time with GOPTS would lead to a higher density of GOPTS on the surface, a greater number of attachment points of PA and the substrate, and therefore shorter “free” segments between the attachment points, but this did not occur. We also observed that the ECL decreased with molecular mass for the series 15,000 MW, 58,000 MW, 900,000 MW. The reason for this is not clear, but the morphology was very different for the 15,000 MW and 58,000 MW samples; it may be more difficult to pull a chain out of the fibrous structure of the 58,000 MW PA. In summary, the GOPTS/PA chains extended far into solution, further than the dipped-PA.

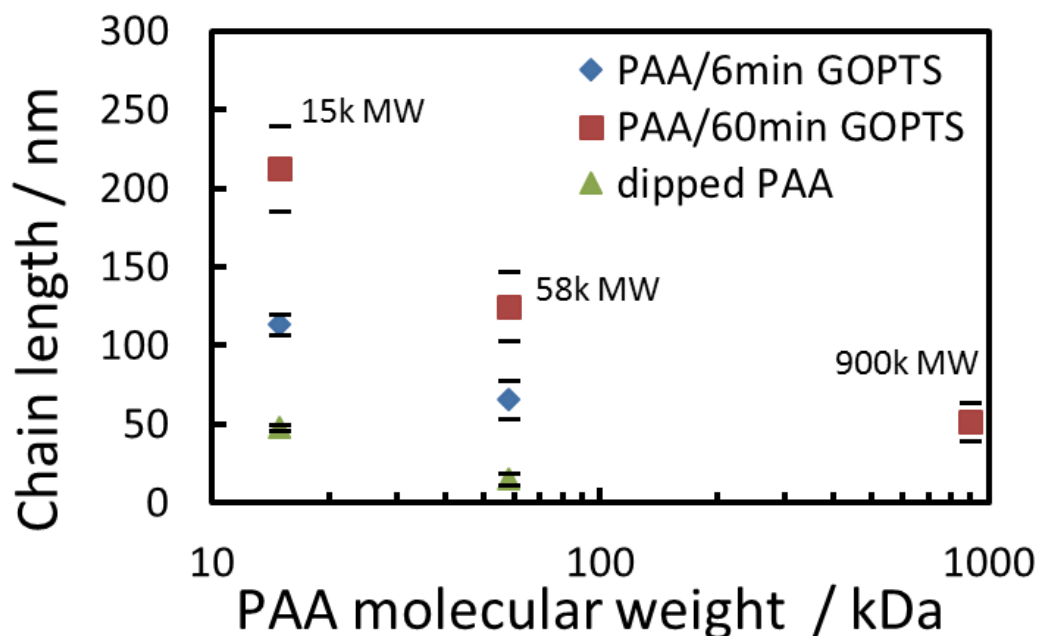


Figure 5.9 Extension of the PA chains into solution as measured using atomic force microscopy.

The error bars indicate the standard error.

5.3.5 Antimicrobial assay

The PA films were tested to determine their antimicrobial performance using a method adopted from Klibanov's group,²⁴ in which bacteria were sprayed onto a surface, briefly air-dried, and then placed in a favorable growth mixture (agar) so that they would grow if the surfaces were not antimicrobial. The efficacy of the method was tested by checking that both clean glass slides and slides coated with GOPTS alone did produce growth of bacteria on the solid surface (negative control), whereas a film that was known to kill bacteria on contact, poly(vynil-N-pyridinium bromide),²⁵ did prevent bacterial growth with the killing efficiency of over 90% (positive control). The test surfaces included 15,000 MW and 58,000 MW PA covalently attached to glass via the GOPTS silane. The application times for GOPTS were varied from 6 to

60 minutes to determine the effect of attachment density. Clean glass was used as the control but we also tested electrostatically attached PA to compare with the covalently bonded films.

The antimicrobial performance of the films was quantified using the killing efficiency parameter defined as:

$$\text{Killing efficiency} = \left(1 - \frac{\# \text{ of colonies on sample}}{\# \text{ of colonies on control}}\right) \times 100\% \quad (5.1)$$

where the control is a clean glass slide. We use the word “killing” because the absence of colonies implies that the sprayed live cells were killed by contact with the surface. The results are presented in Table 5.1. In every experiment at least three slides of each type were used to increase the accuracy of the results. Every value listed in Table 5.1 is an average of at least three separate experiments, except for the values in parenthesis that give preliminary results from a single experiment. The errors are the standard deviations for each experimental set. The most important result is that the very simple GOPTS/PA method is very effective at preventing the growth of a variety of organisms. It is particularly successful against *S. epidermidis* and *S. aureus*, killing about 97% of the organisms. An example of a glass slide is shown in Figure 5.10, showing the dramatic decrease in the number of colonies on GOPTS/PA compared to clean glass.

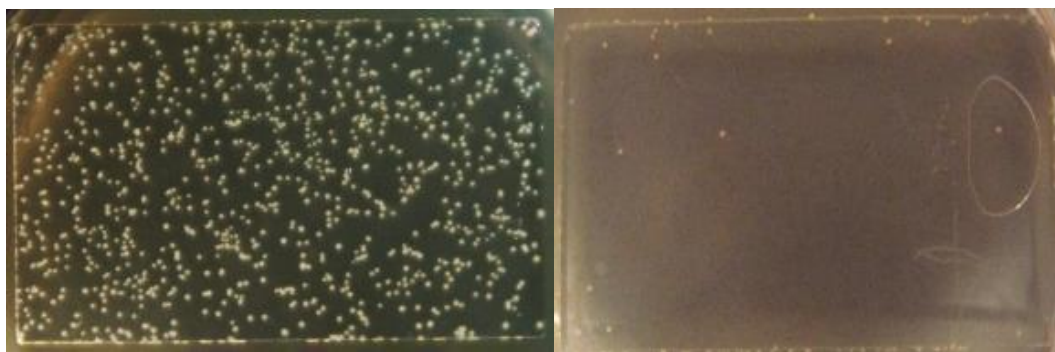


Figure 5.10 *S. aureus* colonies on a control glass slide (left) and the GOPTS/PA treated surface (right) after a 24 hour incubation period.

The GOPTS/PA film was slightly less effective against the Gram-negative *P. aeruginosa* (killing efficiency 88%) when compared with the Gram-positive *S. epidermidis* and *S. aureus* (killing efficiency 97%). It is known that the Gram-negative bacteria have a more compact cell wall with two phospholipid bilayers compared with the Gram-positive bacteria. The lower effectiveness against the Gram-negative microorganism is consistent with previous results showing that the Gram-negative bacteria are less susceptible to antiseptics and disinfectants than the Gram-positive organisms.¹⁶ The cell wall of Gram-positive bacteria are composed of almost exclusively peptidoglycan and teichoic acid that are not effective at excluding antimicrobial agents from the cell. The outer membrane of Gram-negative bacteria on the other hand is an effective barrier to entry and *P. aeruginosa* in particular is known to exhibit high resistance to many disinfectants and antiseptics.^{16,44} For the tethered molecules considered here, diffusion is not an issue, but we expect that the outer membrane of the gram-negative bacteria would also provide a barrier to PA conformations that access the interior membrane.

5.3.6 Effect of PA molecular weight, charge, and deposition techniques on the bacterial killing efficiency

The molecular weight of the PA did not have a strong effect on the antimicrobial effectiveness of the films. The 58,000 MW film had much shorter strands of polymer according to the AFM ECL test (Figure 5.9), but in general, we did not find a correlation between ECL and killing efficiency. For example, the killing efficiency of *S. epidermidis* was about the same for 6 min and 60 min of GOPTS treatment, even though these two treatments produced a factor of two difference in ECL (Table 5.2). In contrast, there was no significant difference between 15,000 MW and 58,000 MW in killing *P. aeruginosa*. As stated above, the time of exposure of the GOPTS, which alters the density of attachment points did not have a significant effect on the killing efficiency of *S. epidermidis* either. Thus, in contrast to other studies that found the antimicrobial polymer length to be important in their system,^{22,24,27} we do not find an effect of tether length on the killing efficiency. However, we can conclude that the covalently attached PA is very effective at killing of a variety of bacteria, almost independent of the preparation conditions. In hopes of optimizing the killing efficiency of the antimicrobial coatings, we varied the application time of the GOPTS, used the GOPTS diluted in dry toluene instead of pure GOPTS, and decreased the concentration of the PA application solution ten-fold. These methods did not show an improvement on the original procedure but they also did not dramatically reduce the effectiveness of the films. For example, in the case of *S. epidermidis*, when the GOPTS application time was varied for the 15,000 MW PA coating between 6 and 60 min (Table 5.1), the film effectiveness remained virtually the same.

The PA films bound to glass using GOPTS showed excellent antimicrobial capability compared with bare glass or PA films that were simply dipped once in the polyelectrolyte solution. This is attributed to the fact that the covalently bonded PA chains had more exposed positive charges on the surface and free polymer chains available to interact with bacteria as confirmed by the zeta potential and the AFM measurements. The alkoxy silane molecules forming the monolayer on the surface removed the negative surface charge so the attractive interactions between the PA polymer chains and the glass surface were eliminated as seen in Figure 5.7. In the case when PA was adsorbed directly from solution and bound to the glass surface via electrostatic attraction, the positively charged amine groups most likely collapsed onto the negatively charged silica and did not “see” the bacterial cells.

5.4 Conclusions

PA covalently bound to glass using GOPTS showed excellent antimicrobial capability compared with bare glass or PA films that were simply dipped in the polyelectrolyte solution. The number of surviving colonies of both Gram-positive (*S. aureus* and *S. epiderimidis*) and Gram-negative (*P. aeruginosa*) organisms were reduced dramatically compared with the control using an aerosol spraying test. The results of zeta potential measurements indicated that the PA surfaces were strongly positively charged and very stable when the PA was reacted with epoxide-functionalized glass. The zeta potential of the GOPTS/PA surfaces varied between 60 and 70 mV depending on the molecular weight of the polymer. Thus, robustness and a high positive zeta potential are important factors in determining killing efficiency. In contrast, the length of free polymer chain was not found to be important in the 100~200 nm range that we examined. Variation in the GOPTS reaction conditions or diluting the PA application solution did not show a strong effect on the antimicrobial properties of the resultant surfaces. When comparing the PA/GOPTS surfaces with the dipped PA control surfaces, it is apparent that the PA/GOPTS surfaces have a strong positive charge and extend much further into solution. This is consistent with previous literature results that indicated the antimicrobial surfaces required a minimum surface charge to be effective as well as the ability to extend from the surface to interact with the bacterial cells. There was no inhibition zone observed. The bacterial killing mechanism was likely due the electrostatic interaction between the bacterial cell membranes and the positively charged PA surfaces as described previously in the literature.

	<i>S. epi</i>	<i>S. aureus</i>	<i>P. aeruginosa</i>
15,000 MW PAA with 60 min GOPTS application	97 ± 2	97 ± 3	88 ± 14
15,000 MW PAA with 6 min GOPTS application	96 ± 5		(98)
58,000 MW PAA 60 min GOPTS application	(98)	90 ± 10	89 ± 5

Table 5.1 Killing efficiency of different surfaces compared with a clean glass control.

	15,000 MW	58,000 MW	900,000 MW
	nm	nm	nm
6 minute GOPTS application	113 ± 7	65 ± 10	
1 hour GOPTS application	210 ± 30	120 ± 20	50 ± 10
Dipped PAA	50 ± 2	15 ± 4	

Table 5.2 The polymer ECL and the standard error of the PA films.

	C1s	N1s	O1s	Si2p	C/N	C/O	C/Si
Clean glass	5.99	0.47	65.5	28.0	12.7	0.091	0.214
GOPTS	8.11	0.22	63.7	28.0	36.8	0.127	0.290
GOPTS+PAH	46.6	9.24	31.3	12.2	5.03	1.489	3.829
GOPTS+PAH+Cys	61.2	7.27	22.0	8.31	8.41	2.789	7.359

Table 5.3 Values for the XPS analysis of the clean, GOPTS-coated, and GOPTS/PA coated wafers, and also the GOPTS/PA coated wafers after a reaction with Fmoc-protected Cysteine amino acids.

References

- (1) Green, J.-B. D.; Fulghum, T.; Nordhaus, M. A. *Biointerphases* **2011**, *6*, MR13.
- (2) Bryers, J. D. *Biotechnology and Bioengineering* **2008**, *100*, 1.
- (3) Bowersock, T. L.; Woodyard, L.; Hamilton, A. J.; DeFord, J. A. *Journal of Controlled Release* **1994**, *31*, 237.
- (4) Sousa, C.; Henriques, M.; Oliveira, R. *Biofouling* **2011**, *27*, 609.
- (5) Geddes, A. *Journal of Antimicrobial Chemotherapy* **2000**, *46*, 873.
- (6) Cozad, A.; Jones, R. D. *American journal of infection control* **2003**, *31*, 243.
- (7) Kramer, A.; Schwebke, I.; Kampf, G. *BMC Infectious Diseases* **2006**, *6*, 130.
- (8) Cunha, B. A. *Critical care clinics* **1998**, *14*, 263.
- (9) Kenawy, E.-R.; Worley, S. D.; Broughton, R. *Biomacromolecules* **2007**, *8*, 1359.
- (10) Han, H.; Wu, J.; Avery, C. W.; Mizutani, M.; Jiang, X.; Kamigaito, M.; Chen, Z.; Xi, C.; Kuroda, K. *Langmuir* **2011**, *27*, 4010.
- (11) Li, Z.; Lee, D.; Sheng, X.; Cohen, R. E.; Rubner, M. F. *Langmuir* **2006**, *22*, 9820.
- (12) Lee, H.-S.; Eckmann, D. M.; Lee, D.; Hickok, N. J.; Composto, R. J. *Langmuir* **2011**, *27*, 12458.
- (13) Wong, S. Y.; Li, Q.; Veselinovic, J.; Kim, B.-S.; Klibanov, A. M.; Hammond, P. T. *Biomaterials* **2010**, *31*, 4079.
- (14) Lichter, J. A.; Rubner, M. F. *Langmuir* **2009**, *25*, 7686.
- (15) Urrutia, A.; Rivero, P. J.; Ruete, L.; Goicoechea, J.; Fernández-Valdivieso, C.; Arregui, F. J.; Matías, I. R. *physica status solidi (c)* **2010**, *7*, 2774.
- (16) Timofeeva, L.; Kleshcheva, N. *Appl Microbiol Biotechnol* **2011**, *89*, 475.
- (17) Malmsten, M. *Soft Matter* **2011**, *7*, 8725.
- (18) Muñoz-Bonilla, A.; Fernández-García, M. *Progress in Polymer Science* **2012**, *37*, 281.
- (19) Tiller, J.; Börner, H. G., Lutz, J.-F., Eds.; Springer Berlin / Heidelberg: 2011; Vol. 240, p 193.
- (20) Page, K.; Wilson, M.; Parkin, I. P. *Journal of Materials Chemistry* **2009**, *19*, 3819.
- (21) Madkour, A. E.; Dabkowski, J. M.; Nüsslein, K.; Tew, G. N. *Langmuir* **2008**, *25*, 1060.
- (22) Klibanov, A. M. *J. Mater. Chem.* **2007**, *17*, 2479.
- (23) Kugler, R.; Bouloussa, O.; Rondelez, F. *Microbiology* **2005**, *151*, 1341.
- (24) Tiller, J. C.; Liao, C. J.; Lewis, K.; Klibanov, A. M. *P Natl Acad Sci USA* **2001**, *98*, 5981.
- (25) Tiller, J. C.; Lee, S. B.; Lewis, K.; Klibanov, A. M. *Biotechnology and Bioengineering* **2002**, *79*, 465.
- (26) Murata, H.; Koepsel, R. R.; Matyjaszewski, K.; Russell, A. J. *Biomaterials* **2007**, *28*, 4870.
- (27) Huang, J.; Koepsel, R. R.; Murata, H.; Wu, W.; Lee, S. B.; Kowalewski, T.; Russell, A. J.; Matyjaszewski, K. *Langmuir* **2008**, *24*, 6785.
- (28) Matias, V. R. F.; Al-Amoudi, A.; Dubochet, J.; Beveridge, T. J. *Journal of Bacteriology* **2003**, *185*, 6112.
- (29) Gazzola, S.; Cocconcelli, P. S. *Microbiology* **2008**, *154*, 3224.
- (30) Dmitriev, B. A.; Toukach, F. V.; Holst, O.; Rietschel, E. T.; Ehlers, S. *Journal of Bacteriology* **2004**, *186*, 7141.

- (31) Agarwal, A.; Weis, T. L.; Schurr, M. J.; Faith, N. G.; Czuprynski, C. J.; McAnulty, J. F.; Murphy, C. J.; Abbott, N. L. *Biomaterials* **2010**, *31*, 680.
- (32) Zasloff, M. *Nature* **2002**, *415*, 389.
- (33) Cunliffe, D.; Smart, C. A.; Alexander, C.; Vulfson, E. N. *APPLIED AND ENVIRONMENTAL MICROBIOLOGY* **1999**, *65*, 4995.
- (34) Todd, S. J.; Scurr, D. J.; Gough, J. E.; Alexander, M. R.; Ulijn, R. V. *Langmuir* **2009**, *25*, 7533.
- (35) Zucolotto, V.; Ferreira, M.; Cordeiro, M. R.; Constantino, C. J. L.; Balogh, D. T.; Zanatta, A. R.; Moreira, W. C.; Oliveira, O. N. *The Journal of Physical Chemistry B* **2003**, *107*, 3733.
- (36) Green, C. P.; Lioue, H.; Cleveland, J. P.; Proksch, R.; Mulvaney, P.; Sader, J. E. *REVIEW OF SCIENTIFIC INSTRUMENTS* **2004**, *75*, 1988.
- (37) Mosse, W. K. J.; Koppens, M. L.; Gengenbach, T. R.; Scanlon, D. B.; Gras, S. L.; Ducker, W. A. *Langmuir* **2009**, *25*, 1488.
- (38) Nispen, J. W. *Pure & Appl. Chem.* **1987**, *59*, 331.
- (39) Pavia, D. L.; Lampman, G. M.; Kriz, G. S. *Introduction to Spectroscopy*; 3rd ed.; Brooks/Cole: United States of America, 2001.
- (40) Elimelech, M.; Chen, W. H.; Waypa, J. J. *Desalination* **1994**, *95*, 269.
- (41) Gupta, M. L.; Brunson, K.; Chakravorty, A.; Kurt, P.; Alvarez, J. C.; Luna-Vera, F.; Wynne, K. J. *Langmuir* **2010**, *26*, 9032.
- (42) Sokolov, I.; Ong, Q. K.; Shodiev, H.; Chechik, N.; James, D.; Oliver, M. *J Colloid Interface Sci* **2006**, *300*, 475.
- (43) Châtellier, X.; Senden, T. J.; Joanny, J.-F.; Meglio, J.-M. d. *Europhys. Lett.* **1998**, *41*, 303.
- (44) McDonnell, G.; Russell, A. D. *Clinical Microbiology Reviews* **1999**, *12*, 147.

Chapter 6

Antimicrobial peptide films

Abstract

A peptide with known antimicrobial properties (Pexiganan) was attached to a silicon substrate using microwave assisted solid phase peptide synthesis. Primary amine groups attached to the silicon surface were used as the peptide binding sites. Different methods of amine functionalization of the substrate were utilized: (1) reaction with (3-aminopropyl)triethoxysilane, (2) attachment of amine-activated poly (ethylene glycol) diamine, and (3) attachment of poly (allyl amine) (PA). It was concluded that the peptide attachment resulted in an effective antimicrobial film when using the GOPTS-PA-Pexiganan reaction schematic due to the longer tether chain length and a large number of amine binding sites.

6.1 Introduction

In recent years the functionality of synthetic or naturally occurring peptide molecules and their potential as antimicrobial agents have been studied extensively.¹ These molecules usually carry a positive charge and therefore have the ability to interact with the overall negatively charged bacterial membranes. The hydrophobic portion of the peptide interacts with the hydrophobic membrane lipid double layer to allow the peptide to enter the bacterial cell. Peptide molecules can interact with the bacterial membrane and with other cell components (DNA, enzymes) inside the cell which results in bacterial death.² It was determined in the previous studies that attaching an oligopeptide to a surface using a spacer allows for surface antimicrobial activity.³ For example in a study by Glinel et al., magainin1 was immobilized on a oligo(ethylene glycol) methacrylate. The results confirmed the effectiveness of the peptide when attached to a surface, and also illustrated that the peptide binding density can be controlled by controlling the tether polymer brush density.⁴

In this study Pexiganan (GIGKFLKKAKKFGKAFVKILKKa) was attached to a substrate to render it antimicrobial. Pexiganan is an analog to a naturally occurring peptide Magainin2 that was extracted from a skin of an African frog.⁵ This peptide was found to have a broad spectrum of activity against different microbial organisms. It was studied in topical applications of diabetic foot ulcers, for treatment of sepsis, and as an anti-fungal agent. This chapter describes the investigations that were performed to determine the best way to attach Pexiganan to a silicon substrate to render it antimicrobial.

6.2 Materials and methods

Poly (ethylene glycol) diamine (3,000 MW) was purchased from Sigma-Aldrich. Silicon slides were pre-treated to expose hydroxyl groups on the surface using concentrated sulfuric acid and hydrogen peroxide mixture. (3-Aminopropyl)triethoxysilane (APTES) was attached to silicon by incubating the wafer in 1% APTES in toluene for 4 minutes at 60°C. 3-

Glycidyoxypropyltrimethoxysilane (GOPTS) was reacted with pre-treated silicon for 1 hour at 37°C. The poly (allyl amine) (PA) was reacted with the GOPTS epoxide-functionalized surface in an aqueous environment at 75°C for 24 hours. *E. coli* (MG1655) was used as the model organism in the bacterial assay study. The bacterial assay was performed by spraying a bacterial suspension on surface-treated glass slides and incubating them under agar. The detailed procedures for the film synthesis and the bacterial assay were described in a previous chapter.

The procedure for PEGDA attachment was adapted from Todd et al.⁶ Briefly, pre-treated silicon slides were exposed to the GOPTS for one hour at 37°C. Two slides were placed in the temperature controlled chamber facing each other, after a droplet of GOPTS was added to the surface of the bottom slide. The silicon wafers were then sonicated in toluene for 3 minutes to remove unreacted or polymerized GOPTS, and washed with toluene and ethanol. The PEGDA powder was then added to the top of the surface, and melted at 75°C for 24 hours. Excess polymer was washed off with water and dried in atmospheric conditions.

The resultant films were analyzed using several surface sensitive techniques: X-ray photoelectron spectroscopy (XPS), attenuated total reflectance infrared spectroscopy (ATR-IR), and secondary ion mass spectrometry (SIMS). The detailed procedures describing how these measurements were performed are given elsewhere in this work.

6.3 Results and discussion

The surface film characterization was performed to confirm successful attachment of peptide binding sites (primary amine groups) to the surface. The presence of APTES and GOPTS was confirmed using the XPS (Figure 6.3). The PA attachment to the surface and the subsequent attachment of a peptide was confirmed using the XPS as well (Figure 5.2). ATR-IR was used to show the availability of the primary amine groups on the GOPTS-PA tether surface (Figure 5.3). Finally, the presence of the correct oligopeptide sequence on the surface was confirmed using the SIMS (Figure 6.2).

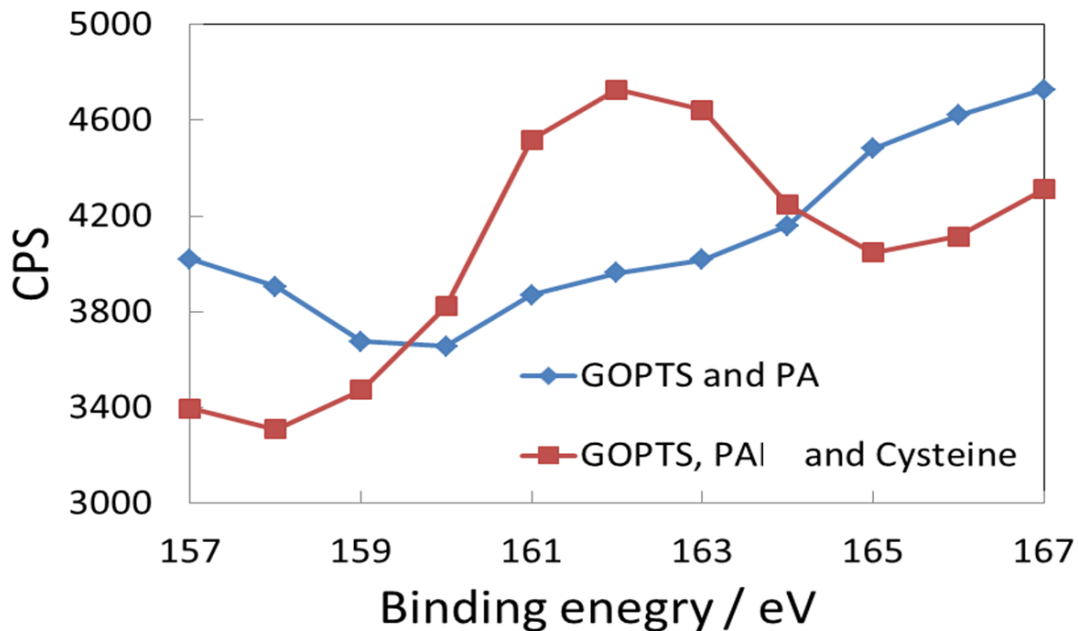


Figure 6.1 S_{2s} peak in the XPS spectrum showing the presence of sulfur, which could only occur if amine groups had been present to bind cysteine. Sulfur was also present in the high resolution S_{2p} scan (not shown).

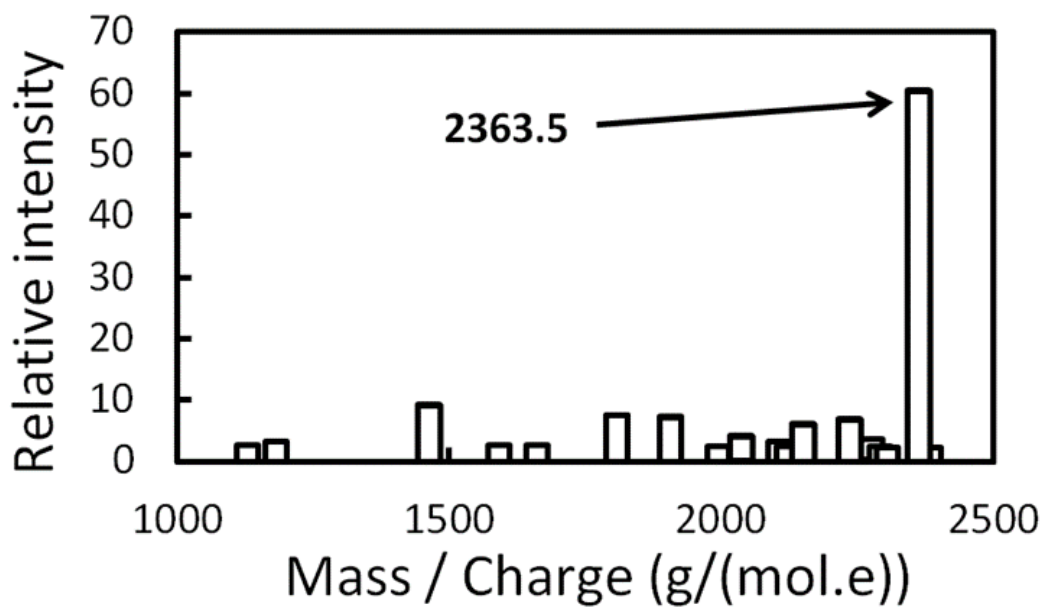


Figure 6.2 Secondary ion mass spectrometry for a Pexiganan which would have a mass of $m/z=2363.5$ if only the intended product were formed. The intense peak at the appropriate mass/charge ratio is consistent with preparation of a film with the appropriate sequence.

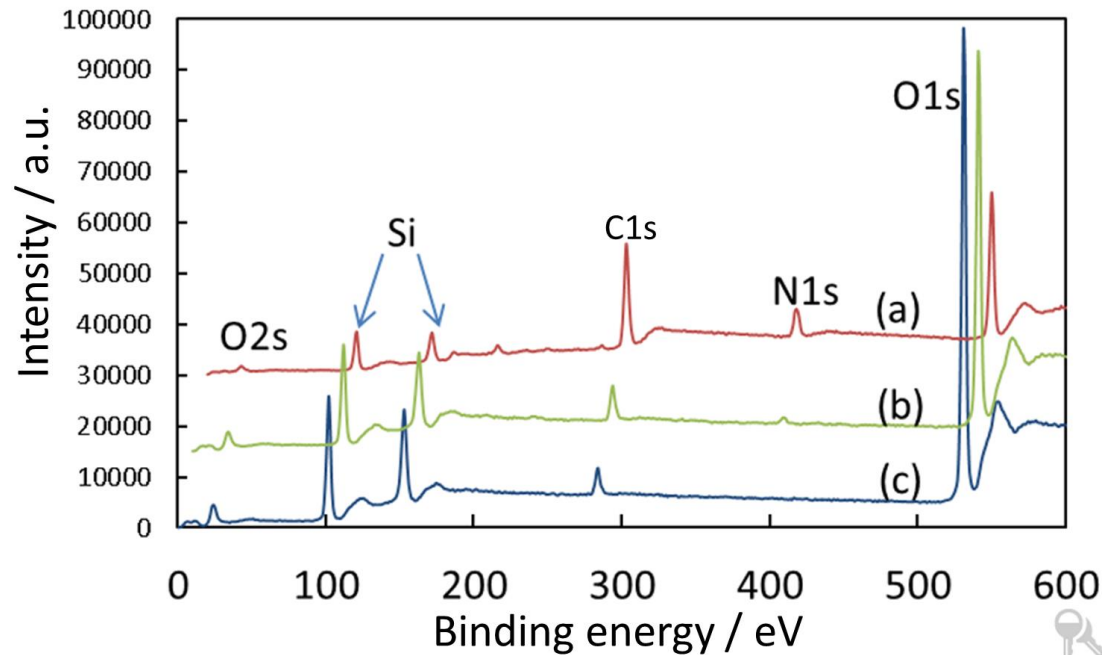


Figure 6.3 The XPS spectrum of the glass film following a 24 hour APTES deposition (a), a 4 minute APTES deposition (b), and of a clean glass control (c).

In order to determine the effectiveness of Pexiganan when bound to glass, we used several attachment methods. Amine functionality was added to the silicon surface using APTES. The surface amine groups served as attachment points for Pexiganan. The APTES coating by itself was determined to have no effect on bacteria compared with glass control slides (Figure 6.4). Adding peptide functionality to the surface did not improve the surface antimicrobial capability. This can be explained because the oligopeptide was bound directly to the surface which hindered its ability to interact with the bacterial cells. Additionally, the peptide may not have the conformational freedom necessary to interact with bacterial cells when in such close proximity to the substrate.

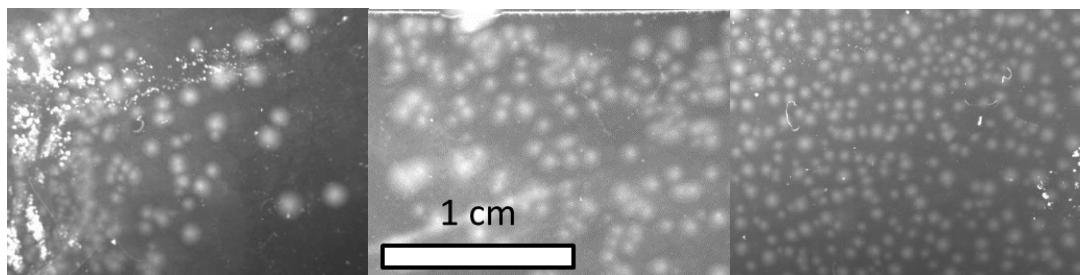


Figure 6.4 Bacterial colonies on a clean glass slide (left), APTES-Pexiganan coating (middle), and GOPTS-PEGDA-Pexiganan (right). Note that there was no reduction in the number of bacterial colonies compared with the clean glass control.

PEGDA was used as an additional tether molecule to attach Pexiganan to the surface. The primary amine groups of the PEGDA molecules served as binding sites for Pexiganan. The 3,000 MW polymer tether was thought to provide a sufficiently long spacer to allow the peptide to interact with bacterial cells. However, no effect on the bacterial cell growth was observed using the PEGDA-Pexiganan system (Figure 6.4). The low molecular weight of the polymer did not provide sufficient freedom for the Pexiganan molecules to extend into solution to interact with the bacterial cell wall. Since the PEGDA polymer had only two amine groups per chain, there was a limited number of accessible sites that the peptide molecules could react with. Each PEGDA molecule could bind to epoxide-functionalized surface with both ends of the polymer chain which would limit the number of the resultant primary amine groups available on the surface. To promote PEGDA attachment to the surface epoxide groups using only one of the two available primary amine groups on each polymer chain, a large excess of PEGDA was used.

Since the APTES and GOPTS-PEGDA binding schemes failed to provide a binding mechanism for the peptide that would retain its antimicrobial properties, a new tether was sought to provide

a better mechanism for attachment. It was determined that the tether molecules had to have a sufficient polymer chain length and a greater number of amine attachment sites than APTES or PEGDA. Poly (allyl amine) (PA) was used as the tether that would satisfy both of these requirements. The higher molecular weight of the polymer (15,000 MW) and a much higher number of possible attachment sites made this tether effective when combined with Pexiganan. Consequently, the PA-Pexiganan coating proved to be effective against *E. coli* when the antimicrobial capability of the film was tested using the bacterial spraying procedure showing 97% reduction in the number of bacterial colonies compared with the glass control. When the PA tether was used by itself, there was a 96% reduction of bacterial colonies, which was within the error of the experiment. Although the GOPTS-PA-Pexiganan film was effective at preventing the growth *E. coli* colonies, it was not significantly more effective than PA alone. The vast increase in effort and cost does not justify its use.

6.4 Conclusions

An effective antimicrobial coating was synthesized using poly(allyl amine) (PA) as the tether molecule for an antimicrobial peptide Pexiganan. The effectiveness of the tether was due to a longer chain length combined with a large number of available amine reactive groups when compared with APTES and GOPTS-PEGDA. The APTES-Pexiganan coating was shown to be ineffective because the peptide was attached directly to the substrate and therefore could not interact with the bacterial cells. The GOPTS-PEGDA-Pexiganan coating also did not exhibit antimicrobial properties when compared with the glass control due to the low molecular weight of the PEGDA tether. We found that peptides grafted from the surface are not biologically active unless there is a tether molecule present that would allow the peptide to interact with bacterial cells. We also found that the tether molecule for the peptide needs to have a minimum chain length to be effective and a sufficient number of binding sites available for peptide grafting.

References

- (1) Zasloff, M. *Nature* **2002**, *415*, 389.
- (2) Jenssen, H.; Hammil, P.; Hancock, R. E. W. *Clin. Microbiol. Rev.* **2006**, *19*, 491.
- (3) Louise Meyer, R.; Zhou, X.; Tang, L.; Arpanaei, A.; Kingshott, P.; Besenbacher, F. *Ultramicroscopy* **2010**, *110*, 1349.
- (4) Glinel, K.; Jonas, A. M.; Jouenne, T.; Leprince, J. r. m.; Galas, L.; Huck, W. T. S. *Bioconjugate Chemistry* **2008**, *20*, 71.
- (5) Gottler, L. M.; Ramamoorthy, A. *Biochimica et Biophysica Acta (BBA) - Biomembranes* **2009**, *1788*, 1680.
- (6) Todd, S. J.; Scurr, D. J.; Gough, J. E.; Alexander, M. R.; Ulijn, R. V. *Langmuir* **2009**, *25*, 7533.

Chapter 7

Conclusions

Oligopeptide molecules were attached to the silicon substrate in order to modify and study frictional interactions as a function of surface chemistry. Lateral force microscopy (LFM) was used to measure the frictional response between a modified surface and a colloidal sphere. We used friction loop analysis to calibrate the photodiode detector together with the thermal deflection method to estimate the torsional spring constant. Frictional and normal surface forces were measured in aqueous environments between a glass colloidal sphere and oligopeptide films grafted from a silicon wafer. Short-chain peptide molecules were synthesized using microwave-assisted solid phase peptide synthesis. Friction force measurements showed that (1) the magnitude of friction increased in the presence of the peptide films compared to a bare silicon wafer, (2) friction had a strong dependence on the nature of the amino acid monomers, (3) friction was lower for hydrophilic films, (4) there was strong adhesion and friction between surfaces of opposite charges, and (5) friction forces were lower in PBS compared to pure water. There was a linear relationship between the frictional force and the applied normal load and this behavior followed the modified version of the Amontons' law. There was a correlation between friction at zero normal load and adhesion between the sphere and the plate. The hydrophobic films and oppositely charged surfaces produced high friction, whereas hydrophilic and like-charged surfaces resulted in low friction. The more hydrophilic films resulted in lower friction. Finally, frictional forces were lower in PBS solution than in water. This was attributed to screening of the double-layer for oppositely charged surfaces and additional separation between the surfaces due to the presence of hydrated salt ions. The grafted chains did not act as

lubricants therefore the friction increased compared with that of two bare hydrophilic glass surfaces. Longer peptides produced lower friction, which suggests that conformational freedom is important for a grafted polymer lubricant.

The second area of investigation focused on antimicrobial properties of thin films. Covalently-bound PA films displayed strong antimicrobial activity compared with bare glass and dipped PA films. An aerosol spraying procedure was used as the metric of microbicidal activity. The cationic PA film displayed strong anti-microbial activity against Gram-positive (*S. aureus* and *S. epidermidis*) and Gram-negative (*P. aeruginosa*) bacteria when evaluated by spraying aqueous suspensions of bacteria on the functionalized glass slides. The zeta potential measurements indicated that covalently-bound PA surfaces had a strong positive charge and high stability. The zeta potential varied between 60 and 70 mV depending on the PA molecular weight. The effectiveness of the PA films is thought to be due to the strong electrostatic interaction between bacterial cell membranes and positively charged PA surfaces. The average length of free polymer chains was not determined to be important as long as the chains extended sufficiently far enough from the surface to interact with the bacterial cell wall. When comparing the PA/GOPTS surfaces with the dipped PA control surfaces, it became apparent that the PA/GOPTS surfaces had a strong positive charge and extended much further from the surface.

An effective antimicrobial coating was synthesized using PA as the tether molecule for an antimicrobial peptide Pexiganan. The effectiveness of the tether was due to a longer chain length combined with a large number of available amine reactive groups when compared with APTES

and GOPTS-PEGDA. The GOPTS-PA tether alone had a strong antimicrobial effect on *E. coli* even without the addition of the peptide. The APTES-Pexiganan coating was not effective because the peptide chain was attached directly to the substrate and therefore could not interact with the bacterial cells. The GOPTS-poly(ethylene glycol) diamine-Pexiganan coating also did not exhibit antimicrobial properties when compared with the glass control due to the low molecular weight of the PEGDA tether.